Recent Progress in the Coordination Chemistry of Verdazyl Radicals

by

Cooper William Johnston
B.Sc., University of British Columbia, 2009

A Thesis Submitted in Partial Fulfillment
of the Requirements for the Degree of

MASTER OF SCIENCE

in the Department of Chemistry

SUPERVISORY COMMITTEE

Recent Progress in the Coordination Chemistry of Verdazyl Radicals

by

Cooper William Johnston
B.Sc., University of British Columbia, 2009

Supervisory Committee

Dr. Robin G. Hicks, (Department of Chemistry)
Supervisor

Dr. J. Scott McIndoe, (Department of Chemistry)
Department Member

ABSTRACT

Supervisory Committee
Dr. Robin G. Hicks, (Department of Chemistry)
Supervisor
Dr. J. Scott McIndoe, (Department of Chemistry)
Department Member

This work expands the investigation into the behaviour of verdazyl radicals and N-alkylated tetrazines as ligands. These new ligands were coordinated to various metals as a means of exploring new properties in the metal-verdazyl and metal-tetrazine products.

The synthesis of *N*,*N*'-diphenyl Kuhn and 6-oxo verdazyl radicals bearing a 2-pyridyl group at the C3 position was accomplished. Palladium(II) dichloride complexes of each of these radicals were prepared in order to study the differences in the structural, electronic, and electrochemical properties compared to corresponding complexes of the previously reported *N*,*N*'-dialkyl-6-oxoverdazyl ligands. The *N*,*N*'-diphenyl verdazyl ligands are structurally bulkier than their dialkyl counterparts resulting in increased interaction between the ligand and palladium as observed in the solid state. The radical complexes were investigated by EPR and shown to exhibit a small amount of spin density on the palladium atoms with most of the spin density remaining on the ligands. The UV-Visible spectra had a noticeable red-shift in the absorbance maxima of the complexes compared to the free ligands. The electrochemistry of the new palladium-

verdazyl complexes showed that there was a positive increase to the reduction and oxidation potentials when compared to the free ligands.

An *N*-benzyl tetrazine and its $Ru(hfac)_2$ complex were synthesized from their corresponding radical species utilizing $Mn_2(CO)_{10}$ to photogenerate benzyl radicals. This method was found to give high yields of the tetrazine and its metal complex. Spectroscopic, structural, and electrochemical properties of the tetrazine and its $Ru(hfac)_2$ complex are reported. These compounds were investigated in regards to the activation energy associated with the homolytic cleavage of the C-N bond in the inert solvent, *tert*-butylbenzene. The activation energy of C-N bond of the tetrazine was 155 $kJmol^{-1}$ while its $Ru(hfac)_2$ complex was 138 $kJmol^{-1}$; this resulted in the rate of dissociation being a factor of ~40 greater for the $Ru(hfac)_2$ complex at 393 K. This work presents the potential of coordination compounds in tuning the properties of molecules associated with the stable free radical polymerization process.

TABLE OF CONTENTS

LIST OF FIGURES

LIST OF SCHEMES

LIST OF TABLES

LIST OF NUMBERED COMPOUNDS

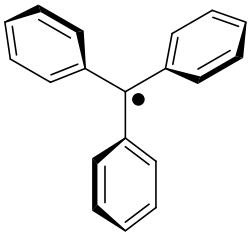

1.1

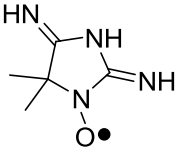

1.2

1.3

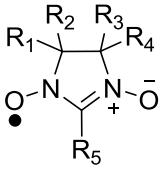

1.4

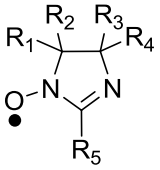

1.5

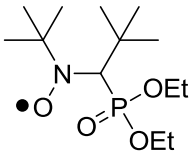

1.6

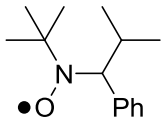

1.7

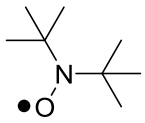

1.8

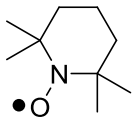

1.9

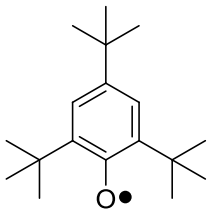

1.10

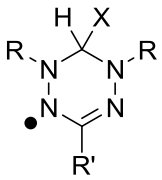

1.11
X = H, alkyl

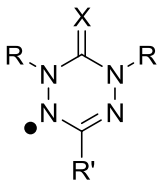

1.12
X = O, S

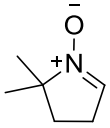

1.13

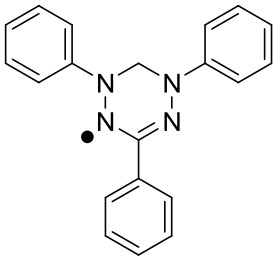

1.14

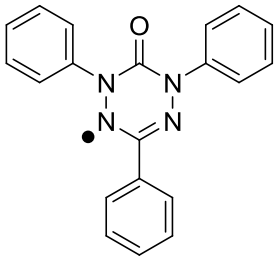

1.15

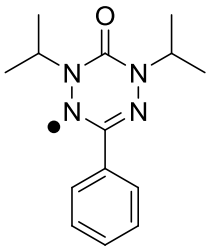

1.16

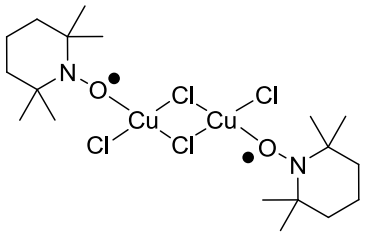

1.17

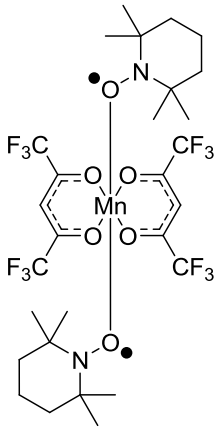

1.18

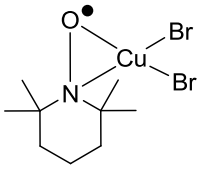

1.19

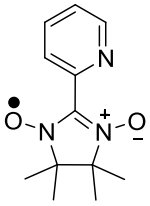

1.20

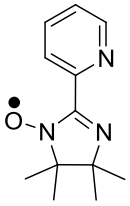

1.21

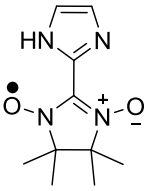

1.22

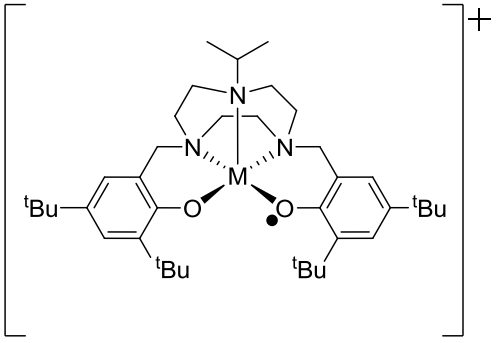

M = Cu, Zn, **1.23**

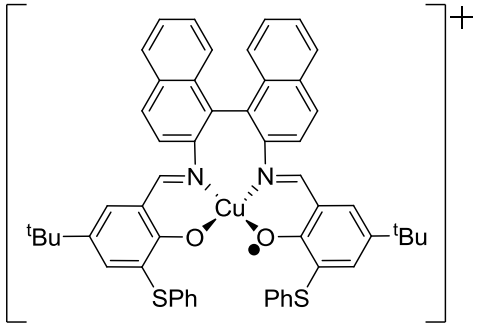

1.24

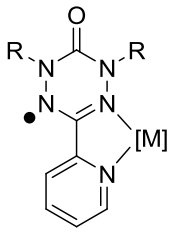

R = Me, [M] = $PdCl_2$ **1.25**
R = ^{i}Pr, [M] = $PdCl_2$ **1.26**
$PtCl_2$ **1.27**
$Ru(acac)_2$ **1.28**
$Ru(hfac)_2$ **1.29**

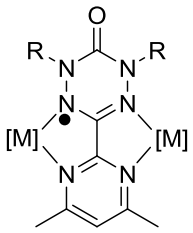

R = Me; [M] = $Ni(hfac)_2$ **1.30**
$Mn(hfac)_2$ **1.31**
R = ^{i}Pr; [M] = $Ru(acac)_2$ **1.32**
$Ru(hfac)_2$ **1.33**

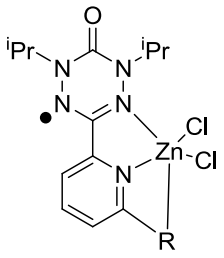

R = 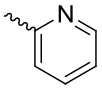 **1.34**

R = 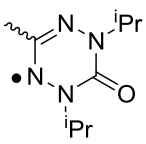 **1.35**

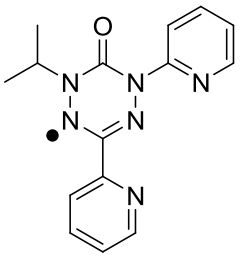

2.1

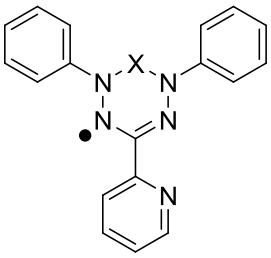

X = CH_2 **2.2**
CO **2.3**

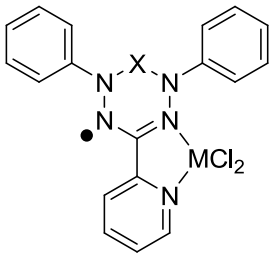

X = CH_2, M = Pd **2.2.PdCl$_2$**
M = Pt **2.2.PtCl$_2$**
X = CO, M = Pd **2.3.PdCl$_2$**
M = Pt **2.3.PtCl$_2$**

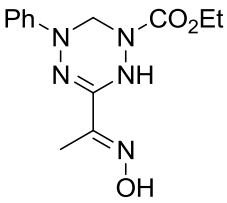

2.4

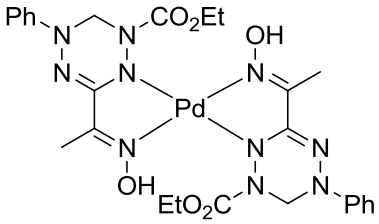

2.5

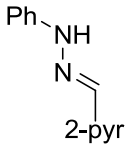

2.6

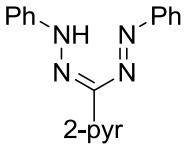

2.7

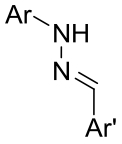

2.8

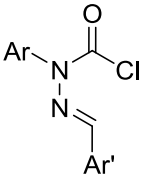

2.9

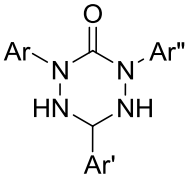

2.10

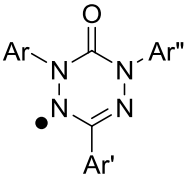

2.11

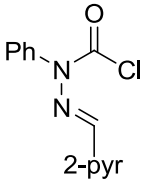

2.12

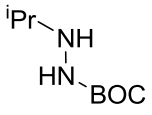

2.13

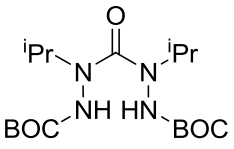

2.14

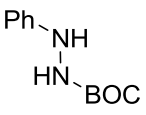

2.15

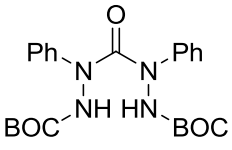

2.16

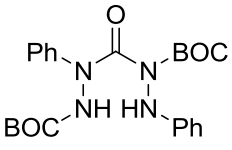

2.17

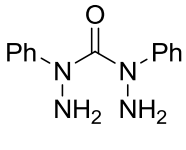

2.18

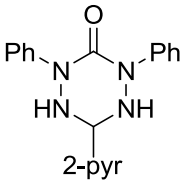

2.19

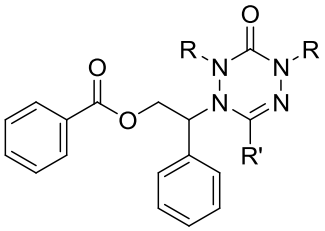

R = R' = Ph **3.1**
R = Me, R' = H **3.2**
R = Me, R'= Et **3.3**
R = Me, R' = Ph **3.4**
R = Me, R' = 4-MeOPh **3.5**
R = Me, R' = 4-NO_2Ph **3.6**

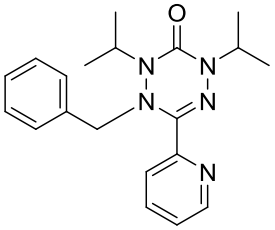

3.7

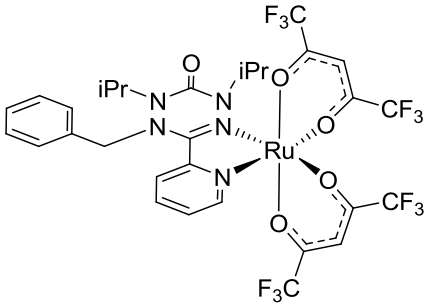

3.7.Ru(hfac)$_2$

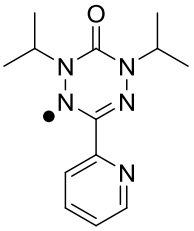

3.8

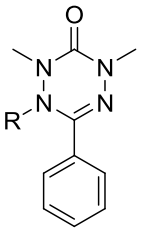

R = Me, Bn **3.9**

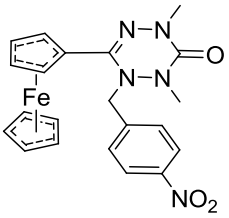

3.10

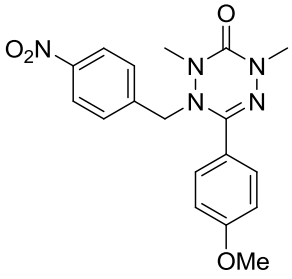

3.11

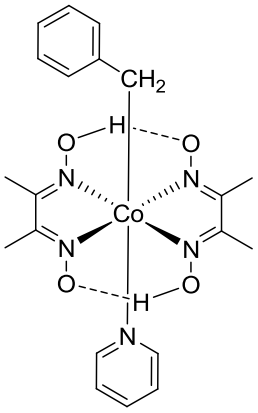

3.12

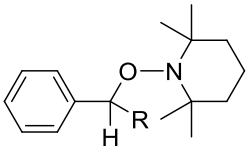

R = H **3.13**
R = Me **3.16**

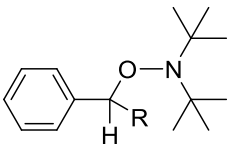

R = H **3.14**
R = Me **3.17**

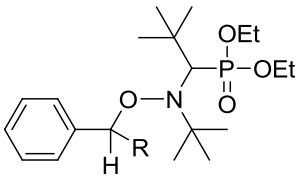

R = H **3.15**
R = Me **3.18**

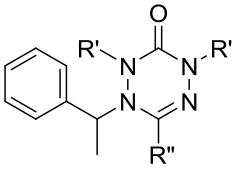

R = Me, R'' = H **3.19**
R = Me, R'' = Et **3.20**
R = Me, R'' = Ph **3.21**
R = Ph, R'' = Ph **3.22**

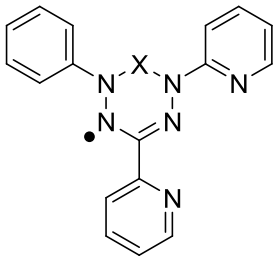

X = CH_2, CO **4.1**

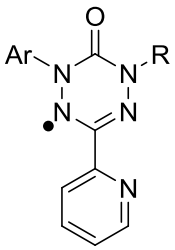

4.2

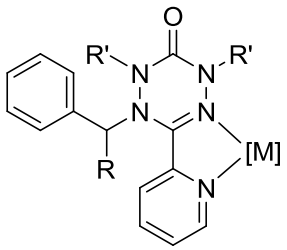

4.3

LIST OF ABBREVIATIONS

1,5-COD	cycloocta-1,5-diene
2-pyr	2-pyridyl
a	hyperfine coupling constant
A	frequency factor
Å	angstroms
a. u.	arbitrary unit
acac	acetylacetonate
Anal. Calc.	analytical calculated
Ar	aromatic group or Argon
BOC	*tert*-butoxycarbonyl
Bn	benzyl
bipy	2,2'-bipyridine
br	broad (IR peak descriptor)
°C	degrees Celsius
cm	centimetre
cm^{-1}	wavenumber
CV	cyclic voltammetry or cyclic voltammogram
d	doublet (NMR peak descriptor)
DBU	1,8-diazabicycloundec-7-ene
DCM	dichloromethane
DDQ	2,3-dichloro-5,6-dicyano-1,4-benzoquinone
DMF	dimethylformamide
DMSO	dimethylsulfoxide

D. N. Al.	deactivated neutral alumina
DPPH	2,2-diphenyl-1-picrylhydrazyl
e^-	electron
E_a	activation energy
E_{cell}	cell potential
E_{ox}	oxidation potential
E_{red}	reduction potential
EPR	electron paramagnetic resonance
ESI	electrospray ionization
Et	ethyl
EtOAc	ethyl acetate
EtOH	ethanol
Et_2O	diethyl ether
Fc/Fc^+	ferrocene/ferrocenium
FT-IR	Fourier transform infrared
g	g-factor or gram
G	Gauss
GAO	galactose oxidase
GHz	gigahertz
h	hour
h	Planck's constant (6.626×10^{-34} Js)
hfac	1,1,1,5,5,5-hexafluoroacetylacetonate
HOMO	highest occupied molecular orbital
HPLC	high-performance liquid chromatography
HR-MS	high-resolution mass spectrometry
Hz	hertz

in vacuo	in a vacuum
^{i}Pr	isopropyl
J	Joule
J	coupling constant
K	Kelvin
k_B	Boltzmann constant (1.381×10^{-23} JK^{-1})
KBr	potassium bromide
k_d	dissociation rate constant
kJ	kilojoules
L	litre
LR-MS	low-resolution mass spectrometry
LUMO	lowest unoccupied molecular orbital
M	molarity or metal
m	medium (IR)
m/z	mass-to-charge ratio
Me	methyl
MeCN	acetonitrile
MeOH	methanol
MHz	megahertz
mg	milligram
min	minute
mL	millilitre
mM	millimolar
mm	millimetre
mmol	millimole
mol	mole

MP	melting point
MS	mass spectrometry
mult	multiplet (NMR)
nm	nanometre
NMR	nuclear magnetic resonance
[O]	oxidant
OAc	acetate
ox	oxidation
PDI	polydispersity index
Ph	phenyl
PhCN	benzonitrile
ppm	parts per million
PRE	persistent radical effect
pyrHOTs	pyridinium tosylate
q	quartet (NMR)
R	gas constant (8.314 $JK^{-1}mol^{-1}$)
R^2	goodness of fit
rbf	round bottom flask
red	reduction
RT	room temperature
s	singlet (NMR), strong (IR) or second
sept	septet (NMR)
SFRP	stable free radical polymerization
SiO_2	silica gel
SOMO	singly occupied molecular orbital
T	temperature

t	triplet (NMR) or time
^{t}Bu	*tert*-butyl
TEMPO	2,2,6,6-tetramethylpiperidine 1-oxyl
THF	tetrahydrofuran
TEA	triethylamine
UV	ultraviolet
V	volt
Vis	visible
w	weak (IR)
$\Delta H^{\ddagger}$	enthalpy of activation
$\Delta S^{\ddagger}$	entropy of activation
δ	chemical shift
ε	molecular extinction coefficient
λ	wavelength
λ_{max}	wavelength of maximum electronic absorption

ACKNOWLEDGEMENTS

I would like to thank my supervisor, Dr. Robin G. Hicks, who has allowed me the chance to learn synthetic chemistry and explore new chemistry that was previously unknown. He has granted me the freedom to develop skills pertaining to chemistry both inside and outside of the laboratory.

Many thanks go out to past and present members of the Hicks group: Dr. Kevin Anderson, Gen Boice, Dr. Steve McKinnon, Graeme Nawn, Emma Nicholls-Allison, Dr. Daniel Plaul, Corey Sanz, and Dr. Tyler Trefz. To all the non-group members: Aman Bains, Jordan Cramen, Dr. Brynn Dooley, Aiko Kurimoto, Dr. Tom Whitesides, and Mark Zsombor. Your experience, knowledge, and patience have been invaluable to me in learning about inorganic synthetic chemistry.

The faculty and staff in the chemistry department deserve acknowledgements and thanks. Thanks to the instrument shop for maintaining the computers and electronics that I have relied upon during my studies. I would like to thank the teaching staff with whom I have had the pleasure of interacting and for having made the experience enjoyable.

I would like to thank my friends and family who has managed to put up with me over the many years. Finally, thanks to Gillian Blaine for having joined me on this ride we call "life".

CHAPTER 1

INTRODUCTION AND BACKGROUND

1.1 Stable Organic Free Radicals

Radicals are molecules which possess at least one unpaired electron and for the most part are reactive and short-lived. The reason for their transient nature lies in the multitude of pathways for their decomposition (e.g. dimerization, hydrogen abstraction, disproportionation) which are thermodynamically favored[1]. Many of these decomposition pathways are kinetically very fast due to the low activation energy barrier associated with these degradations. In contrast to typical organic compounds which are closed-shell and possess the appropriate valence as expected by the octet rule and Lewis structures, radicals are open-shell molecules and subvalent meaning that they have one less bond than expected.

Yet, not all radicals are created equal and each has its own unique lifetime which can vary from seconds to days in solution and hours to years in the solid state. When these lifetimes are long enough for the compound of interest to be investigated by spectroscopic methods, they are referred to as *persistent*[2]. Organic radicals which can be isolated and handled as a pure compound are referred to as *stable*. Stable radicals have been made which are unreactive to both air and water.

In 1900, Gomberg proposed the existence of the first organic free radical[3], the triphenylmethyl radical (**1.1**). While Gomberg experienced difficulty in convincing the

scientific community of his discovery due to the controversial nature of what he was proposing[4], we now know that he was correct in his interpretation of his results. While radicals that can be isolated are not new, they continue to be viewed as exotic molecules.

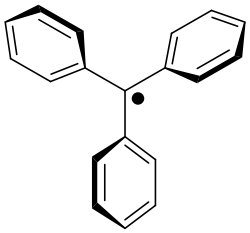

1.1

The seminal work by Gomberg encouraged the development of the field of organic radical chemistry. Organic radicals, both persistent and stable, have been made which are carbon-centered, nitrogen-centered, oxygen-centered, and heavier p-block element (S, Se, Te, etc.)-centered. The number of different types of radicals is a testament to human ingenuity and the richness of chemistry.

Since the discovery of **1.1** there have been numerous advancements in the field of organic radicals (e.g. synthesis, stability, classes). Research into free radicals has had an effect on numerous other fields of study including environmental[5,6], medicinal[7,8], material[9-11], and mechanistic[12-14] chemistry. Three different classes of stable organic radicals (nitroxides, phenoxyls, and verdazyls) will be discussed in regards to their structure, redox properties, and metal compounds.

1.1.1 Nitroxide Radicals

The first isolated stable organic radical was the nitroxide radical, porphyrexide (**1.2**), which was prepared by Piloty and Schwerin in 1901[15]. Since this time, there has been tremendous effort in the study of the nitroxides chiefly due to their high stability, ease of synthesis, and variety of uses. This has led to the development of various types of nitroxides: nitroxides[16,17] (**1.3**), nitronyl nitroxides[18] (**1.4**), and imino nitroxides[19] (**1.5**).

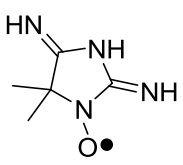

1.2

1.3

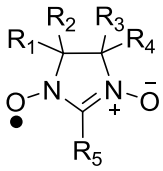

1.4

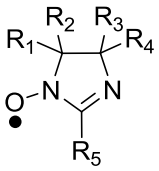

1.5

The aminoxyl group of the nitroxide consists of a three-electron N-O π system. The spin density of the nitroxide radical is distributed on the nitrogen and oxygen atoms with a slightly higher distribution on the oxygen atom[20]. The stability of nitroxides can vary depending on the substituents on the nitrogen. Generally, nitroxides which possess a hydrogen atom on the carbon atom directly attached to nitrogen atom are not stable due to a thermodynamically favored disporportionation reaction which results in the formation of a hydroxylamine and nitrone[21-23]. This instability can be overcome by the introduction of steric bulk in the form of alkyl or aryl groups α to the nitrogen atom such as *N*-*tert*-butyl-*N*-[1-diethylphosphono-(2,2-dimethylpropyl) nitroxide][24,25] (**1.6**) and *N*-*tert*-butyl-N-[1-phenyl-(2-methylpropyl) nitroxide][26] (**1.7**), but if steric strain becomes exceedingly high these compounds will give rise to a nitroso compound and alkyl radical through homolytic cleavage of the C-N(O) bond. Nitroxides possessing

quartenary carbons such as di-*tert*-butyl nitroxide[27] (**1.8**) or TEMPO[28] (**1.9**) are indefinitely stable as a result of the elimination of the disproportionation pathway.

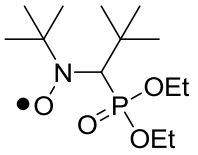

1.6

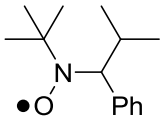

1.7

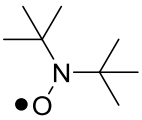

1.8

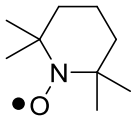

1.9

1.1.2 Phenoxyl Radicals

The phenoxyl radical was first proposed in 1922 to help explain the formation of some diaryl peroxides[29]. Yet, it was not until 1953 that Cook[30] and Müller[31], independent of each other, discovered the first stable phenoxyl radical, 2,4,6-tri-*tert*-butylphenoxyl (**1.10**). In 2008, the X-ray structure of **1.10** was finally obtained[32].

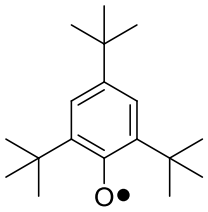

1.10

Phenoxyl radicals are electron deficient molecules[33] that are often perceived to be "oxygen-based" radicals, but through resonance they are stabilized by delocalizing the spin density onto the *ortho* and *para* positions of the benzene ring (**Figure 1.1**). A result of this delocalization is that the reactivity is increased at these positions of the benzene ring necessitating the need for substituents to stabilize the phenoxyl radical. In addition

to adding steric bulk to the molecule at the *ortho* and *para* positions, substituents that add electron density also contribute to the stability of this class of radicals[34].

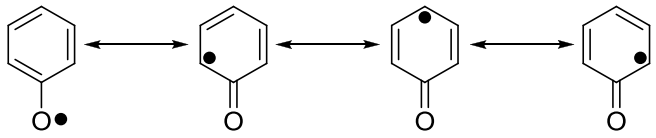

Figure 1.1: Resonance structure of phenoxyl radicals.

1.1.3 Verdazyl Radicals

Verdazyl radicals were discovered in 1963 by Kuhn and Trischmann[35] likely accidently during the course of their research into the alkylation of aryl formazans. The first example of a verdazyl radical (**1.11**) had a methylene (CH_2) moiety at the C6 position and aryl substituents at the N1 and N5 positions (verdazyls of this structure type will be referred to as "Kuhn verdazyls"). Since then, many variants have been made by varying the group attached at the C3 position (e.g. alkyl, aryl). Verdazyls have also been made where the C6 position is either a carbonyl (CO) ("6-oxoverdazyls") or a thiocarbonyl (CS) ("thioxoverdazyls") group (**1.12**)[36-39]; the substituents at the N1 and N5 positions are most commonly alkyl (Me, ^{i}Pr, or benzyl) or aryl groups. The generalized structures and numbering scheme of the verdazyl radical core are shown in **Figure 1.2**.

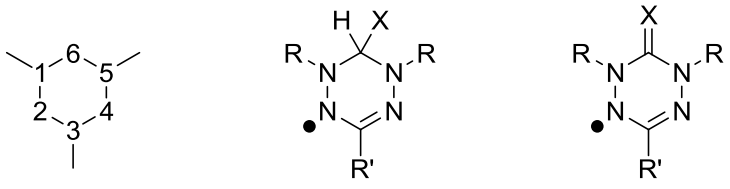

1.11 **X = H, alkyl**

1.12 **X = O, S**

Figure 1.2: General verdazyl radical structures with ring atom numbering scheme.

Verdazyl radicals are one of the few classes of radicals that are stable; most of these radicals are unreactive to air and water and do not suffer from dimerization in the solid state[40]. However, if there is a Me group at either the N1 or N5 positions, the resulting radicals are prone to decomposition via disproportionation[38,41]. The use of EPR spectroscopy has allowed for the observation that the spin density is delocalized mainly over the four nitrogen atoms which can be rationalized by the use of resonance structures (**Figure 1.3**).

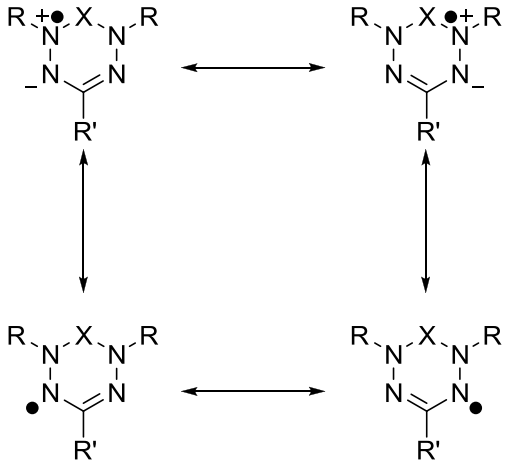

Figure 1.3: Resonance structures of verdazyl radicals.

1.2 Uses of Stable Radicals

Due to the presence of an unpaired electron on the stable radical, multiple uses for these radicals have been explored. In the 1960s, McConnell[42] developed a technique known as spin labeling which allows the study of biological systems by EPR spectroscopy. The radical serves as a "spin label", whereby it is incorporated into the (bio)macromolecule. The EPR spectra of the labeled species can be used to explore the environment surrounding the spin label. The main requirements of the radical is that it is stable to the biological conditions and that it can act as a reporter of the chemical environment, but does not perturb the molecule in which it is incorporated.

In order to investigate whether a particular chemical process generates unstable, transient radicals during the course of a reaction, much work has been placed into the research of the ways to "trap" the short-lived radical either by a spin trap or the persistent radical effect (PRE). Spin traps work by allowing the transient radical to react with a nitrone such as 5,5-dimethyl-1-pyrroline-*N*-oxide (**1.13**) which generates a persistent nitroxide[43,44] (**Scheme 1.1**). This compound can then be analyzed by EPR spectroscopy to elucidate the structure of the transient radical.

The PRE is a phenomenon which results in the formation of a cross-coupled product between two radicals[45,46]. If two or more radicals exist and are formed at equal rates in solution and one is more persistent than the other then the persistent radical will dictate the direction of the subsequent reactions due to its build up over time. This process can be used to study transient radicals by introducing an excess of a stable

radical, such as **1.9**, into a reaction and allowing it to react with the transient radical that is generated during the course of the reaction (**Scheme 1.1**). The product can be collected and analyzed by NMR spectroscopy to determine the structure of the transient radical.

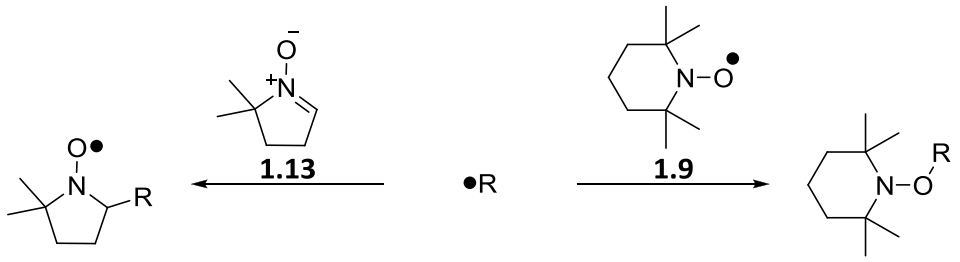

Scheme 1.1: Reaction of a transient radical (**R·**) via spin trap (left) and PRE (right).

Another field that has benefited from stable radicals is molecule-based magnetism. The first example of an organic radical to demonstrate bulk magnetic ordering was a nitroxide[47,48]. Other stable radicals[49,50] have also been used for the study of molecule-based magnetism. Recently there has been a large push to develop molecule-based magnets due to the advantages that these solids would provide compared to traditional metal based magnets, e.g. low density, solubility, optics, and mechanics.

In 1956, early work by Otsu[51] showcased how radicals could be used for polymerization; unfortunately, the dithiocarbamates used in these studies decomposed into other radical species and gave wide molecular weight distributions[52]. This work was carried forward by Georges who in 1993 demonstrated that utilizing stable radicals in the process of stable free radical polymerization (SFRP) can narrow the polydispersity of the polymer[53] giving it controllable molecular weights. In this process, a stable radical

can reversibly bond to the end of the growing polymer and this allows for the reduction of the number of reactive chains through the formation of an unreactive polymer-radical couple (**Scheme 1.2**). This lowers the number of irreversible termination reactions yielding a polymerization method that gives more controlled and predictable results.

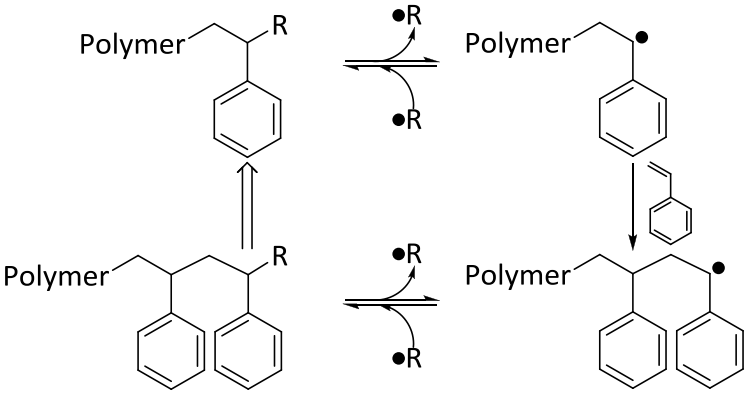

Scheme 1.2: General mechanism for living radical polymerization with a stable radical (**R·**).

1.3 Redox Properties of Stable Radicals

Many stable radicals have been explored electrochemically using cyclic voltammetry (CV). When considering the redox properties of open-shell compounds, it is important to understand how neutral closed-shell compounds are affected by similar events. In neutral closed-shell species, the oxidation process involves removal of an electron from the HOMO of the molecule thereby generating a radical cation; the reduction process involves the addition of an electron to the LUMO resulting in a radical anion (**Figure 1.4(a)**). In radicals, both redox events involve the SOMO of the molecule and result in a closed-shell species (**Figure 1.4(b)**). In both cases, the stability of the "new" species is different when compared to its parent compound. This fundamental difference

between the redox properties of closed-shell and open-shell compounds makes stable radicals an attractive option when considering systems which require a redox-active species.

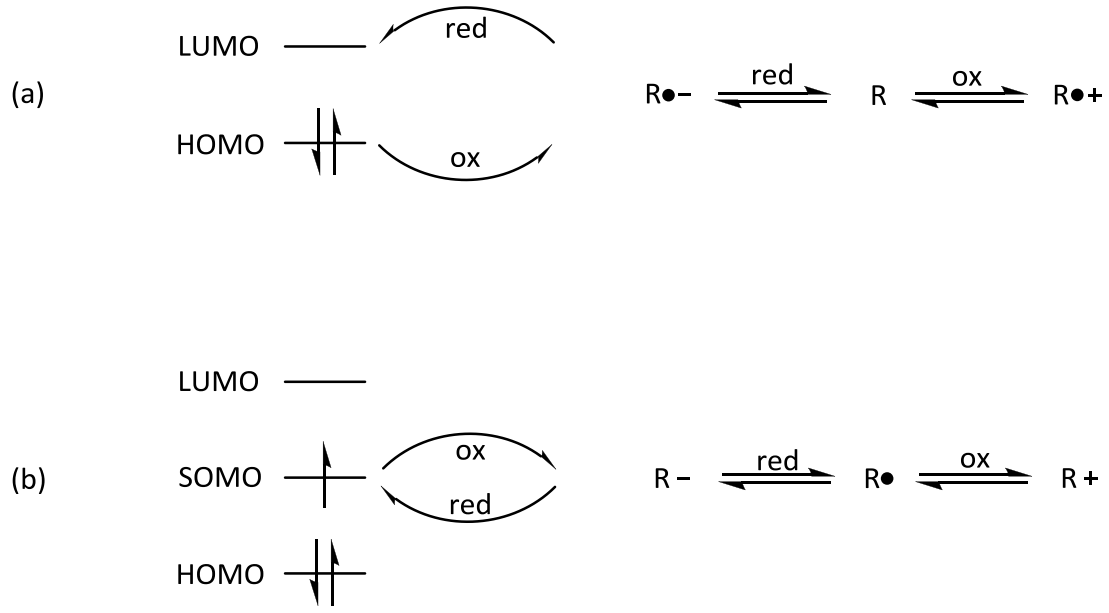

Figure 1.4: Redox processes involving (a) closed shell molecules and (b) open shell molecules and their corresponding change to the chemical species.

1.3.1 Nitroxide Radical Redox Properties

The oxidation of a nitroxide is a one-electron event that gives rise to the oxoammonium cation while the reduction results in the formation of a deprotonated hydroxylamine (**Figure 1.5**). It is the nitroxide's flexibility that impacts the oxidation and reduction, albeit it is the ease with which the nitrogen atom can be pyramidalized in the hydroxylamine and planarized in the oxoammonium cation which impacts the stability[54]. Substituents play a smaller role in affecting the redox potentials[55].

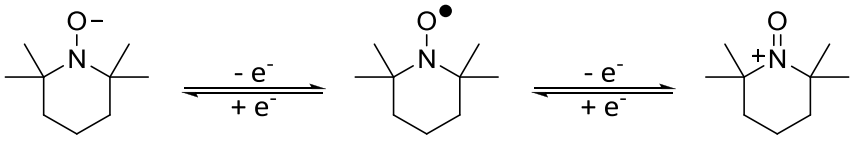

1.9

Figure 1.5: Redox chemistry of the nitroxide, TEMPO (**1.9**).

Nitroxide radicals have been explored as oxidation catalysts as a result of their redox activity. **1.9** has been used in catalytic amounts along with two co-oxidants for the oxidation of alcohols to aldehydes[56]. **1.9** has also been used as an oxidant in copper-catalyzed C-N and C-O bond cross-coupling reactions[57] of arylboronic acids with a variety of substrates.

1.3.2 Phenoxyl Radical Redox Properties

Although more prone to dimerization, phenoxyl radicals have also been examined electrochemically. Phenoxyl radicals can undergo two one-electron events, a reduction resulting in the phenolate anion and an oxidation giving the corresponding cation (**Figure 1.6**). The oxidation process does not give rise to an oxygen centered cation, but rather the positive charge is delocalized over the *ortho* and *para* positions of the ring; this highly reactive species reacts with acetate when it is present during the oxidation[58].

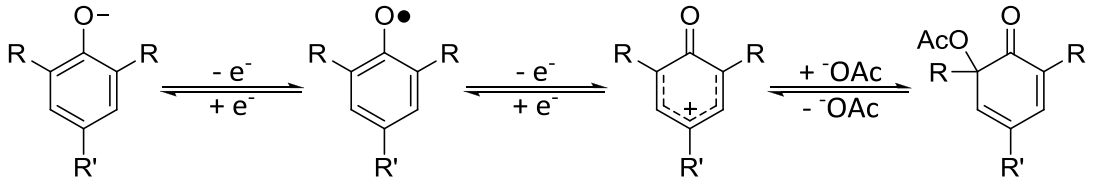

Figure 1.6: Redox chemistry of phenoxyl radicals.

Much of the recent work on the electrochemistry of phenoxyl radicals has focused on metal-phenoxyl radical systems. The interaction between the metal and radical will be discussed in more detail in section 1.4.3.

1.3.3 Verdazyl Radical Redox Properties

Similar to the other stable radicals presented previously, verdazyl radicals can undergo a one-electron reduction to the verdazyl anion or undergo a one-electron oxidation to the verdazylium cation (**Figure 1.7**).

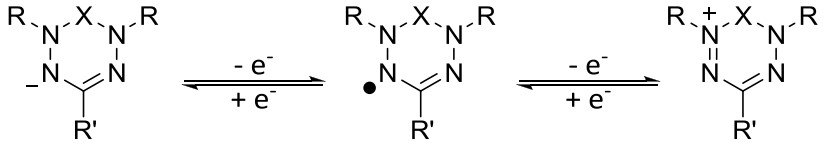

Figure 1.7: Redox chemistry of verdazyl radicals.

Most verdazyl radicals have reduction potentials in the range of -1.3 to -1.0 V (vs. Fc/Fc^+); their oxidation potentials are in the range of –0.2 to +0.5 V (vs. Fc/Fc^+) depending on the substituents attached at the N1 and N5 positions and the type of verdazyl. A study correlating the redox properties of some verdazyl radicals through the use of CV has been performed by our group[59] and a few of the representative compounds illustrating the different structural features are presented (**Table 1.1**). The cell potential, E_{cell}, is presented ($E_{cell} = |E_{ox}^{\circ} - E_{red}^{\circ}|$) for various verdazyl radicals.

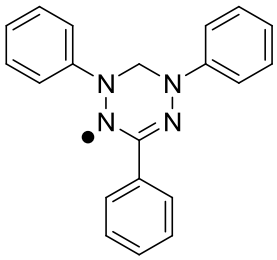

1.14

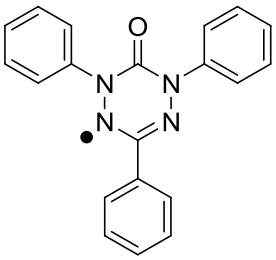

1.15

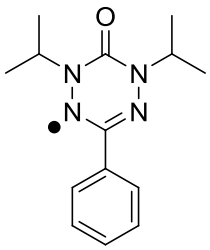

1.16

Table 1.1: Electrochemical properties of a selection of verdazyl radicals (V vs. Fc/Fc^+). Conditions: MeCN solution, 1 mM analyte, 0.1 M $n Bu_4NBF_4$, scan rate 100 mVs^{-1}, and temperature 295 K. Reduction (E_{red}) and oxidation (E_{ox}) half potentials are averages of anodic and cathodic peaks for a given redox process[59].

Verdazyl	E_{red}°	E_{ox}°	E_{cell}
1.14	-1.23	-0.22	1.01
1.15	-0.94	+0.44	1.38
1.16	-1.38	+0.18	1.56

Kuhn verdazyl radicals such as 1,3,5-triphenyl verdazyl (**1.14**) have an oxidation potential in the range of -0.4 to -0.2 V (vs. Fc/Fc^+ in MeCN), while 6-oxoverdazyl radicals such as 1,3,5-triphenyl 6-oxoverdazyl (**1.15**) is on the order of ~0.6 V higher (for the same C and N substituents)[59]. When electron donating substituents are introduced at the N1 and N5 positions as in **1.16**, the verdazyl radical becomes more difficult to reduce and easier to oxidize (compared to **1.15**); electron withdrawing substituents demonstrate the opposite effects in terms of redox properties. The groups at the C3 position have a somewhat smaller effect due to their attachment on the verdazyl ring on a SOMO nodal plane[40].

1.4 Metal Coordinated Stable Radicals

Coordination compounds involving transition metals and radicals allow for the investigation of the combined properties of the two components. Radical-metal combinations have also been shown to be involved in a number of biological processes[60].

It is of importance that the radical ligand system can be easily modified when probing the coordination compounds in order to allow for the determination of the interplay between metal and radical. While compounds containing the radicals O_2 and NO have been synthesized, these small inorganic ligands have no substituents and therefore are not tunable. The following sections will showcase organic radicals that can be functionalized and incorporated onto metals.

1.4.1 Redox-Active Ligands and Non-Innocent Ligands

In 1967, Robin and Day invented a classification system meant to organize bimetallic compounds based on the amount of electron communication between the two metal centres. Their system involves 3 categories: class I where there is no communication, class II where there can be some communication depending on conditions, and class III where there is strong communication over the molecule resulting in a complex where the electron is effectively delocalized.

This classification system can be extended further to describe the electronic communication between any two redox-active centres whether they are metals or not. Ligands that show redox activity are termed redox-active ligands; when the metal-based

and ligand-based frontier orbitals are similar enough in energy these ligands become "non-innocent" ligands and give rise to a number of possible ground state electronic configurations. This confusion regarding the ground state electronic structure is the basis for Jørgensen's original definition of a non-innocent ligand[61].

Non-innocence is seen when the orbitals of the ligand and the metal are similar enough in energy that they interact. This was observed from the series of dithiolene complexes of the nickel family whereby assigning formal oxidation states to the metal and the ligands was controversial[62]. Due to the difficulty with interpreting the spectroscopic properties, a large number of resonance structures are possible leading to the suggestion that the ligand was involved with the changes, thus the ligand can be termed a non-innocent ligand (**Figure 1.8**).

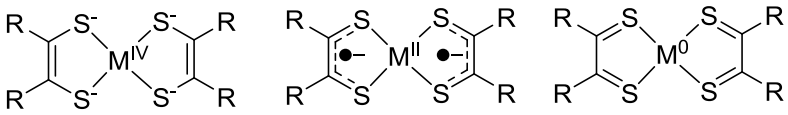

Figure 1.8: Resonance descriptions for square planar metal bis(dithiolene) complexes (M = Ni, Pd, Pt).

1.4.2 Metal-Nitroxide Complexes

One of the most common nitroxide radicals is TEMPO (**1.9**); this stable radical has been incorporated into a wide range of coordination compounds. Interestingly, the fashion of coordination of nitroxides such as **1.9** is not always predictable due to these compounds being weak donors[63]. Coordination compounds of **1.9** have been made using strong Lewis acids and some of these compounds have had **1.9** bind solely through

the oxygen atom in an "end-on" fashion, **1.17**[64] and **1.18**[65,66], and, less commonly, through the nitrogen and oxygen atoms by a "side-on" fashion, **1.19**[64,67]. This is only a selection of the wide variety of nitroxide-metal complexes and the geometries that exist.

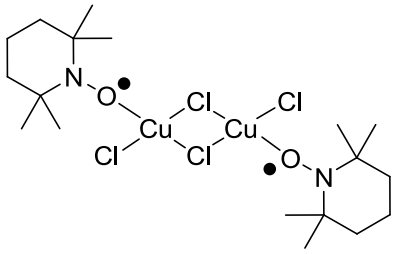

1.17

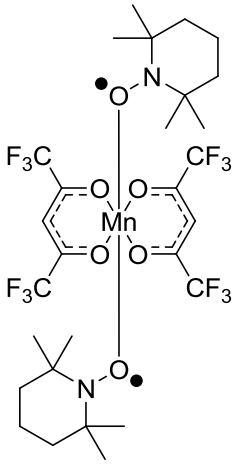

1.18

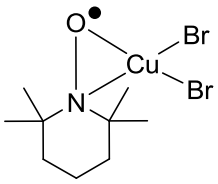

1.19

Due to the poor predictability of the geometries of metal-nitroxide complexes, introduction of substituents that can help control the shape of metal-nitroxide complexes have been developed. By taking advantage of the chelate effect, stronger binding and defined geometries are obtained. Introduction of a 2-pyridyl group into the nitronyl nitroxides and imino nitroxides has allowed for the formation of metal complexes that incorporated **1.20**[68] and **1.21**[69-71], respectively. A one-dimensional manganese coordination polymer using the bis(bidentate) ligand **1.22** has been synthesized[72] and it has also been used in the preparation of two-dimensional manganese structures[73].

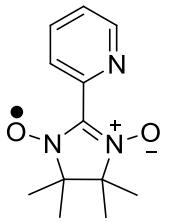

1.20

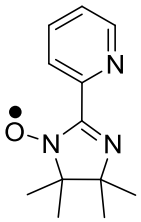

1.21

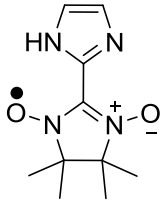

1.22

Metal-nitroxide complexes have been explored primarily for their magnetic properties, but this does not mean that they have not been used for chemical reactions. The oxidation of alcohols that is performed by TEMPO can also be done with transition metals involving TEMPO while using O_2 as the co-oxidant[74,75]. The exact structure of the active species involved is not known, but it has been determined to be a metal-TEMPO adduct[76].

1.4.3 Metal-Phenoxyl Complexes

Systems that require the use of metal-radical combinations to perform useful chemistry are quite common and even necessary to human life (e.g. Vitamin B_{12}). One of the best-known metallo-radical-based metalloenzymes is the copper-phenoxyl enzyme, galactose oxidase (GAO)[77]. This system catalyzes the two-electron oxidation of D-galactose to D-galactohexodialdose in tandem with the reduction of O_2 to H_2O_2[78-81] (**Figure 1.9**).

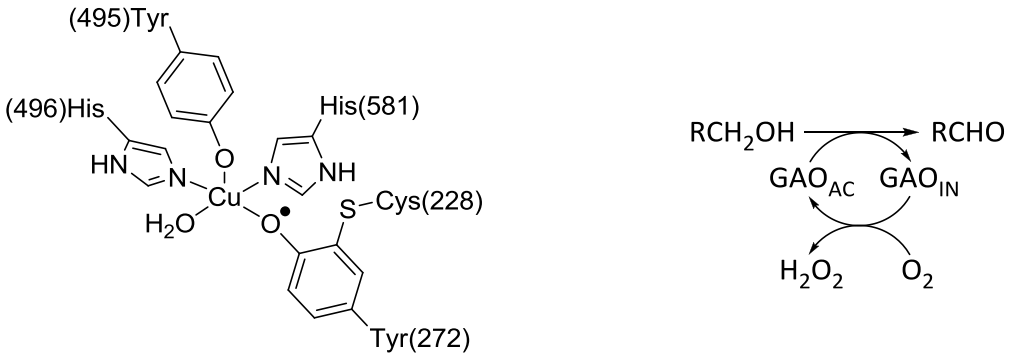

Figure 1.9: Structure of GAO and generalized reaction of GAO. GAO_{AC} and GAO_{IN} represent the active and inactive forms of the enzyme, respectively.

Much research has focused on biomimetic systems in which metal-phenoxyl complexes that are made under controlled conditions are able to perform similar reactions to GAO. In 1996, Tolman *et al*.[82] presented a model compound for the active site of GAO based on the 1,4,7-triazacyclononane ligand. This work was advanced by making complexes using copper(II) and zinc(II) while experimenting with either one or two coordinated phenolates[83]. A one electron oxidation of the neutral bis(phenolate) metal complex gave the corresponding metal-phenoxyl complex (**1.23**).

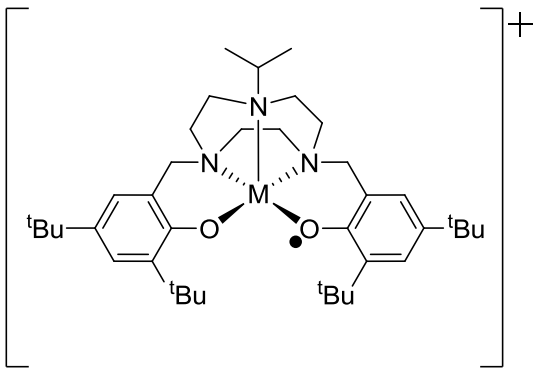

M = Cu, Zn, **1.23**

A number of research groups attempted to make complexes to mimic the active site of GAO[84-86] and they explored the electrochemistry of these complexes. Wang and

Stack[87] reported the development of a copper-phenoxyl complex (**1.24**) that was capable of oxidizing primary alcohols to aldehydes under a nitrogen atmosphere, albeit with low turnover numbers. They further improved their system[88] by performing the reaction under an oxygen atmosphere and using neat substrate which allowed **1.24** to oxidize benzyl alcohol to benzaldehyde with much higher turnover numbers.

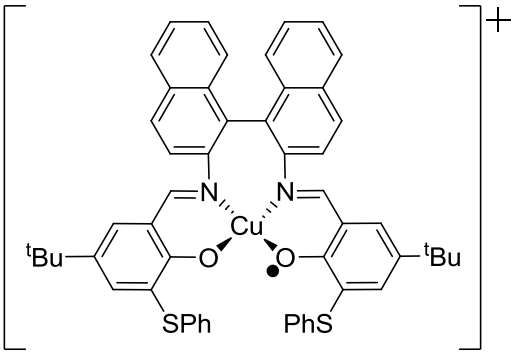

1.24

1.4.4 Metal-Verdazyl Complexes

Recently, work into the coordination chemistry of verdazyl radicals and the exploration of the properties that these materials possess has commenced[89]. Most of this work has been using the 6-oxoverdazyls where the radical can be directly coordinated to the metal center[90]. Kuhn verdazyls bearing 4-pyridyl groups that can be bound to copper[91] have been synthesized and some of these verdazyls have been coordinated to palladium to make spin cage materials[92,93], but no examples of the Kuhn verdazyls where the radical is directly bound to metal centre exist. Below are a few of the examples of 6-oxoverdazyl radicals that have been used as bidentate ligands (**1.25**-**1.29**[94,95], **1.30**-**1.33**[96,97]); 6-oxoverdazyls radicals have even been incorporated into metal complexes as tridentate ligands involving zinc chloride[98] (**1.34**-**1.35**).

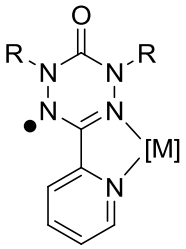

R = Me, [M] = $PdCl_2$ **1.25**
R = ^{i}Pr, [M] = $PdCl_2$ **1.26**
$PtCl_2$ **1.27**
$Ru(acac)_2$ **1.28**
$Ru(hfac)_2$ **1.29**

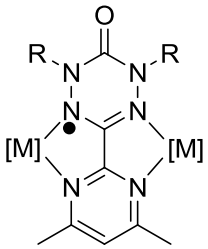

R = Me; [M] = $Ni(hfac)_2$ **1.30**
$Mn(hfac)_2$ **1.31**
R = ^{i}Pr; [M] = $Ru(acac)_2$ **1.32**
$Ru(hfac)_2$ **1.33**

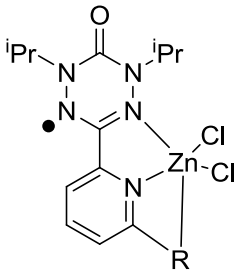

R = 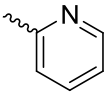 **1.34**

R = 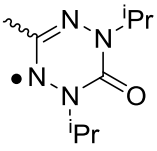 **1.35**

Most of the work involving coordination compounds of verdazyl radicals has largely focused on the magnetic properties of these compounds[94,96,99-104]. It is only within the last few years that the electrochemistry of the coordinated verdazyl compounds have been investigated[94,98].

Compounds **1.28** and **1.29** have been examined because these molecules contain a redox active ruthenium(II) metal centre. The frontier orbitals between the verdazyl radical and the metal centre in **1.28** and **1.29** do interact with each other resulting in non-innocent ligand behavior (**Table 1.2**). The net result is that the reduction of the complex can be assigned to the verdazyl ligand, but the oxidation processes cannot accurately be assigned to one part of the molecule or the other. The extent of this effect is dependent upon the nature of the ancillary ligands attached to the metal resulting in a change to the redox potentials.

Table 1.2: Electrochemical properties of a selection of metal-verdazyl complexes (V vs. Fc/Fc^{+}). Conditions: MeCN solution, 1 mM analyte, 0.1 M $n Bu_4NBF_4$, scan rate 100 mVs^{-1}, and temperature 295 K. Redox ($E_{1/2}$) half potentials are averages of anodic and cathodic peaks for a given redox process[94,98].

Metal-Verdazyl Complex	$E_{1/2}$ (V)
1.28	-1.35, -0.42, +0.88
1.29	-0.84, +0.13
1.34	-0.87, +0.43
1.35	-0.75, +0.35

Compounds **1.34** and **1.35** bearing one and two verdazyl radical units, respectively, do not demonstrate non-innocent ligand behavior because they are coordinated to a redox inert metal. The coordination of the zinc metal causes the reduction potentials of these compounds to be shifted ~0.5 V more positive relative to the free ligand[98] and a smaller, but noticeable positive shift in the oxidation potential does occur. These effects are rationalized qualitatively by the presence of the electropositive zinc ion which is argued to make reduction easier, but oxidation tougher. While this view may be a simplification, it does account for the contrasting electrochemical effects that have been explored with other verdazyl radicals[59].

1.5 Thesis Objectives

Previous work in the Hicks group has largely focused on the synthesis, design, and characterization of verdazyl radicals and their metal-verdazyl complexes (section 1.4.4). While much work has been done on the magnetism of these compounds, the current focus of research in our group has shifted towards the electrochemistry of verdazyls radicals and their metal complexes[94,98]. The main thrusts of this thesis focus on metal complexes of (i) new types of verdazyl radical ligands and (ii) N-alkylated tetrazines, i.e. benzyl radical adducts of verdazyl radicals. Chapter 2 focuses on the synthesis and characterization of the first metal complexes of *N,N'*-diaryl verdazyl radicals ligands based both on the Kuhn verdazyl and 6-oxoverdazyl skeleton. The impact of the bridge position of the verdazyl radical on the physiochemical (spectroscopic, redox) properties of these compounds is examined. Chapter 3 explores the synthesis of closed shell *N*-benzyl tetrazine ligands derived from verdazyls and their metal complexes, with a view to studying the homolytic cleavage of the N-alkyl group and to what degree it is affected by metal coordination.

CHAPTER 2

SYNTHESIS AND COORDINATION COMPLEXES OF *N,N'*-DIARYL VERDAZYL RADICALS

2.1 Introduction

The design of verdazyl radicals that are suitable to form coordination compounds with transition metals has relied heavily on the introduction of groups at the C3 position that can assist in metal binding through chelation; this is chiefly due to the fact that the verdazyl radical core is a poor ligand[104] necessitating the assistance from other moieties in the molecule for coordination. Incorporation of a bipy-like core (**Figure 2.1**) has been utilized to enhance the coordination ability of the verdazyl through exploitation of the chelate effect and has been utilized in the synthesis of various metal-verdazyl complexes including copper[89,101,105,106], manganese and nickel[96,100,107], ruthenium[94], and palladium and platinum complexes[95].

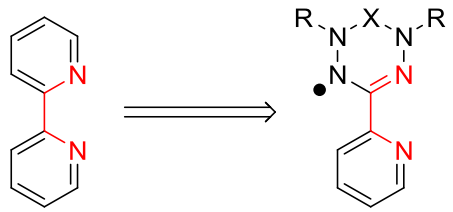

Figure 2.1: Bipy-like core incorporated in a verdazyl radical.

Our group and many others have primarily used the 6-oxoverdazyl with alkyl groups at the N1 and N5 positions in their quest to make various coordination compounds. While this has proven fruitful, there were no examples of verdazyl radicals suitable for coordination that possessed aryl groups at either the N1 or N5 positions until Brook *et*

al.[104] published an example of an asymmetric 6-oxoverdazyl (**2.1**) bearing an alkyl and aryl group on N1 and N5, respectively, that was capable of coordination to nickel(II). *N*, *N'*-diaryl verdazyl radicals that are suitable for coordination are still non-existent and no examples of Kuhn verdazyls that can coordinate to a metal centre exist despite the 50 years since the first report of a Kuhn verdazyl radical.

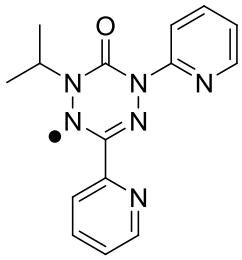

2.1

There are a number of differences between the Kuhn (**1.14**) and 6-oxo (**1.15**) verdazyls. While both have a similar central 6-membered ring core with the electron delocalized over the four nitrogens atoms (albeit different distributions), they differ with respect to their structures, spectroscopic and redox properties. The focus of this chapter is on the synthesis and electrochemical properties of the palladium(II) complexes of *N*,*N'*-diaryl Kuhn and 6-oxo verdazyls.

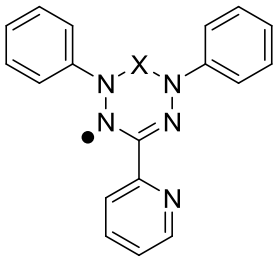

X = CH_2 **2.2**
CO **2.3**

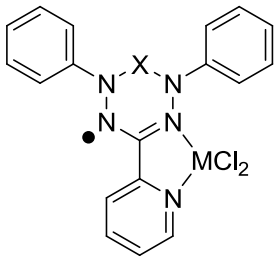

X = CH_2, M = Pd **2.2.$PdCl_2$**
M = Pt **2.2.$PtCl_2$**
X = CO, M = Pd **2.3.$PdCl_2$**
M = Pt **2.3.$PtCl_2$**

2.2 Synthesis of a Kuhn Verdazyl Ligand and its $PdCl_2$ Complex

Kuhn verdazyls are the oldest class of verdazyl radicals. Originally wanting to make alkylated formazans, Kuhn found that reacting formazans with methyl iodide in the presence of base in air gave a green solid[35]; this solid was found to be both stable and a radical. Since this time, a number of new Kuhn verdazyls have been synthesized[59] and even polymers containing this type of verdazyl have been made[108-114]. In 2004, Awadallah *et al.*[115] published the synthesis of a tetrazine (**2.4**) and a palladium complex (**2.5**) thereof; while neither compound is paramagnetic, **2.5** is the first compound bearing a structural resemblance to the Kuhn verdazyl radical bound to a metal.

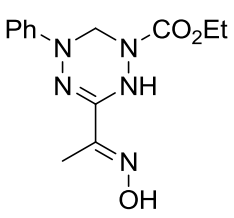

2.4

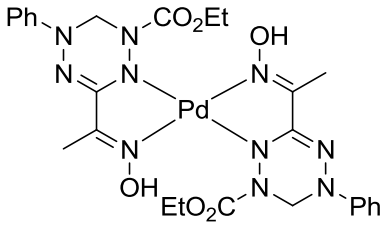

2.5

*2.2.1 Synthesis of the Kuhn Verdazyl (**2.2**)*

The synthesis of **2.2** utilizes the methodology established by our group[59,116], but had to be slightly modified. The first step of the synthesis involves the formation of the dark red formazan (**2.7**) by reacting 2-pyridine phenylhydrazone (**2.6**) with the appropriate diazonium salt in basic solution (**Scheme 2.1**); this compound has a tendency to remain a viscous oil, but can be coaxed into a solid by dissolving in EtOAc, removing the solvent *in vacuo*, and repeating these steps until a solid is obtained. The Kuhn verdazyl (**2.2**) is obtained by reacting **2.7** with formaldehyde and base while being exposed to air (**Scheme 2.1**); like **2.7**, the radical has a propensity to "oil out", but it was obtained as a solid by performing column chromatography using neutral alumina and adding TEA to the eluent. Despite numerous attempts, elemental analysis of **2.2** was consistently low for nitrogen. Other data used in the characterization of **2.2** is consistent with the proposed structure including CV, EPR, and UV-Vis.

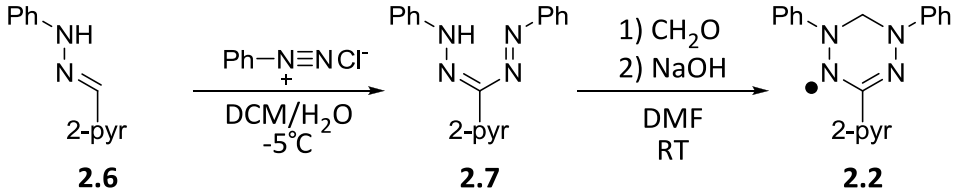

2.6 **2.7** **2.2**

Scheme 2.1: Synthesis of **2.2** from 2-pyridine phenylhydrazone (**2.6**).

Like other Kuhn verdazyls, **2.2** undergoes a disproportionation reaction in the presence of acid[35,117], but also shows signs of decomposition in neutral and basic aqueous solutions. This is thought to be a result of the proximity of the nitrogen atom

of the pyridyl group to the nitrogen atoms of the verdazyl core that had not been introduced into other Kuhn verdazyls.

Having introduced the bipy-like core into the Kuhn verdazyl, the coordination chemistry was then explored (**Scheme 2.2**). The reaction of **2.2** with palladium dichloride in refluxing MeCN followed by cooling and slow evaporation allowed for the collection of pure **2.2.PdCl$_2$**. Numerous attempts to prepare **2.2.PtCl$_2$** were unsuccessful in obtaining a pure product. Several sources of "$PtCl_2$" were explored, such as $(DMSO)_2PtCl_2$, $(PhCN)_2PtCl_2$, and [1,5-COD]$PtCl_2$, and other reaction conditions such as solvent, temperature, and reaction time were varied without success.

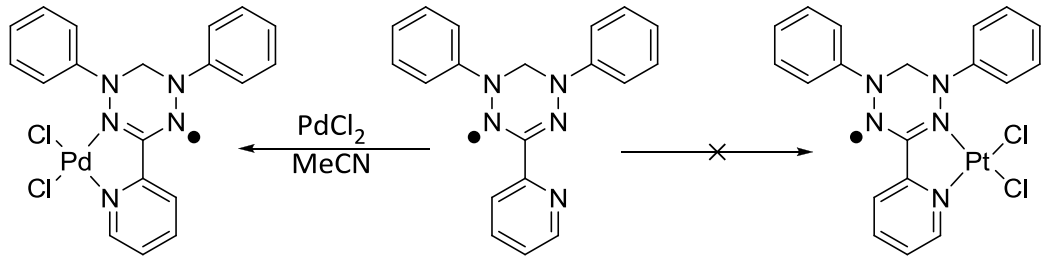

2.2.PdCl$_2$ **2.2** **2.2.PtCl$_2$**

Scheme 2.2: Synthesis of **2.2.PdCl$_2$**.

2.3 Synthesis of *N*,*N*'-diphenyl-6-oxoverdazyl Ligand and its PdCl$_2$ Complex

In the 1990s, Milcent *et al.* established a methodology for the synthesis of 1,3,5-triaryl-6-oxoverdazyls by a stepwise manner[39] (**Scheme 2.3**). The diaryl hydrazone (**2.8**) is first reacted with phosgene in the presence of pyridine to generate the 2-chloroformylhydrazone (**2.9**) which is then reacted with the two equivalents of an arylhydrazine to form the corresponding tetrazane (**2.10**). The tetrazane can then be

reacted with an oxidizing agent such as Ag_2O or DDQ to convert it to the 6-oxoverdazyl radical (**2.11**). In principle, the Milcent procedure allows for the synthesis of tetrazanes and radicals with a variety of substituents at the C3, N1, and N5 positions.

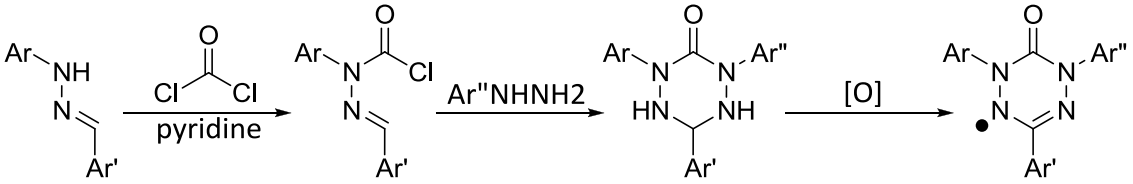

2.8 **2.9** **2.10** **2.11**

Scheme 2.3: Milcent procedure for aryl verdazyls.

*2.3.1 Synthesis of the 6-oxoverdazyl (**2.3**)*

In the generation of a 6-oxoverdazyl, the corresponding tetrazane is a requirement of its synthesis. This is true also for **2.3** and a summary of the various methods explored in the generation of **2.3** will be presented.

In 2010, Brook *et al.*[104] published a paper outlining the synthesis of **2.1** which followed a modified Milcent procedure in its synthesis. Our attempts to employ the Milcent procedure using **2.6** and phosgene (**Scheme 2.4**) failed to yield the corresponding chloroformylhydrazone (**2.12**). During the course of the reaction, the colour and goo-like consistency were uncharacteristic of a reaction between phosgene and a hydrazone and the ^{1}H NMR spectrum was extremely complex and provided no evidence for the formation of **2.12**.

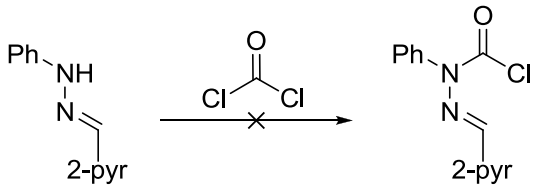

2.6 **2.12**

Scheme 2.4: Unsuccessful Milcent procedure using **2.6**.

Due to the failure of the Milcent procedure, it was thought that reaction of *N*-BOC-*N*'-isopropyl hydrazine (**2.13**) which is used in the synthesis of **2.14**[118] (**Scheme 2.5(a)**) would be a suitable reaction to mimic. An *N*-BOC-*N*'-phenyl hydrazine (**2.15**) was synthesized[119] and subsequently reacted with phosgene in the attempt to synthesize **2.16**, but was found to yield **2.17** (**Scheme 2.5(b)**) which cannot be used to make a verdazyl radical because both terminal nitrogen atoms must be unsubstituted to proceed.

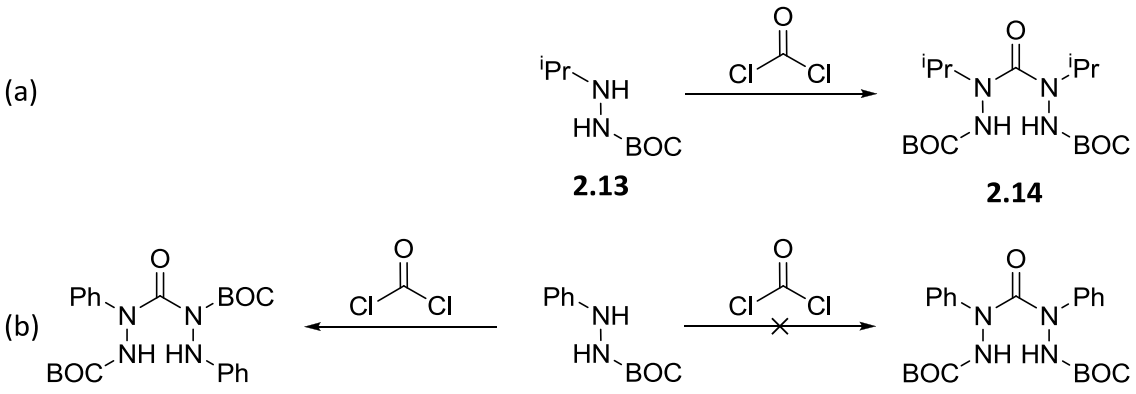

2.13 **2.14**

2.17 **2.15** **2.16**

Scheme 2.5: Reaction of phosgene with (a) **2.13** in the synthesis of **2.14** and (b) **2.15** showing the desired reaction (right) and actual reaction (left).

A summary of the chemical shifts of various BOC protected hydrazines and the product from the reaction of **2.15** with phosgene is shown below (**Table 2.1**). Had **2.16** been formed, it would show only one NH signal due to symmetry while **2.17** would show two NH signals. The observation of two NH signals by NMR leads to the conclusion that **2.17** was the obtained product.

Table 2.1: Summary of chemical shifts of various BOC protected hydrazines and the condensed products.

Compound	^{1}H NMR (NH δ, ppm)	Solvent	Reference
2.13	6.03, 3.92	$CDCl_3$	[120]
2.14	6.48	$CDCl_3$	[118]
2.15	6.53, 5.92	$CDCl_3$	[119]
Phosgene Condensed Product (**2.17**)	6.53, 5.84	CD_2Cl_2	

Another synthetic approach was explored based on an N-arylation of carbonohydrazide by Masuda *et al.*[121]. Masuda *et al.* were able to prepare a verdazyl radical using 2,4-diphenylcarbonohydrazide (**2.18**) from the coupling of iodobenzene and carbonohydrazide (**Scheme 2.6**). While they were able to obtain **2.18** in ~21% yield, all of our attempts to reproduce their procedure failed to yield the desired product.

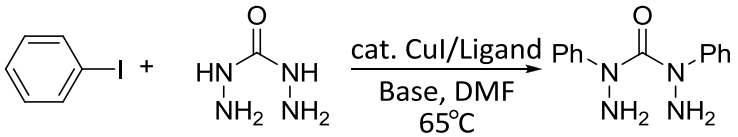

2.18

Scheme 2.6: N-arylation of carbonohydrazide to form **2.18**.

Molecule **2.18** seems to be a reasonable target for synthesis, so it was hypothesized that it would be ideal for synthetic planning. Since the condensation reaction of **2.18** and an aldehyde yields a tetrazane, is it reasonable to think of a tetrazane as a cyclic aminal which can be converted into a bishydrazide and aldehyde similar to the cleavage of an acetal?

The successful synthesis of **2.18** required the initial synthesis of **1.15** which was made based on the Milcent procedure[39]. **1.15** was cleaved at the N1-C6 and N5-C6 bonds using concentrated HCl yielding benzaldehyde (discarded) and **2.18** in 76% yield. **2.18** was then condensed with 2-pyridine carboxaldehyde using pyridinium tosylate (pyrHOTs) as a catalyst to yield the tetrazane (**2.19**). This molecule was then oxidized using Ag_2O on celite to generate the verdazyl radical (**2.3**) (**Scheme 2.7**).

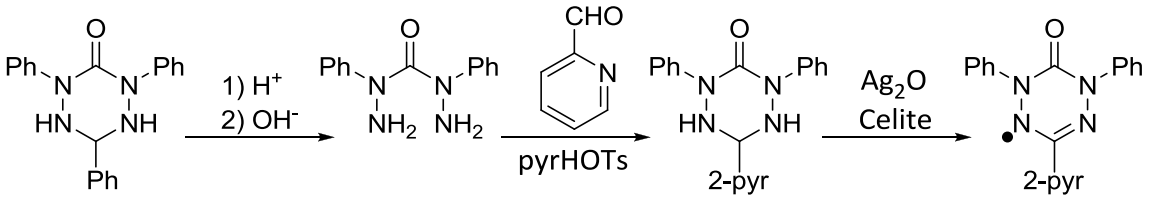

1.15 **2.18** **2.19** **2.3**

Scheme 2.7: Synthesis of **2.3** using acidic cleavage of **1.15**.

Having now introduced the bipy-like core into the 6-oxoverdazyl, a coordination complex with palladium could be made (**Scheme 2.8**). The reaction of **2.3** with palladium chloride in refluxing MeCN followed by cooling and sitting undisturbed allowed for the collection of pure **2.3.PdCl$_2$**. **2.3.PtCl$_2$** could not be synthesized successfully as a pure product using a variety of reaction conditions as was the case for the attempted synthesis of a Pt complex of a Kuhn verdazyl, **2.2**.

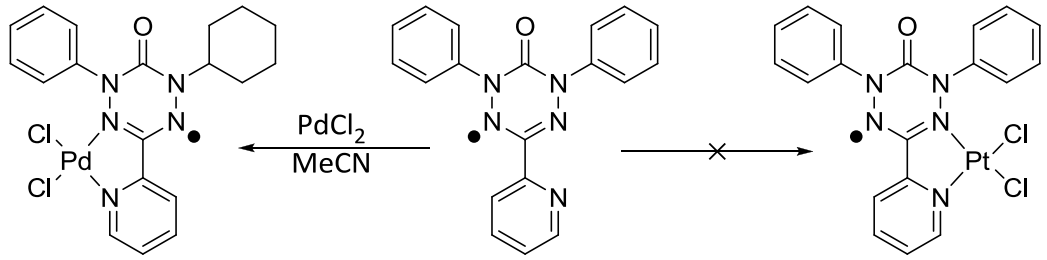

2.3.PdCl$_2$ **2.3** **2.3.PtCl$_2$**

Scheme 2.8: Synthesis of **2.3.PdCl$_2$**.

2.4 Results and Discussion

This section will compare and contrast the Kuhn and 6-oxo verdazyls by examining the properties that both sets of metal-verdazyl complexes possess. This analysis will focus on the structural (X-ray crystallography), spectroscopic (UV-Vis, EPR), and electrochemical (CV) properties that the two palladium-verdazyl complexes exhibit.

2.4.1 Structural Properties

The molecular structures of **2.2.PdCl$_2$** and **2.3.PdCl$_2$** are shown in **Figure 2.2** with selected bond lengths in **Table 2.2**. In **2.3.PdCl$_2$**, there is a difference in the C-N bond lengths within the verdazyl core, specifically the values for the C-N bonds in the lower portion of the verdazyl ring (C(2)-N(1), 1.322(13) Å; C(2)-N(4), 1.371(12) Å) compared to the values for the same C-N bonds in **2.3** [~1.34 Å]. The bond lengths of the N-N bond in **2.3.PdCl$_2$** are within experimental error of each other (N(1)-N(2), 1.358(11) Å; N(3)-N(4), 1.348(10) Å).

In **2.2.PdCl$_2$**, there is a slight difference of the C-N bond lengths of the verdazyl core, but they are not as pronounced as in **2.3.PdCl$_2$**. **2.2.PdCl$_2$** does have a difference in the N-N bond lengths with N(1)-N(2) [1.335(2) Å] being shorter than N(3)-N(4) [1.381(2) Å].

The metal-verdazyl and metal-pyridine bond lengths are approximately the same within each complex with **2.2.PdCl$_2$** [N(4)-Pd(1), 2.025(1) Å; N(5)-Pd(1), 2.031(1) Å] exhibiting shorter N-Pd bond lengths than **2.3.PdCl$_2$** [N(4)-Pd(1), 2.064(7) Å; N(5)-Pd(1), 2.076(7) Å].

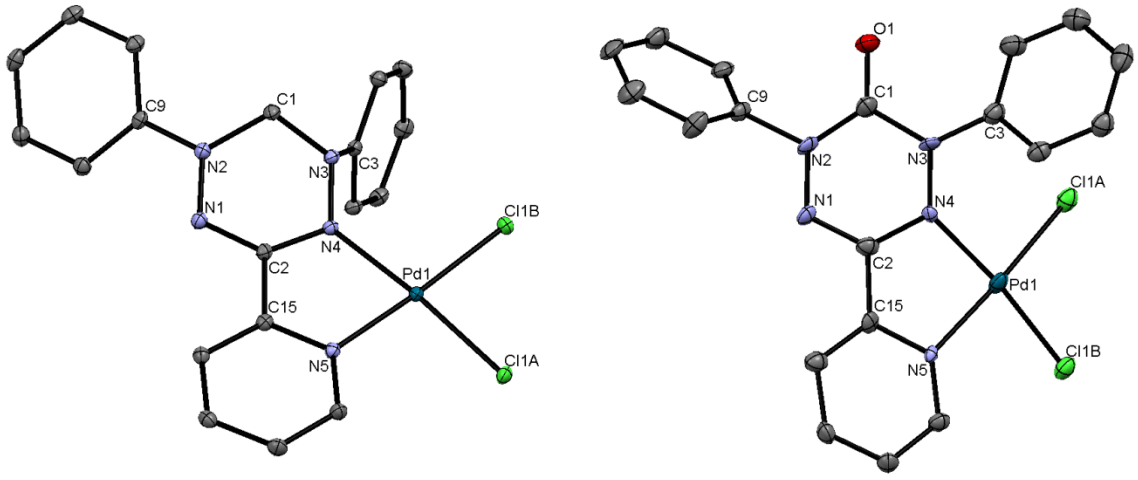

Figure 2.2: Solid state structure of **2.2.PdCl$_2$** (left) and **2.3.PdCl$_2$** (right). Hydrogen atoms have been omitted for clarity. Thermal ellipsoids are shown at the 30% probability level.

Table 2.2: Selected bond lengths and interatomic distances for structures **2.2.PdCl$_2$** and **2.3.PdCl$_2$** (estimated standard deviations are in parentheses).

Bond	2.2.PdCl$_2$	2.3.PdCl$_2$
C(1)-N(2)	1.470(2)	1.359(13)
C(1)-N(3)	1.453(2)	1.417(13)
C(1)-O(1)	—	1.220(12)
C(2)-N(1)	1.336(2)	1.322(13)
C(2)-N(4)	1.341(2)	1.371(12)
N(1)-N(2)	1.335(2)	1.358(11)
N(3)-N(4)	1.381(2)	1.348(10)
N(4)-N(5)	2.610(2)	2.692(9)
N(4)-Pd(1)	2.025(1)	2.064(7)
N(5)-Pd(1)	2.031(1)	2.076(7)
Pd(1)-Cl(1A)	2.2945(4)	2.281(3)
Pd(1)-Cl(1B)	2.2870(4)	2.282(3)

The selected bond angles are shown in **Table 2.3**. Variations between the two compounds arise at the nitrogen atoms at the N1 and N5 positions. In **2.2.PdCl$_2$**, the sum of the angles vary around N1 and N5 (N(2), Σ° = 359.9; N(3), Σ° = 349.1) indicating that N(3) is being distorted upon coordination due to the close proximity of the phenyl group to the palladium atom evidenced by the difference in torsion angles (C(2)-N(1)-N(2)-C(9), 164.9°; C(3)-N(3)-N(4)-C(2), -119.2°). In **2.3.PdCl$_2$**, the sum of the angles around N1 and N5 are comparable to each other (N(2), Σ° = 359.8; N(3), Σ° = 359.3) with a much smaller difference in torsion angles. Unlike **2.2.PdCl$_2$**, **2.3.PdCl$_2$** is unable to undergo distortion at these nitrogen atoms due to the carbonyl group which creates a carbamide-like bridge. The distortions around the nitrogen atoms are shown in **Figure 2.3**.

Table 2.3: Selected bond angles for structures **2.2.PdCl$_2$** and **2.3.PdCl$_2$** (estimated standard deviations are in parentheses).

Atom	2.2.PdCl$_2$	2.3.PdCl$_2$
C(1)-N(2)-C(9)	125.7(1)	119.7(8)
C(1)-N(2)-N(1)	115.8(1)	125.0(8)
C(9)-N(2)-N(1)	118.4(1)	115.1(8)
C(1)-N(3)-C(3)	119.8(1)	123.7(9)
C(1)-N(3)-N(4)	112.4(1)	119.7(8)
C(3)-N(3)-N(4)	116.9(1)	115.9(8)
Cl(1A)-Pd(1)-Cl(1B)	89.61(1)	90.04(10)
Cl(1A)-Pd(1)-N(5)	93.68(4)	92.9(2)
Cl(1B)-Pd(1)-N(4)	96.64(4)	95.9(2)
N(4)-Pd(1)-N(5)	80.08(5)	81.1(3)

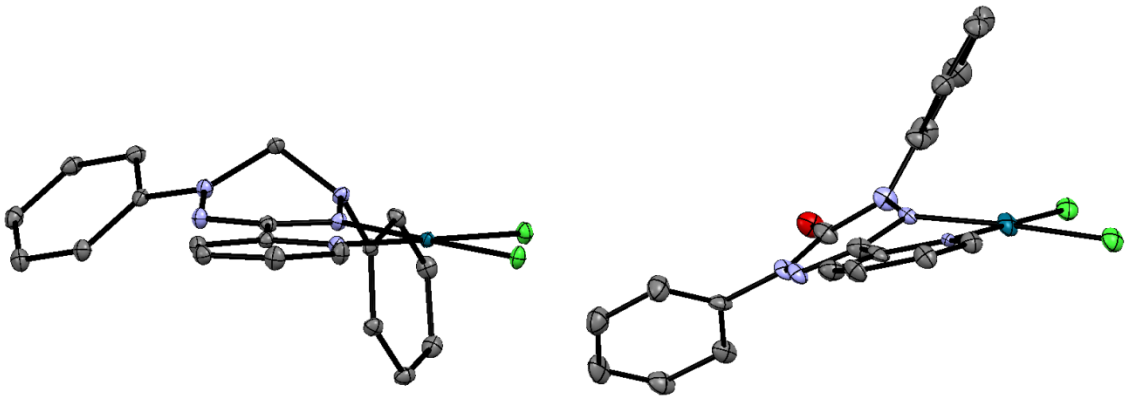

Figure 2.3: Alternative view of the solid state structures of **2.2.PdCl$_2$** (left) and **2.3.PdCl$_2$** (right). Hydrogen atoms have been omitted for clarity. Thermal ellipsoids are at the 30% probability level.

Examining the structures of the palladium-verdazyl complexes showed that the pyridyl group and the lower portion of the verdazyl ring core of the ligand in **2.2.PdCl$_2$** is nearly planar while the ligand in **2.3.PdCl$_2$** is twisted, demonstrated by the torsion angle in **2.3.PdCl$_2$** (N(1)-C(2)-C(15)-N(5), 167.1°). Overall, there is a large degree of twisting in **2.3.PdCl$_2$** compared to **2.2.PdCl$_2$** as demonstrated by the differences in torsion angles (**Table 2.4**) leading to poor interaction between the verdazyl core and the palladium centre (torsion angle defined by (C(15)-C(2)-N(4)-Pd(1), 25°)).

Table 2.4: Selected torsion angles for structures **2.2.PdCl$_2$** and **2.3.PdCl$_2$** (estimated standard deviations are in parentheses).

Atom	2.2.PdCl$_2$	2.3.PdCl$_2$
C(15)-C(2)-N(4)-Pd(1)	0.1(2)	25(1)
N(1)-C(2)-C(15)-N(5)	-179.6(1)	167.1(9)
C(2)-C(15)-N(5)-Pd(1)	-5.5(2)	-6(1)
C(2)-N(1)-N(2)-C(9)	164.9(1)	175.0(9)
C(2)-N(4)-N(3)-C(3)	-119.2(1)	150.4(9)
C(2)-N(4)-Pd(1)-N(5)	-2.3(1)	-21.2(6)
C(15)-N(5)-Pd(1)-N(4)	4.4(1)	14.5(6)

2.4.2 UV-Vis Spectroscopy

The electronic absorption spectrum of **2.2** was recorded in MeCN and **2.2.PdCl$_2$** was recorded in two different solvents, MeCN and DCM (**Figure 2.4**). The spectra of **2.2.PdCl$_2$** in both solvents is red-shifted from the free ligand, **2.2** (**Table 2.5**) and the spectrum in DCM is slighty red-shifted from the one in MeCN. In addition to this red shift, there is an increase in ε by a factor of ~2.5 in DCM compared to MeCN.

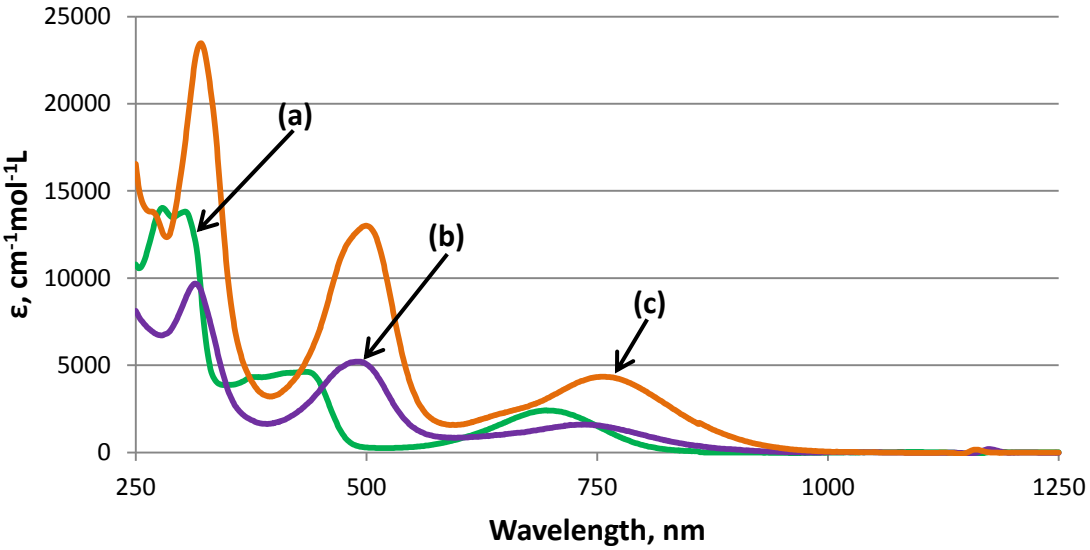

Figure 2.4: Room temperature UV-Vis of (a, green) **2.2** in MeCN, (b, purple) **2.2.PdCl$_2$** in MeCN, and (c, orange) **2.2.PdCl$_2$** in DCM.

Table 2.5: Absorption maxima for **2.2** in MeCN and **2.2.PdCl$_2$** in MeCN and DCM (wavelength is listed with ε in parentheses).

Complex	λ_{max}/nm (ε/cm^{-1}mol^{-1}L)
2.2 (MeCN)	279 (14000), 304 (14000), 435 (4600), 693 (2400)
2.2.PdCl$_2$ (MeCN)	314 (9700), 489 (5200), 733 (2000)
2.2.PdCl$_2$ (DCM)	321 (23000), 499 (13000), 756 (4300)

The spectra of **2.3** and **2.3.PdCl$_2$** are shown in **Figure 2.5**. Compared to **2.3**, the main visible absorptions in **2.3.PdCl$_2$** are red-shifted (**Table 2.6**). In DCM, the complex exhibits four peaks at 299 nm, 486 nm, 597 nm, and 647 nm. In MeCN, the first peak separates into two peaks at 283 nm and 307 nm, the peak at 486 nm in DCM appears at 478 nm in MeCN, but the last two peaks that are observed in DCM coalesce together into a broad band 550-700 nm (ε = 2000 $cm^{-1}mol^{-1}L$) in MeCN.

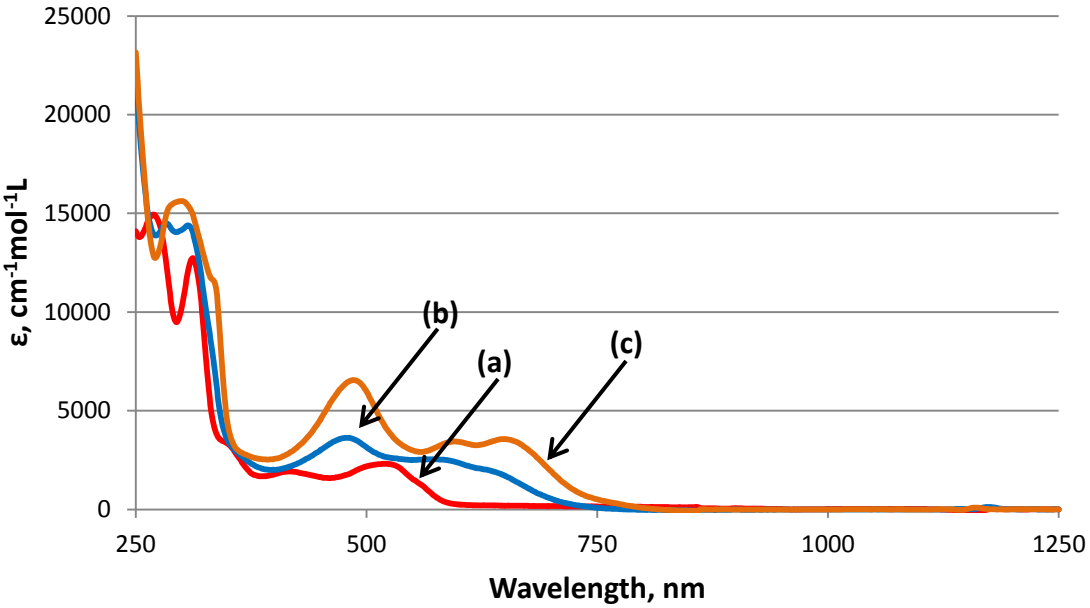

Figure 2.5: Room temperature UV-Vis of (a, red) **2.3** in MeCN, (b, blue) **2.3.PdCl$_2$** in MeCN, and (c, orange) **2.3.PdCl$_2$** in DCM.

Table 2.6: Absorption maxima for **2.3** in MeCN and **2.3.PdCl$_2$** in MeCN and DCM (wavelength is listed with ε in parentheses).

Complex	λ_{max}/nm (ε/$cm^{-1}mol^{-1}L$)
2.3 (MeCN)	269 (15000), 312 (13000), 418 (1900), 520 (2300)
2.3.PdCl$_2$ (MeCN)	283 (14000), 307 (14000), 478 (3600), 550-700 (2000)
2.3.PdCl$_2$ (DCM)	299 (16000), 486 (6600), 597 (3400), 647 (3600)

2.4.3 EPR Spectroscopy

The room temperature EPR spectra of **2.2** and **2.3** demonstrate a 9-line pattern that is expected for the type of verdazyl radical each compound represents. Their spectra are comparable in hyperfine structure and g-values to other Kuhn and 6-oxo verdazyls[40] (**Figure 2.6**). Simulations of the EPR spectra were obtained by modeling the experimental spectra using WinSim 2002; the parameters for **2.2** and **2.3** were constrained such that the molecules were treated as symmetric. A summary of the g-values, hyperfine coupling constants, and the goodness of fit (R^2) between experimental and simulated data for the free ligands and palladium complexes are given in **Table 2.7**.

Table 2.7: Summary of EPR data for **2.2**, **2.2.PdCl$_2$**, **2.3**, and **2.3.PdCl$_2$**. Hyperfine coupling constants are given in G.

Complex	g-value	*a*/N	*a*/N	*a*/N	*a*/N	R^2
2.2	2.0042	5.78	5.78	5.87	5.87	0.9905
2.2.PdCl$_2$	2.0120	—	—	—	—	—
2.3	2.0028	4.57	4.57	6.49	6.49	0.9954
2.3.PdCl$_2$	2.0087	4.74	4.79	5.76	8.04	0.9836

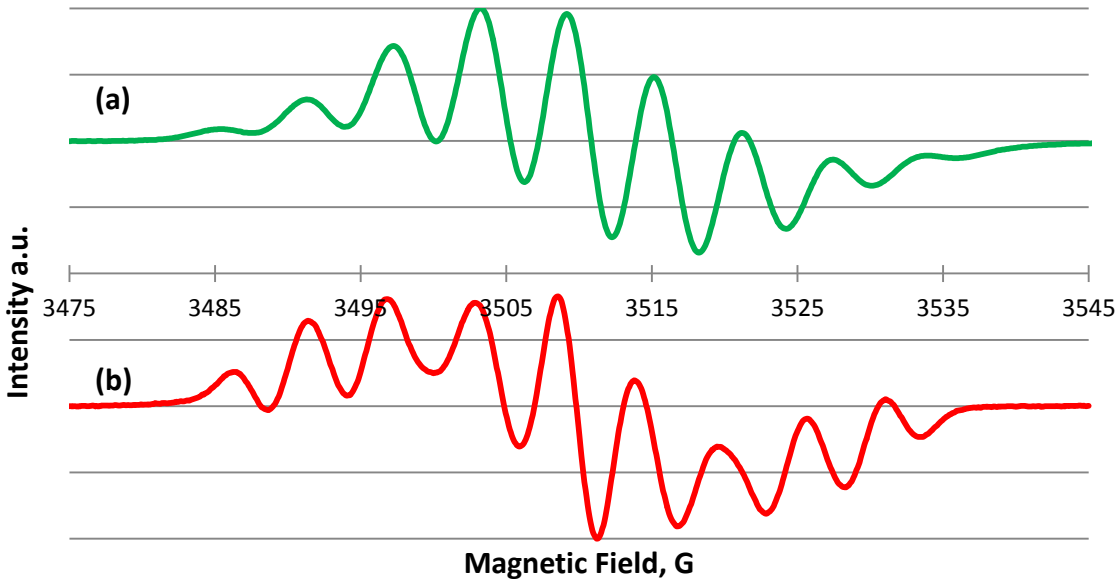

Figure 2.6: Room temperature EPR spectra of the verdazyl ligands in DCM (a) **2.2** and (b) **2.3**.

The spectrum of **2.2.PdCl$_2$** is shown in **Figure 2.7**. The spectrum is broad and lacks hyperfine structure. Because of the lack of fine structure, it was impossible to extract hyperfine coupling constants. The total spectral width is ~70 Gauss which is comparable in size to the free ligand, **2.2**. The g-value for **2.2.PdCl$_2$** was determined to be 2.0120 compared to 2.0042 for **2.2**. The higher g-value compared to the free ligand indicates that there is some spin density on palladium due to interaction between palladium and the nitrogen atom of the verdazyl core to which it is bonded.

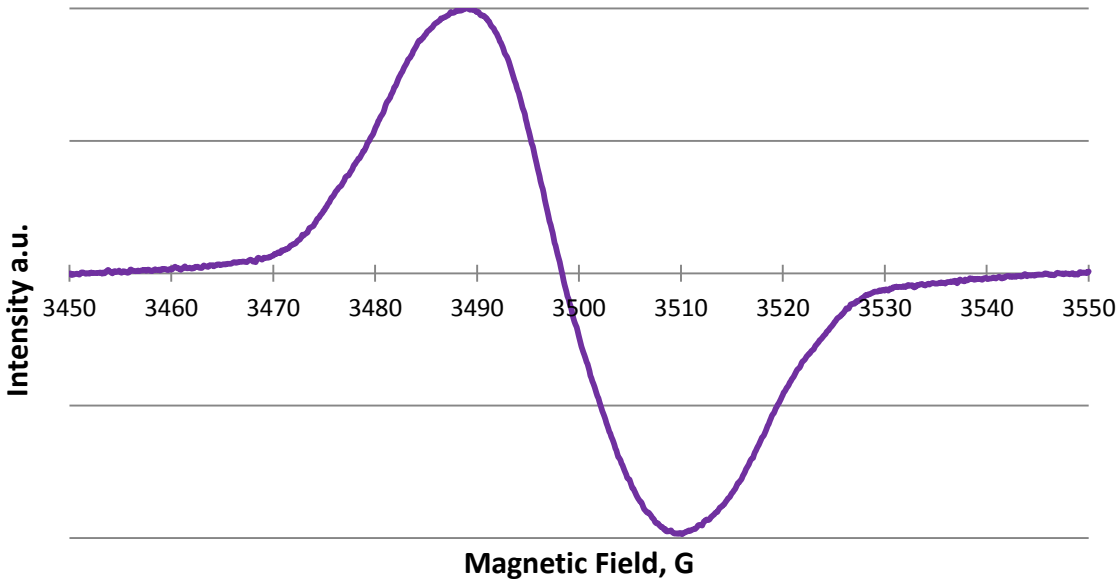

Figure 2.7: Room temperature EPR spectrum of **2.2.PdCl$_2$** in DCM.

The EPR spectrum of **2.3.PdCl$_2$** is shown in **Figure 2.8**. The spectrum demonstrates hyperfine structure. It was possible to extract hyperfine coupling constants from this spectrum (**Table 2.7**). The total spectral width is ~60 Gauss which is similar to that of the free ligand, **2.3**. The g-value for **2.3.PdCl$_2$** was determined to be 2.0087 compared to 2.0028 for **2.3**. The g-value is higher than **2.3**, but less than **2.2.PdCl$_2$**.

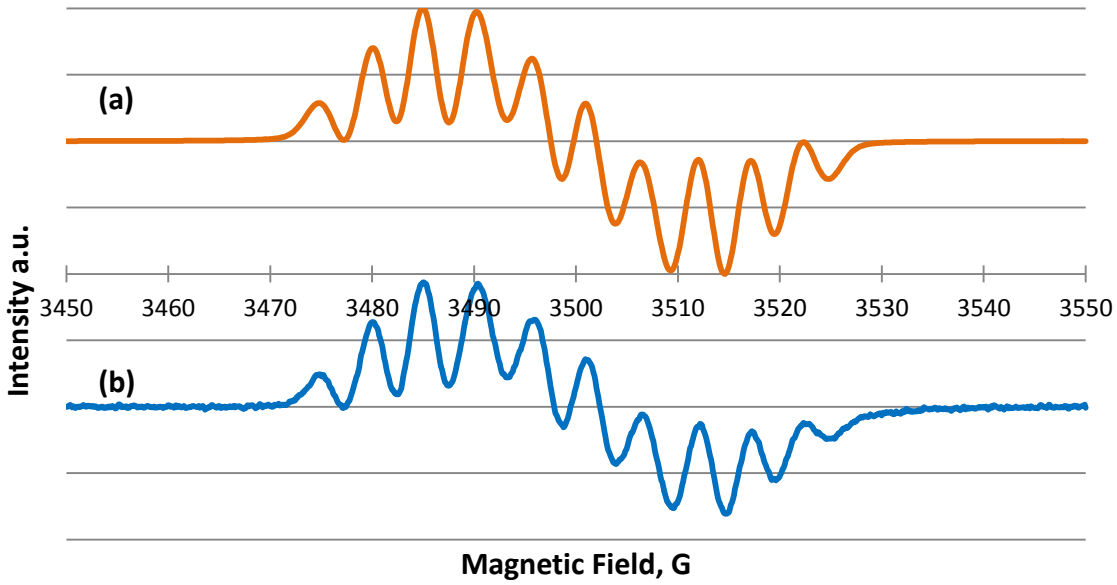

Figure 2.8: Room temperature EPR spectra of **2.3.PdCl$_2$** in DCM (a) simulation and (b) experimental.

2.4.4 Cyclic Voltammetry

The CVs of the verdazyl radicals and palladium-verdazyl complexes were run in DCM due to solubility issues in MeCN and are shown in **Figure 2.9**. Compounds **2.2** and **2.3** demonstrate characteristic reversible redox waves for verdazyl radicals and at nearly the same potentials as other verdazyl radicals of similar structure (**Table 2.8**).

The palladium-verdazyl complexes show two reversible redox processes. In both complexes there is an increase in the reduction potential by ~0.9 V compared to the values for the free ligands. The oxidation potential demonstrates an increase in both complexes, **2.2.PdCl$_2$** (~0.6 V) and to a lesser extent in **2.3.PdCl$_2$** (~0.3 V). While palladium is a redox active metal, it appears to not be involved with the redox processes in either metal-verdazyl complexes, but instead acts as an electropositive atom causing

the increase in both reduction and oxidation potentials. In both complexes the E_{cell} is smaller compared to the free ligand. The percent contraction of the E_{cell} (contraction = $(E_{cell(ligand)} - E_{cell(complex)})/E_{cell(ligand)}$) is larger in **2.3.PdCl$_2$** (34%) compared to **2.2.PdCl$_2$** (23%).

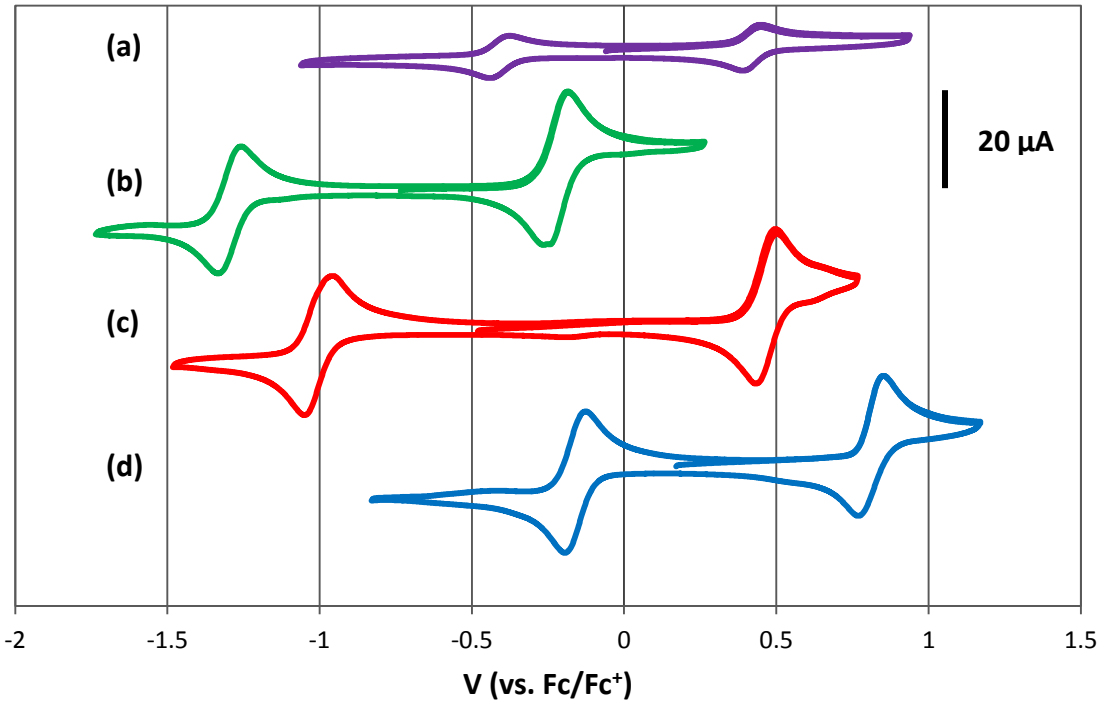

Figure 2.9: CVs of (a) **2.2.PdCl$_2$**, (b) **2.2**, (c) **2.3**, and (d) **2.3.PdCl$_2$**. Conditions: DCM solution, 1 mM analyte, 0.1 M *n*Bu$_4$NBF$_4$, scan rate 100 mVs^{-1}, and temperature 295 K. Scans shown were initiated in the positive direction.

Table 2.8: Electrochemical properties of **2.2.PdCl$_2$**, **2.2**, **2.3**, and **2.3.PdCl$_2$** (V vs. Fc/Fc$^+$). Conditions: DCM solution, 1 mM analyte, 0.1 M *n*Bu$_4$NBF$_4$, scan rate 100 mVs^{-1}, and temperature 295 K.

Complex	E_{red}° (V)	E_{ox}° (V)	E_{cell} (V)
2.2.PdCl$_2$	-0.41	+0.42	0.83
2.2	-1.30	-0.22	1.08
2.3	-1.00	+0.47	1.47
2.3.PdCl$_2$	-0.16	+0.81	0.97

2.5 Conclusions

This work expands on previous metal-verdazyl coordination chemistry and is the first study to investigate the *N*,*N'*-diaryl verdazyl radicals as ligands and the electrochemistry of palladium-verdazyl compounds. The challenges in the synthesis of **2.2** and **2.3** have been discussed and have been overcome to obtain the desired ligands. The palladium(II) dichloride complexes of **2.2** and **2.3** have been made and characterized.

Examination of the solid state structure reveals planarity around palladium and in the ligand in **2.2.PdCl$_2$**, but slight deviations are observed in **2.3.PdCl$_2$**. The UV-Vis spectra of the free ligands and the palladium-verdazyl complexes reveal a red-shift in the absorbance maximums of the metal complexes compared to the free ligand. EPR spectroscopy was helpful in observing spin distributions of the different complexes and indicated that a low amount of spin was being transferred onto palladium. The electrochemistry of the verdazyl radicals (**2.2** and **2.3**) have redox potentials near those of other verdazyl radicals of similar structures and the coordination complexes with palladium, **2.2.PdCl$_2$** and **2.3.PdCl$_2$**, demonstrate a positive increase to both the reduction and oxidation potentials while retaining reversible redox events.

2.6 Experimental

2.6.1 Materials and Methods

1,3,5-Triphenyl 6-oxotetrazane[39] and 2-pyridinecarboxaldehyde phenylhydrazone[122] were synthesized using literature methods. All solvents and reagents were purchased from Aldrich and used as received without further purification unless otherwise stated.

^{1}H and ^{13}C NMR spectra were recorded on a Bruker AC300 (300 MHz) instrument. FT-IR spectra were recorded on a Perkin-Elmer Spectrum One FT-IR spectrometer as pressed KBr discs. EPR spectra were recorded on a Bruker EMX instrument (9.51 GHz) with samples prepared as dilute (~10^{-4} M) and deoxygenated (sparging with Ar through the solution) solutions. A DPPH radical standard (g = 2.0036) was used as a field reference. The EPR spectra were simulated using the WinSim 2002 program. UV-Vis spectra were recorded on a Perkin-Elmer Lambda 1050 spectrometer. Melting points were determined using a Gallenkamp melting point apparatus and are uncorrected. Elemental analyses were performed by Canadian Microanalytical Services Ltd., Delta, British Columbia, Canada. CV experiments were performed using a Bioanalytical Systems E2 Epsilon Electrochemical Analyzer with a cell consisting of a glassy carbon working electrode, platinum wire counter electrode, and a silver wire reference electrode. Low-resolution mass spectrometry data was collected on an ESI-Ion Trap and high-resolution mass spectrometry data was collected on an ESI-Orbitrap by Ori Granot (University of Victoria).

1,5-Diphenyl-3-(pyridin-2-yl)formazan (2.7)

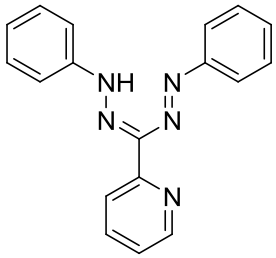

To a solution of EtOH (10 mL), H_2O (70 mL), and DCM (120 mL) at RT was added 2-pyridinecarboxaldehyde phenylhydrazone (2.19 g, 11.1 mmol). The solution was allowed to cool to -5°C using a brine/ice bath. $Na_2CO_3 \cdot H_2O$ (5.57 g, 44.9 mmol) and nBu$_4$NBr (0.44 g, 1.4 mmol) were added to the solution. A second solution containing the diazonium salt was made by mixing H_2O (10 mL), aniline (1.20 mL, 13.0 mmol), and 37% HCl (4 mL, 46.6 mmol) followed by cooling to -5°C; a solution of $NaNO_2$ (1.04 g, 15.1 mmol) at -5°C was added dropwise to it and the resulting solution was allowed to stir for 30 min.

The diazonium salt solution was added dropwise to the biphasic solution producing a gradual colour change (yellow to blood red). It was then stirred for 1 h at -5°C. The solution was added to a separatory funnel and DCM (100 mL) was added to the funnel. The organic layer was washed with H_2O (5X100 mL) and stored on $MgSO_4$.

The solvent was removed *in vacuo* until near dryness and column chromatography was performed (D. N. Al.; hexanes:DCM, 8:2) collecting the red portion followed by (SiO_2; hexanes:DCM:EtOAc, 7:2:1) collecting the red fraction. The collected product was taken up in EtOAc and the solvent was removed *in vacuo*, this was repeated until a dark red solid was obtained (1.30 g, 39.0%). ^{1}H NMR (300 MHz, DCM-d_2, 300 K): δ 15.61 (s, 1H, NH), 14.25 (s, 1H, NH), 8.76 (ddd, 1H, J = 5,2,1 Hz), 8.71 (ddd, 1H, J = 5,2,1 Hz), 8.27 (dt, 1H, J = 8,1 Hz), 8.14 (dt, 1H, J = 8,1 Hz), 7.95 (dd, 2H, J = 8,2 Hz), 7.91 (td, 1H, J = 8,2 Hz),

7.79 (td, 1H, J = 8,2 Hz), 7.74 (dd, 4H, J = 8,2 Hz), 7.35 (m, 15H), 7.04 (tt, 1H, J=7,2 Hz) ppm. ^{13}C NMR (300 MHz, DCM-d_2, 300 K): δ 155.5, 153.8, 153.0, 149.7, 148.1, 147.5, 144.0, 143.3, 141.9, 137.3, 136.7, 129.9, 129.8, 129.5, 128.2, 124.1, 123.3, 123.2, 122.9, 122.7, 121.7, 119.3, 115.3 ppm. FT-IR (KBr): 3369 (w), 3049 (m), 1599 (m), 1584 (s), 1565 (m), 1501 (s), 1470 (s), 1450 (s), 1430 (s), 1351 (s), 1240 (s), 1076 (s), 1058 (s), 1036 (s), 994 (m), 926 (w), 894 (w), 792 (m), 767 (m), 754 (s), 741 (s), 696 (m), 685 (s), 653 (m), 633 (m), 588 (m), 546 (w), 501 (w) cm^{-1}. UV-Vis (DCM): λ_{max} 262 nm (ε = $1.4x10^4$ $L{\cdot}mol^{-1}{\cdot}cm^{-1}$), 308 nm (ε = $1.9x10^4$ $L{\cdot}mol^{-1}{\cdot}cm^{-1}$), 464 nm (ε = $1.9x10^4$ $L{\cdot}mol^{-1}{\cdot}cm^{-1}$). MS (ESI): *m/z* LR-MS 324 ($M+Na^+$, 100%), HR-MS: theor 302.14057 ($M+H^+$), expt 302.13969 ($M+H^+$, 100%). MP: 106-109°C.

1,5-Diphenyl-3-(pyridin-2-yl)verdazyl (2.2)

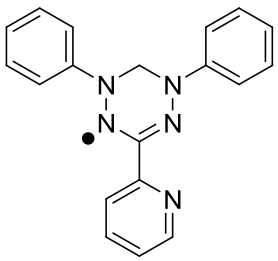

To 1,5-diphenyl-3-(pyridin-2-yl)formazan (522 mg, 1.73 mmol) was added DMF (25 mL). A 37% solution of formaldehyde (1.9 mL, 26 mmol) was added and the resulting solution was left to stir for 1 h. A solution of 2 M NaOH (5.5 mL, 11 mmol) was added dropwise. The solution was allowed to stir at RT and open to air for 23 h. It was poured into Et_2O (200 mL), washed with H_2O (5X50 mL), and the organic layer was stored on Na_2CO_3.

The solvent was removed *in vacuo* and column chromatography was performed (D. N. Al, hexanes:DCM:TEA, 14:6:1) isolating the green band. The solvent was removed *in*

vacuo to yield a dark green solid (81.5 mg, 15.0%). FT-IR (KBr): 3057 (w), 2957 (w), 1685 (w), 1588 (s), 1567 (m), 1495 (s), 1476 (s), 1457 (m), 1393 (m), 1368 (m), 1314 (m), 1304 (m), 1270 (m), 1216 (w), 1147 (m), 1130 (m), 1076 (w), 1028 (w), 994 (w), 940 (w), 894 (w), 789 (m), 748 (s), 687 (m), 650 (w), 628 (w), 622 (w), 612 (w), 603 (m) cm^{-1}. UV-Vis (MeCN): λ_{max} 279 nm ($\varepsilon = 1.4x10^4$ $L{\cdot}mol^{-1}{\cdot}cm^{-1}$), 304 nm ($\varepsilon = 1.4x10^4$ $L{\cdot}mol^{-1}{\cdot}cm^{-1}$), 435 nm ($\varepsilon = 4.8x10^3$ $L{\cdot}mol^{-1}{\cdot}cm^{-1}$), 699 nm ($\varepsilon = 2.6x10^3$ $L{\cdot}mol^{-1}{\cdot}cm^{-1}$). MS (ESI): *m/z* LR-MS 315 ($M+H^+$, 100%), HR-MS: theor 314.14057(M^+), expt 314.13997 (M^+, 100%). Anal. Calc. for $C_{19}H_{16}N_5$: C, 72.59; H, 5.13; N, 22.28. Found: C, 72.47; H, 5.08; N, 20.87. MP: 80-84°C.

[1,5-Diphenyl-3-(pyridin-2-yl)verdazyl]palladium(II) chloride (2.2.$PdCl_2$)

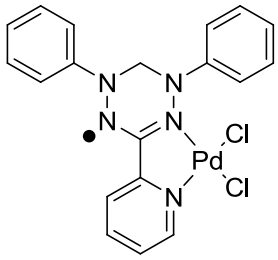

Solid $PdCl_2{\cdot}2H_2O$ (37.4 mg, 0.175 mmol) was added to MeCN (20 mL) and the solution was heated to reflux. A solution of 1,5-diphenyl-3-(pyrdin-2-yl)verdazyl (59.4 mg, 0.189 mmol) in MeCN (5 mL) was added dropwise. The resulting dark coloured solution was stirred for 15 min at reflux, stirring was arrested, and it was left to sit for 72 h at RT exposed to air. A dark purple solid was collected by filtration (41.5 mg, 48.1%). FT-IR (KBr): 3466 (br, m), 3047 (s), 2920 (w), 1607 (m), 1584 (m), 1487 (s), 1458 (s), 1424 (s), 1392 (m), 1344 (m), 1288 (m), 1266 (m), 1243 (m), 1199 (m), 1161 (m), 1146 (m), 1136 (m), 1108 (m), 1100 (m), 1077 (w), 1050 (w), 1035 (w), 1027 (w), 1003 (w), 969 (w), 951 (m), 906 (w), 766 (s), 755 (s), 700 (m), 680 (m), 655 (m), 629 (m), 602 (w), 575 (w), 535

(w) cm^{-1}. UV-Vis (MeCN): λ_{max} 314 nm ($\varepsilon = 9.7x10^3$ $L \cdot mol^{-1} \cdot cm^{-1}$), 489 nm ($\varepsilon = 5.2x10^3$ $L \cdot mol^{-1} \cdot cm^{-1}$), 733 nm ($\varepsilon = 1.6x10^3$ $L \cdot mol^{-1} \cdot cm^{-1}$). Anal. Calc. for $C_{19}H_{16}N_5PdCl_2$: C, 46.41; H, 3.28; N, 14.24. Found: C, 46.35; H, 3.15; N, 14.32. MP: 202-208°C.

2,4-Diphenylcarbonohydrazide (2.18)

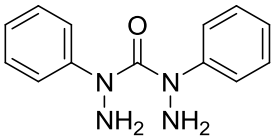

2,4,6-Triphenyl tetrazane (2.480 g, 7.507 mmol) was combined with 37% HCl (80 mL) and H_2O (30 mL). The solution was stirred at RT for 24 h followed by reflux for 2 h. The solution was added to a separatory funnel and was washed with DCM (3X50 mL). DCM (60 mL) was added to the funnel and the solution was basified using 2 M NaOH until pH 14 was reached. It was then extracted with DCM (4X60 mL) and the organic layer was dried using $MgSO_4$. The solvent was removed *in vacuo* leaving a yellowish oil which solidified *in vacuo*. The yellowish solid was collected (1.375 g, 75.6%). ^1H NMR (300 MHz, DMSO-d6, 300 K): δ 7.29 (dd, 4H, J = 8,1 Hz), 7.20 (t, 4H, J = 7 Hz), 6.95 (2H, tt, J = 7,1 Hz), 5.24 (4H, s) ppm. ^{13}C NMR (300 MHz, DMSO-d6, 300 K): δ 160.8, 145.5, 127.9, 123.0, 121.5 ppm. FT-IR (KBr): 3342 (s), 3313 (s), 3282 (s), 3063 (m), 3039 (m), 1653 (s), 1620 (s), 1585 (s), 1494 (s), 1363 (s), 1305 (s), 1179 (m), 1091 (m), 1076 (m), 1024 (m), 921 (s), 901 (s), 775 (s), 766 (s), 748 (s), 693 (s), 658(m), 603 (m), 536 (m) cm^{-1}. UV-Vis (MeCN): λ_{max} 266 nm ($\varepsilon = 1.2x10^4$ $L \cdot mol^{-1} \cdot cm^{-1}$). MS (ESI): m/z LR-MS 265 ($M+Na^+$, 100%), HR-MS: theor 243.12459 ($M+H^+$), expt 243.12385 ($M+H^+$, 100%). Anal. Calc. for $C_{13}H_{14}N_4O$: C, 64.45; H, 5.82; N, 23.13. Found: C, 64.47; H, 5.65; N, 23.22. MP: 74-77°C.

2,4-Diphenyl-6-(pyridin-2-yl)-1,2,4,5-tetrazinan-3-one (2.19)

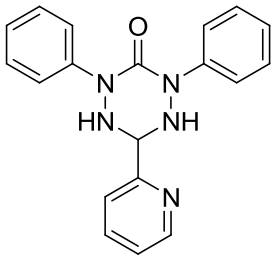

To MeOH (15 mL) was added 2,4-diphenylcarbonohydrazide (317 mg, 1.31 mmol) and 2-pyridinecarboxaldehyde (0.11 mL, 1.2 mmol) followed by pyridinium tosylate (108 mg, 0.430 mmol). The bright yellow solution was stirred at room temperature for 48 h. It was then poured into H_2O (90 mL) and stirred for 3 h. A white precipitate was collected by filtration and washed with H_2O. The solid was dried overnight to yield a white solid (371 mg, 94.7%). ^{1}H NMR (300 MHz, DMSO-d_6, 300 K): δ 8.56 (ddd, 1H, J = 5,2,1 Hz), 7.84 (td, 1H, J = 8,2 Hz), 7.64-7.53 (mult, 5H), 7.39 (ddd, 1H, J = 8,5,1 Hz), 7.30 (tt, 4H, J = 8,2 Hz), 7.05 (tt, 2H, J = 7,1 Hz), 6.49 (d, 2H, J = 10 Hz), 5.40 (t, 1H, J = 10 Hz) ppm. ^{13}C NMR (300 MHz, DMSO-d_6, 300 K): δ 156.8, 156.3, 148.7, 142.8, 137.2, 128.0, 123.8, 123.3, 122.7, 121.1, 73.4 ppm. FT-IR (KBr): 3222 (m), 3066 (w), 3029 (w), 1653 (s), 1596 (s), 1570 (w), 1484 (s), 1455 (m), 1440 (m), 1360 (s), 1299 (s), 1111 (w), 1090 (w), 1031 (w), 997 (m), 898 (s), 796 (m), 751 (s), 706 (m), 693 (s), 647 (w), 593 (w), 568 (m) cm^{-1}. UV-Vis (MeCN): λ_{max} 263 nm (ε = 2.3x10^4 L·mol^{-1}·cm^{-1}). MS (ESI): *m/z* LR-MS 354 (M+Na^+, 100%), HR-MS: theor 332.15114 (M+H^+), expt 332.15031 (M+H^+, 100%). Anal. Calc. for $C_{19}H_{17}N_5O$: C, 68.87; H, 5.17; N, 21.13. Found: C, 69.28; H, 4.99; N, 21.25. MP: 143-147°C.

1,5-Diphenyl-3-(pyridin-2-yl)-6-oxoverdazyl (2.3)

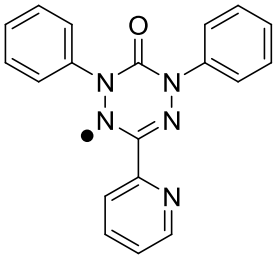

To MeOH (5 mL) was added 2,4-diphenyl-6-(pyridin-2-yl)-1,2,4,5-tetrazinan-3-one (97.0 mg, 0.293 mmol), celite (92.0 mg), and silver oxide (101.8 mg, 0..439 mmol). The resulting solution was stirred and a colour change (colourless to red) was observed after 10 min. It was stirred for a further 1 h. Column chromatography was performed (SiO_2; hexanes:EtOAc:DCM, 2:1:1) and the major red fraction was collected (56.0 mg, 58.3%). FT-IR (KBr): 3089 (w), 3065 (w), 3013 (w), 1743 (w), 1696 (s), 1589 (m), 1570 (m), 1485 (s), 1457 (m), 1401 (m), 1368 (m), 1298 (m), 1258 (m), 1238 (m), 1136 (m), 1125 (m), 1088 (w), 1044 (w), 1024 (w), 994 (w), 897 (w), 798 (w), 758 (s), 713 (w), 692 (s), 654 (m), 631 (m), 619 (m), 612 (m), 601 (s) cm^{-1}. UV-Vis (MeCN): λ_{max} 269 nm (ε = $1.5x10^4$ $L{\cdot}mol^{-1}{\cdot}cm^{-1}$), 312 nm ($\varepsilon$ = $1.3x10^4$ $L{\cdot}mol^{-1}{\cdot}cm^{-1}$), 416 nm ($\varepsilon$ = $1.5x10^3$ $L{\cdot}mol^{-1}{\cdot}cm^{-1}$), 518 nm ($\varepsilon$ = $2.5x10^3$ $L{\cdot}mol^{-1}{\cdot}cm^{-1}$). MS (ESI): *m/z* LR-MS 351 ($M+Na^+$, 100%), HR-MS: theor 329.12767 ($M+H^+$), expt 329.12661 ($M+H^+$, 100%). Anal. Calc. for $C_{19}H_{14}N_5O$: C, 69.50; H, 4.30; N, 21.33. Found: C, 69.43; H, 4.16; N, 21.37. MP: 206-209°C.

[1,5-Diphenyl-3-(pyridin-2-yl)-6-oxoverdazyl]palladium(II) chloride (2.3.$PdCl_2$)

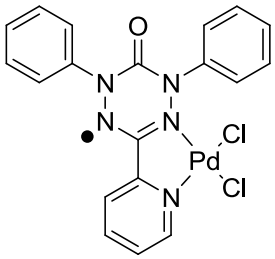

Solid $PdCl_2$ (25.0 mg, 0.141 mmol) was added to MeCN (20 mL) and the resulting solution was heated to reflux. A solution of 1,5-diphenyl-3-(pyrdin-2-yl) 6-oxoverdazyl (45.9 mg, 0.140 mmol) in

MeCN (5 mL) was added dropwise. The dark coloured solution was stirred for 20 min at reflux, stirring was stopped, and it was left to sit for 72 h at RT exposed to air. A dark green solid was collected by filtration (47.2 mg, 66.8%). FT-IR (KBr): 3440 (br, m), 3067 (w), 1714 (s), 1605 (m), 1485 (m), 1458 (m), 1447 (m), 1373 (w), 1299 (m), 1241 (m), 1157 (m), 1143 (m), 1104 (m), 1024 (w), 913 (w), 780 (m), 755 (m), 696 (m), 688 (m), 642 (w), 620 (m), 608 (w), 508 (w) cm^{-1}. UV-Vis (MeCN): λ_{max} 283 nm ($\varepsilon = 1.4x10^4$ $L \cdot mol^{-1} \cdot cm^{-1}$), 307 nm ($\varepsilon = 1.4x10^4$ $L \cdot mol^{-1} \cdot cm^{-1}$), 478 nm ($\varepsilon = 3.6x10^3$ $L \cdot mol^{-1} \cdot cm^{-1}$), 550-700 nm ($\varepsilon = 2.0x10^3$ $L \cdot mol^{-1} \cdot cm^{-1}$). Anal. Calc. for $C_{19}H_{14}N_5Cl_2OPd$: C, 45.13; H, 2.79; N, 13.85. Found: C, 44.70; H, 2.56; N, 13.73. MP: >320°C.

CHAPTER 3

SYNTHESIS AND STUDIES OF AN *N*-BENZYL TETRAZINE AND ITS RUTHENIUM COMPLEX

3.1 Introduction

Owing to their ability to be functionalized at a variety of positions that affect the properties of the molecule, verdazyl radicals are one of the few classes of stable radicals that offer richness in diversification. Studies exploring the structure-property relationships with respect to spectroscopy and electrochemistry of these molecules have been reported[59,123-125]. Verdazyl radicals have also been modified to incorporate substituents which can allow for the formation of coordination compounds with a variety of metal systems, some of which were shown in section 1.4.4. One goal of these new metal-verdazyl compounds is to explore the properties that arise as a result of the interaction between the metal centre and verdazyl radical ligand.

Verdazyl radicals behave similarly to other radicals in that they can be used as a radical trap. The resulting species can be either the leuco verdazyl (addition of an H atom) or the N-alkylated tetrazine (addition of an alkyl group) (**Figure 3.1**). Examples of isolated leuco verdazyls are rare, as the leuco compounds of Kuhn verdazyls have a relatively weak N-H bond[40] and are generally converted back to the verdazyl radical in the presence of oxygen. The N-alkylated tetrazines have been synthesized using a variety of organometallic reagents[126-128]; tetrazine compounds are more common than the leuco verdazyls as a result of their increased stability. One field of study that

benefits from these weak bonds is stable free radical polymerization (SFRP), but this area has yet to be fully explored with verdazyl radicals and the N-alkylated compounds.

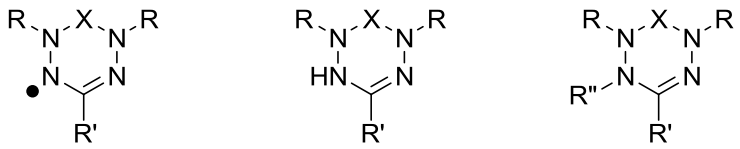

Figure 3.1: Verdazyl radical (left), leuco verdazyl (center), and N-alkylated tetrazine (right).

The process of SFRP has received attention chiefly due to its ability to form polymers with narrow polydispersity indexes (PDIs). This ability is a result of the weak and reversible nature of the bond between the growing polymer chain and the stable radical (**Scheme 1.2**). SFRP can lead to a reduction in the number of termination reactions allowing for the continued growth of a polymer as long as monomer is present. Since the initial work by Georges *et al.*[53] into SFRP, much work in this field has focused on the use of nitroxide radicals. Other radicals have been tested in the SFRP process such as arylazooxyls[129], borinates[130,131], and triazolinyls[132-134], but none of these radicals have been examined to the same extent as the nitroxides.

Verdazyl radicals were explored by Yamada *et al.* who used **1.14** in the polymerization of styrene and methyl methacrylate[135,136]. However, the end groups of the growing polymer chains were not uniform in length arising from the bimolecular termination reactions which lead to relatively high PDIs (1.9 to 3.7 depending on concentration) and **1.14** was found not to be stable at operational temperatures. While **1.14** was found not to be useful in SFRP, a series of N-alkylated tetrazines based on the

6-oxoverdazyls radicals (**3.1**-**3.4**) were evaluated by Georges, Hicks *et al.*[137] and further studies into the effect of changing the R' substituents (**3.2**, **3.4**-**3.6**) has on the polymerization results were carried out by Raynor *et al*.[138].

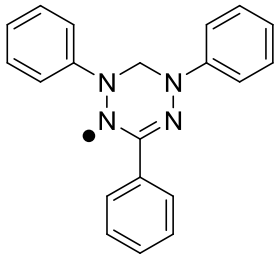

1.14

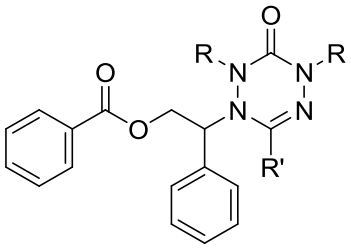

R = R' = Ph	**3.1**
R = Me, R' = H	**3.2**
R = Me, R'= Et	**3.3**
R = Me, R' = Ph	**3.4**
R = Me, R' = 4-MeOPh	**3.5**
R = Me, R' = 4-NO_2Ph	**3.6**

While **3.1** was found to give results similar to Yamada for the polymerization of styrene, it is believed the large phenyl groups at N1 and N2 introduce a steric problem when the radical tries to recombine with the propagating chain[137]. Compounds **3.2**-**3.4** were used for the polymerization of *n*-butyl acrylate or styrene and found to give low PDIs (~1.1-1.5) and efficient conversions compared to **3.1**. The main difference between **3.1** and **3.2**-**3.6** is the substituents at the N1 and N5 positions (phenyl and methyl, respectively). The initiators **3.5**-**3.6** have electron donating and withdrawing groups, respectively; the rates of polymerization are higher for **3.5** than for **3.6** leading to the use of **3.5** in the polymerization of styrene at a lower temperature (100°C)[138] compared to conventional polymerization temperatures (~130°C).

A better understanding of polymerization results as a function of sterics and electronics of the tetrazines was investigated by Lukkarila[139]. The presence of phenyl substituents at the N1 and N5 positions such as in **3.1** results in a lower dissociation

constant (k_d) compared to compounds with methyl substituents. The effect of varying the R' substituent from electron donating to withdrawing substituents has yet to be studied to the same degree.

The ability to modify the structure/substituents of verdazyl radicals creates the ability to alter the spin distribution and redox properties (section 1.3.3). Both of these aspects could also be perturbed through the formation of metal-verdazyl complexes with some demonstrating non-innoncence as in **1.28** and **1.29**. As such, the ability to form coordination compounds of verdazyl radicals presents another avenue of altering and controlling the radical-type reactivity on the verdazyl ligand that is not possible for the nitroxide based systems.

This chapter presents the synthesis and studies of the *N*-benzyl tetrazine ligand (**3.7**) and its ruthenium complex (**3.7.Ru(hfac)$_2$**). The synthesis and properties of each compound will be discussed followed by an investigation into the homolytic C-N bond dissociation activation energy for these compounds by a new UV-Visible spectroscopy-based method.

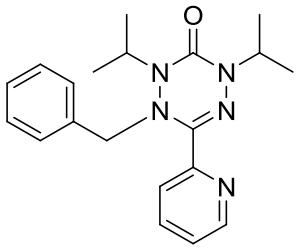

3.7

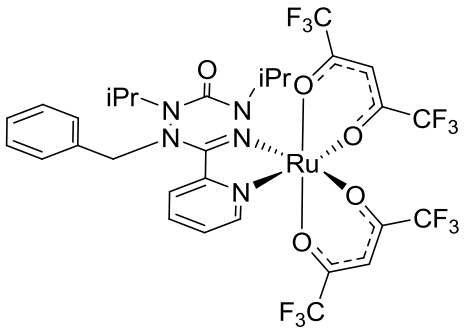

3.7.Ru(hfac)$_2$

3.2 N-Benzyl Tetrazine and its Ru Complex

The verdazyl radical chosen for this work was the bidentate chelating compound, 1,5-diisopropyl-3-(pyridin-2-yl)-6-oxoverazyl (**3.8**) because it can mimic the coordination of bipy. **3.8** has been utilized in the formation of numerous metal compounds including **1.26**-**1.29**[94,95]. The metal centre in this study was ruthenium because ruthenium-verdazyl complexes of **3.8** were previously studied[94], one bearing two acac ligands (**1.28**) and the other with two hfac ligands (**1.29**).

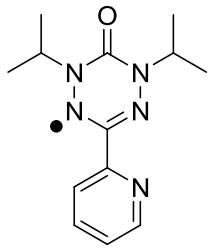

3.8

Tetrazines derivatives of the Kuhn verdazyl, **1.14**, have been synthesized using a variety of organometallic reagents[126-128]. Various tetrazine derivatives of 6-oxoverdazyls have been synthesized through the alkylation of a leuco verdazyl as in **3.9**[38] and the trapping of a radical from a *p*-nitrobenzyl cobaloxime[140] as in **3.10** and **3.11** or an alkoxyamine as in **3.1**-**3.3**[137]. The organocobaloxime used for **3.10** and **3.11** is able to release a *p*-nitrobenzyl radical upon exposure to UV light and the released radical couples with the appropriate verdazyl radical thereby generating the tetrazines.

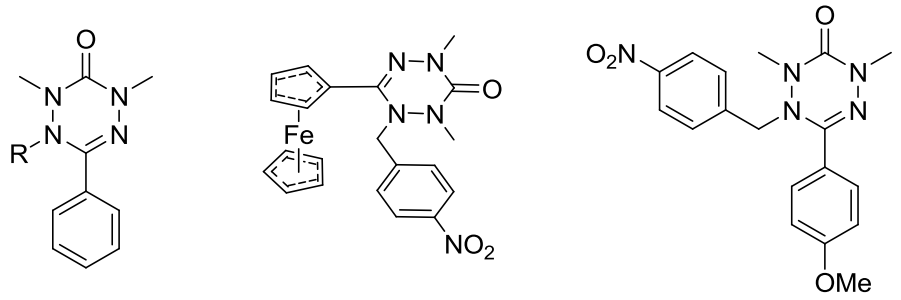

R = Me, Bn **3.9** **3.10** **3.11**

Initial attempts to prepare **3.7** using benzyl cobaloxime[141] (**3.12**) (**Scheme 3.1**) resulted in low yields (10-15%) of the desired compound, **3.7**. In addition to the low yields, the purification procedure was time consuming leading to the abandonment of this method.

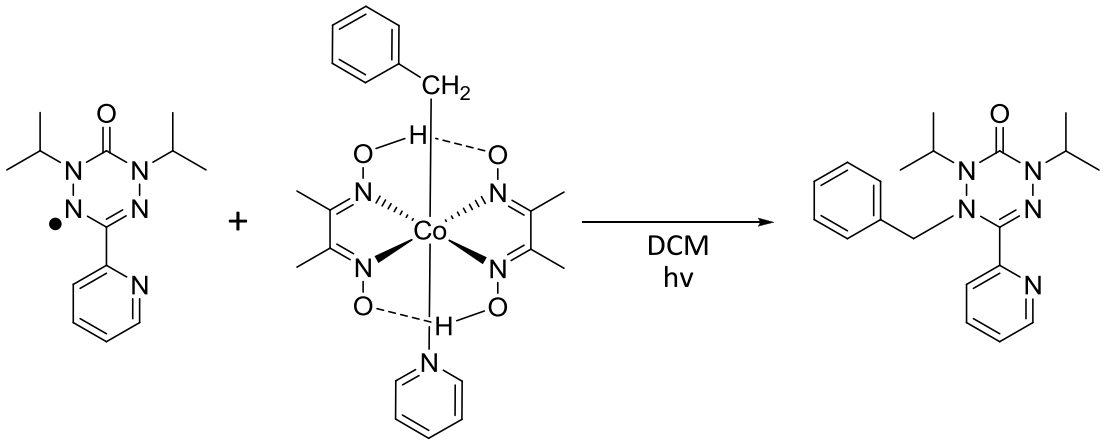

3.8 **3.12** **3.7**

Scheme 3.1: Trapping of benzyl radical released from benzyl cobaloxime using **3.8**.

Dimanganese decacarbonyl, $Mn_2(CO)_{10}$, can be used with benzyl bromide to generate benzyl radicals in the presence of a full spectrum light source. Gilbert *et al.*[142,143] investigated the use of this reagent to perform radical cyclization reactions and coupling of **1.9** with benzyl radicals to form an N-alkoxyamine. The radical, **3.8**, was

combined with $Mn_2(CO)_{10}$ in dry DCM and placed in a full spectrum light box for 24 h during which **3.7** was formed (**Scheme 3.2(a)**); the product could be isolated in pure form and in a higher yield (60%) by straightforward aqueous extraction. This synthetic method was also amenable to the formation of **3.7.Ru(hfac)$_2$** from **1.29** (**Scheme 3.2(b)**), but required purification by column chromatography to yield a pure product in 85% yield.

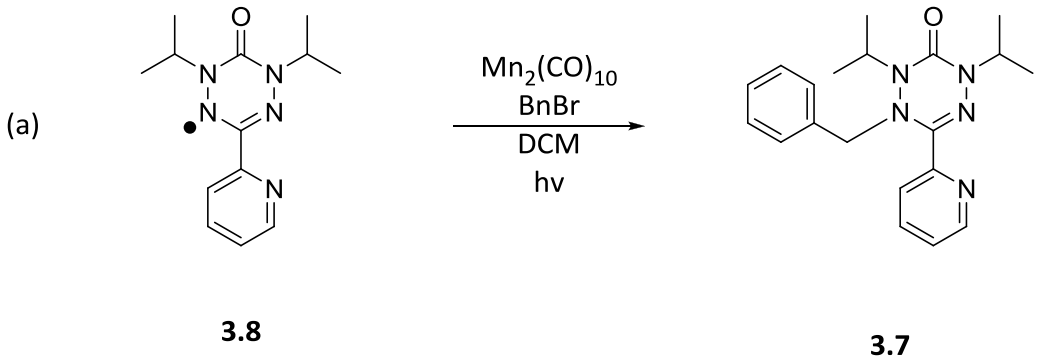

3.8 **3.7**

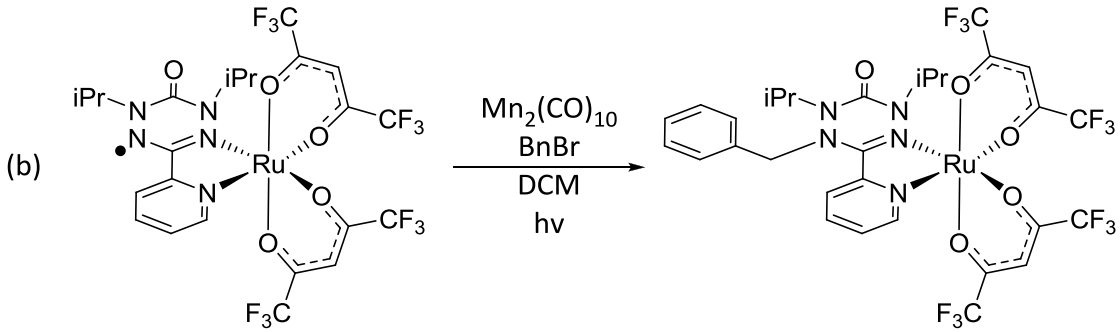

1.29 **3.7.Ru(hfac)$_2$**

Scheme 3.2: C-N bond formation reaction using $Mn_2(CO)_{10}$ with (a) **3.8** and (b) **1.29**.

The attempted synthesis of the acac analogue of **3.7.Ru(hfac)$_2$** using the synthetic method illustrated above did not yield a pure sample of the desired complex "**3.7.Ru(acac)$_2$**". Unlike **1.29**, calculations of the spin density distribution in **1.28** has shown a near equal sharing between the verdazyl radical ligand and the ruthenium ion[94]

thereby affecting the position at which a benzyl radical might react with **1.28**. The reactions of the free ligand **3.7** with *cis*-$[Ru(acac)_2(MeCN)_2]$[144] in EtOH or *cis*-$[Ru(acac)_2(\eta^2\text{-cyclooct-1-ene})_2]$[145] in THF also failed to produce **3.7.Ru(acac)$_2$**.

3.3 Properties of N-Benzyl Tetrazine and its Ru Complex

The new compounds, **3.7** and **3.7.Ru(hfac)$_2$**, were characterized by FT-IR, ^{1}H, ^{13}C, and ^{19}F NMR, and UV-Vis spectroscopy. A comparison of these new compounds to their radical parent molecules, **3.8** and **1.28**, will be discussed. The methods of comparison include structural features by X-ray crystallography, electronic transitions by UV-Vis spectroscopy, and electrochemical by the use of CV.

3.3.1 NMR Spectroscopy

The collection of the NMR spectra of **3.7** required that the sample be cooled to 250 K to resolve the methyl signals of the isopropyl substituents and are as expected. The room temperature NMR spectra of **3.7.Ru(hfac)$_2$** suggests that the isolated product is a mixture of isomers. The spectra of ^{1}H, ^{13}C, and ^{19}F NMR all show double the number of signals than are expected. For example, in the ^{19}F NMR, one isomer would show four distinct signals with each signal having the same relative integration as a result of four different environments for the CF_3 groups, but a total of seven signals are observed (two signals appear to overlap near -75.3 ppm, **Figure 3.2**). This is thought to be caused by diastereomers (up/down orientation of the benzyl group) as a result of the fluxionality of the new C-N bond; the changing nature of this bond (up/down) is too slow on the NMR timescale to be observed as a single set of signals.

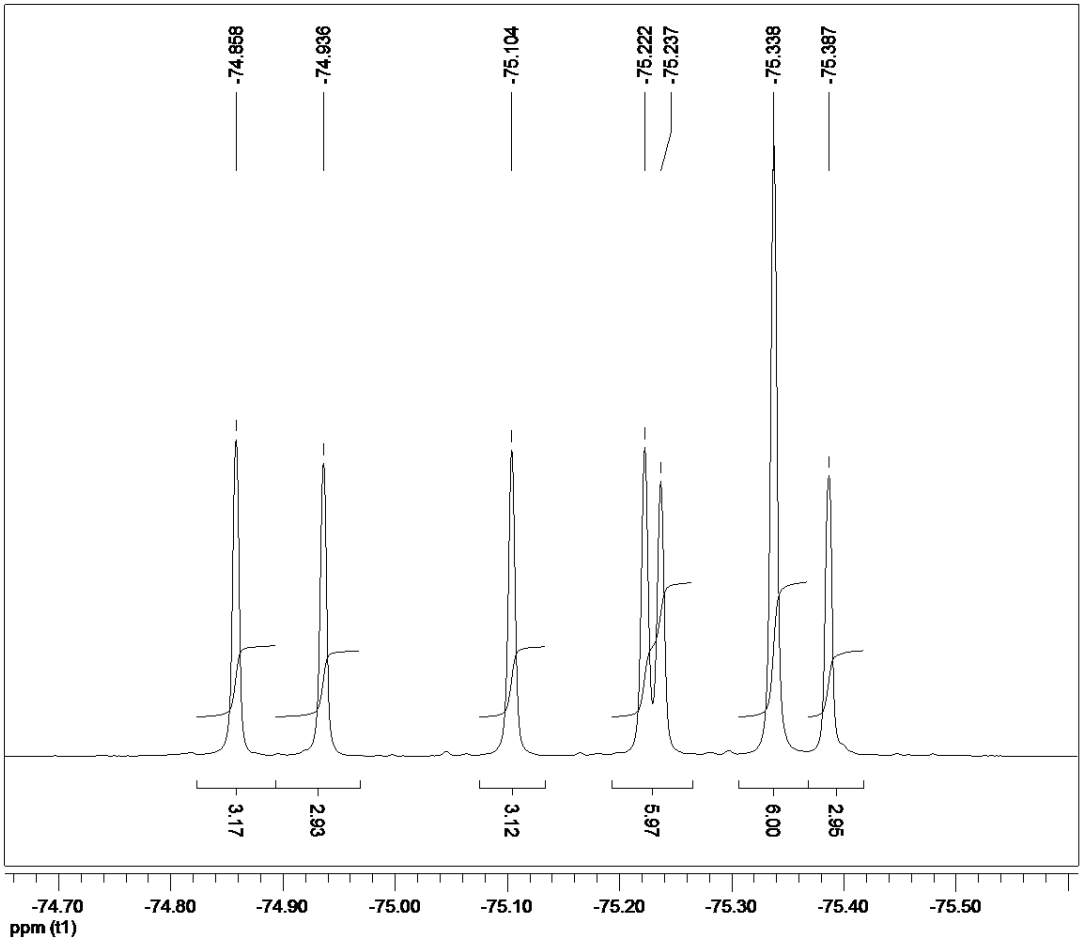

Figure 3.2: Room temperature ^{19}F NMR spectrum of **3.7.Ru(hfac)$_2$**.

3.3.2 Structural Properties

The solid state structures of **3.7** and **3.7.Ru(hfac)$_2$** and the numbering format for **3.8** and **1.29** are presented in **Figure 3.3**; selected bond lengths for these compounds are given in **Table 3.1**. Compared to the parent radical compounds (**3.8** and **1.29**), there is a lengthening of the N(1)-N(2) and N(3)-N(4) bonds in the N-benzyl tetrazine species (**3.7** and **3.7.Ru(hfac)$_2$**). Also, while **3.8** does not demonstrate significant differences in the bond lengths of C(2)-N(1) and C(2)-N(4), the corresponding bond in **3.7** are consistent with single and double bonds, respectively. The ruthenium-verdazyl complex (**1.29**) has

bond lengths in the lower portion of the verdazyl core of the ligand that are similar to each other [C(2)-N(1), 1.304(5) Å; C(2)-N(4), 1.358(4) Å] while **3.7.Ru(hfac)$_2$** demonstrated more pronounced single and double bonds [C(2)-N(1), 1.407(1) Å; C(2)-N(4), 1.280(1) Å]. The Ru-N distances in **1.29** are similar to one another [Ru-N(4), 2.020(3) Å; Ru-N(5), 2.035(3) Å], but the difference becomes more pronounced in **3.7.Ru(hfac)$_2$** [Ru-N(4), 2.067(2) Å; Ru-N(5), 2.019(2) Å] with the 2-pyridyl group behaving as a better donor than the nitrogen atom of the tetrazine core.

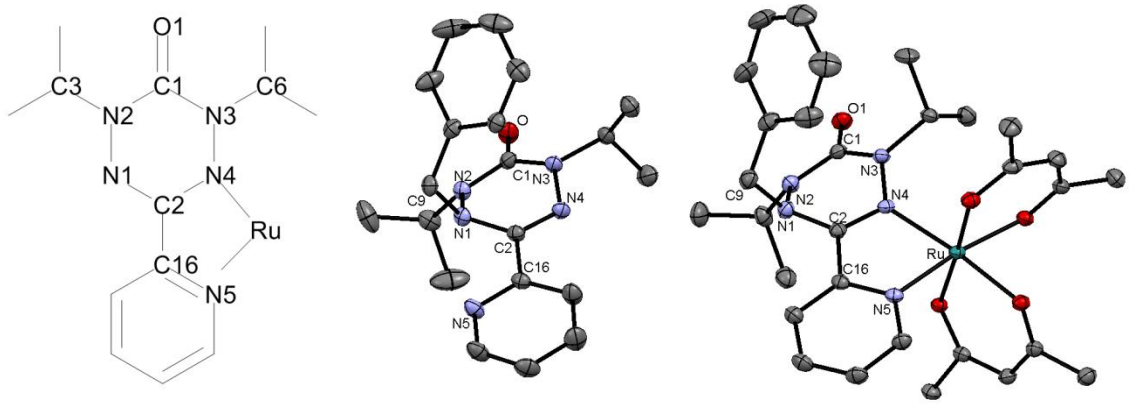

Figure 3.3: Numbering format of **3.8** and **1.29** (left) and solid state structure of **3.7** (middle) and **3.7.Ru(hfac)$_2$** (right). Hydrogen and fluorine atoms have been omitted for clarity. Thermal ellipsoids are at the 30% probability level.

Table 3.1: Selected bond lengths for **3.8**, **1.29**, **3.7**, and **3.7.Ru(hfac)$_2$** (estimated standard deviations are in parentheses).

Bond	**3.8**[106]	**1.29**[a,94]	**3.7**	**3.7.Ru(hfac)$_2$**
C(1)-O(1)	1.216(2)	1.223(5)	1.220(1)	1.217(3)
N(1)-N(2)	1.365(2)	1.372(5)	1.419(1)	1.416(2)
N(3)-N(4)	1.365(2)	1.392(2)	1.391(1)	1.402(3)
C(9)-N(1)	—	—	1.487(2)	1.493(4)
C(1)-N(2)	1.373(2)	1.375(2)	1.379(3)	1.379(2)
C(1)-N(3)	1.374(3)	1.379(5)	1.386(2)	1.373(2)
C(2)-N(1)	1.324(2)	1.304(5)	1.386(3)	1.407(1)
C(2)-N(4)	1.322(2)	1.358(4)	1.304(2)	1.280(1)
C(2)-C(16)	1.488(3)	1.474(5)	1.459(3)	1.489(1)
Ru-N(4)	—	2.020(3)	—	2.067(2)
Ru-N(5)	—	2.035(3)	—	2.019(2)

[a]data for one of two independent molecules in the asymmetric unit.

3.3.3 UV-Vis Spectroscopy

The electronic absorption spectra of the radical and tetrazine compounds were recorded in MeCN and are shown in **Figure 3.4** and a summary of their absorption maxima are given in **Table 3.2**. Upon formation of the *N*-benzyl tetrazine compounds from their corresponding parent compounds, there is a loss of the higher wavelength transitions. While **3.8** has a transition at 408 nm, the absorption maximum for **3.7** occurs at 332 nm and with a much higher molar extinction coefficient. The ruthenium-radical complex (**1.29**) has low energy transitions at 584 nm and 696 nm which are not present in **3.7.Ru(hfac)$_2$**. The absorption spectrum of **3.7.Ru(hfac)$_2$** has a highly intense band in the visible region at 495 nm which is likely a charge transfer transition.

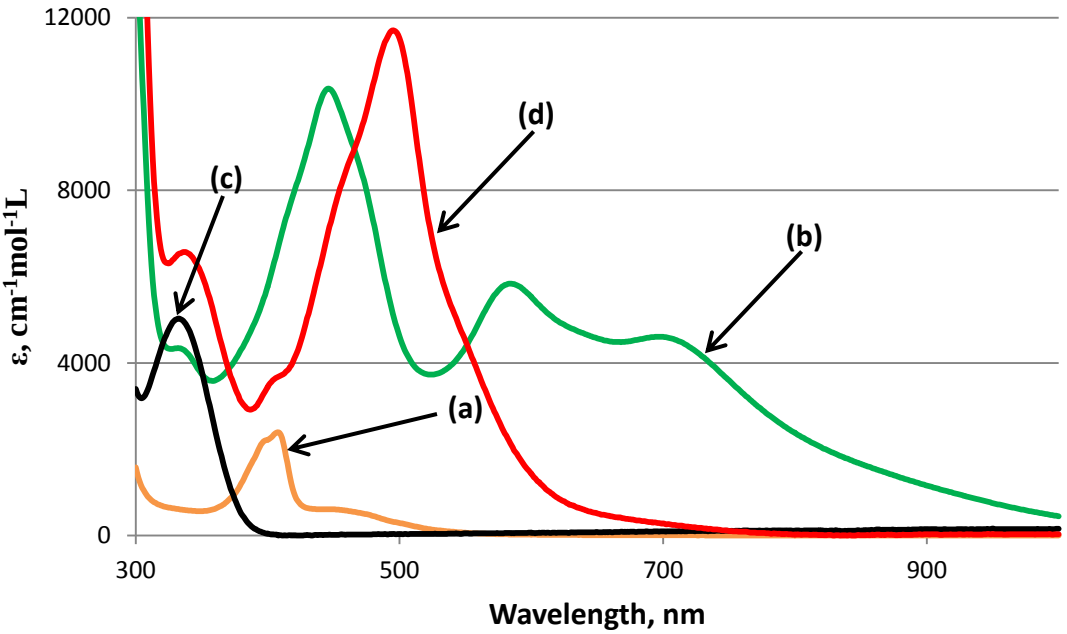

Figure 3.4: Room temperature UV-Vis spectra in MeCN of (a, orange) **3.8**, (b, green) **1.29**, (c, black) **3.7**, and (d, red) **3.7.Ru(hfac)$_2$**.

Table 3.2: Absorption maxima of **3.8**, **1.29**, **3.7**, and **3.7.Ru(hfac)$_2$** (wavelength is listed with ε in parentheses).

Compound	λ_{max}/nm (ε/cm^{-1}mol^{-1}L)
3.8	408 (2400)
1.29	332 (4600), 446 (10000), 584 (5800), 696 (4600)
3.7	332 (5000)
3.7.Ru(hfac)$_2$	337 (6600), 495 (12000)

3.3.4 Cyclic Voltammetry

The CVs of the tetrazine compounds (**3.7** and **3.7.Ru(hfac)$_2$**) and radical compounds (**3.8** and **1.29**) were recorded in MeCN and referenced to Fc/Fc$^+$ and are shown in **Figure 3.5**. A summary of the redox processes for the *N*-benzyl species and their parent compounds is given in **Table 3.3**. The free ligand, **3.7**, has an irreversible reduction at -2.57 V, a reversible oxidation at +0.63 V, and an irreversible oxidation at +1.25 V. The

oxidation potential of **3.7** at +0.63 V is similar to the value for a related N-alkylated tetrazine, **3.11**[140] (+0.60 V vs. Fc/Fc^{+}). The parent radical, **3.8**, has two reversible processes occurring at -1.36 V and +0.20 V corresponding to the reduction and oxidation, respectively. It is not possible to speculate as to which part of the molecule is being reduced in **3.7** as a result of the extremely low potential. The oxidation potentials in **3.7** when compared to **3.8** are much higher indicating that the removal of an electron is much more difficult.

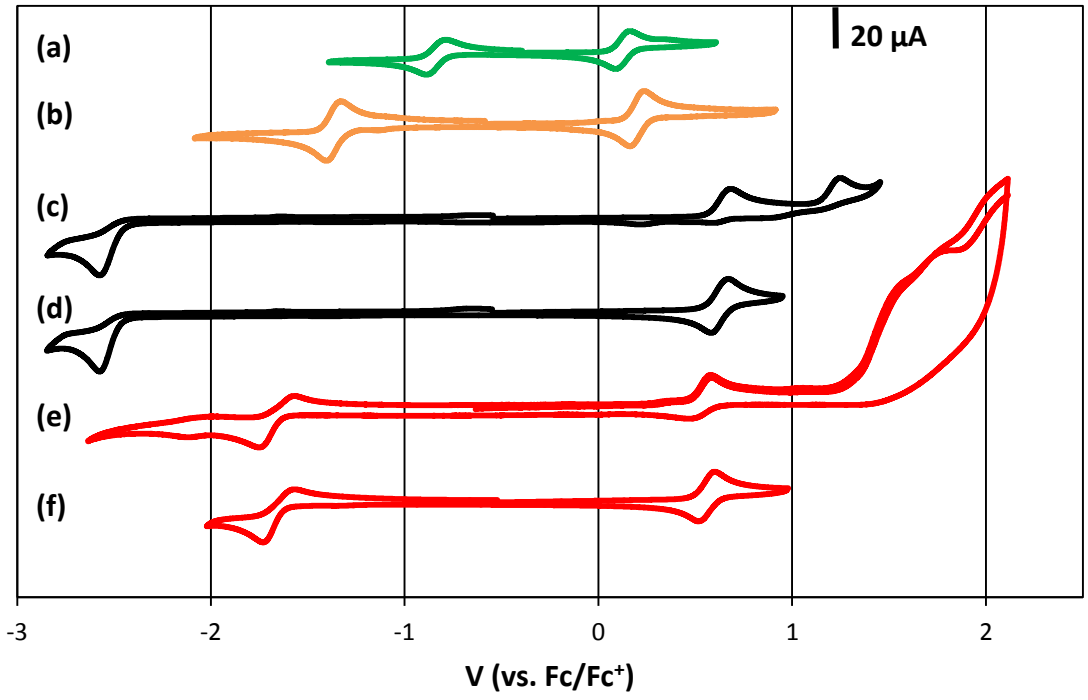

Figure 3.5: CVs of (a) **1.29**, (b) **3.8**, (c) **3.7** (full), (d) **3.7** (1^{st} oxidation only), (e) **3.7.Ru(hfac)$_2$** (full), and (f) **3.7.Ru(hfac)$_2$** (1^{st} oxidation only). Conditions: MeCN solution, 1 mM analyte, 0.1 M nBu$_4$NBF$_4$, scan rate 100 mVs^{-1}, and temperature 295 K. Scans shown were initiated in the positive direction.

Table 3.3: Electrochemical properties of **3.8**, **1.29**, **3.7**, and **3.7.Ru(hfac)$_2$** (V vs. Fc/Fc$^+$). Conditions: MeCN solution, 1 mM analyte, 0.1 M *n*Bu$_4$NBF$_4$, scan rate 100 mVs^{-1}, and temperature 295 K.

Compound	$E_{1/2}$ (V)
3.8	-1.36, +0.20
1.29	-0.84, +0.13
3.7	-2.57[a], +0.63, +1.25[a]
3.7.Ru(hfac)$_2$	-1.65[b], +0.56

[a]irreversible, [b]quasi reversible.

The ruthenium-tetrazine complex, **3.7.Ru(hfac)$_2$**, has two redox processes, a quasi-reversible reduction at -1.65 V (as observed by the difference in anodic and cathodic peak heights) and a reversible oxidation at +0.56 V. Compared to **3.7** the reduction potential is nearly 1 V more positive, a result of coordination to the electropositive ruthenium centre. The oxidation potential is nearly the same as that of the free ligand, but may be either a ligand-centered, metal-centered or non-innocent event.

Compared to the ruthenium-verdazyl complex (**1.29**) which has two redox processes at -0.84 V and +0.13 V, **3.7.Ru(hfac)$_2$** is tougher to reduce and oxidize. McKinnon, Hicks *et al*.[94] assigned the redox processes of **1.29** as being a ligand-centered reduction and a non-innocent oxidation resulting from the interaction of the ruthenium and verdazyl ligand thereby making assignment to one part of the molecule or the other "inappropriate". The reduction of **3.7.Ru(hfac)$_2$** is likely a ligand-centered event due to the low potential; the oxidation is more difficult to assign as there may be orbital mixing as in **1.29**, but more likely it is a result of the oxidation of ruthenium(II) to ruthenium(III)

since the value for **3.7.Ru(hfac)$_2$** (+0.56 V vs. Fc/Fc$^+$) is similar to the oxidation of ruthenium in Ru(bipy)(hfac)$_2$[146] (+0.51 V vs. Ag/AgNO$_3$, +0.41 V vs. Fc/Fc$^+$).

3.4 C-N Bond Strength Studies

3.4.1 Determining the C-N Bond Strength in Tetrazines

In order to determine the strength of the C-N bond in both **3.7** and **3.7.Ru(hfac)$_2$**, it is necessary to calculate the rate constant associated with the homolytic cleavage of this bond. The rate constant is dependent on the temperature of the reaction and can be related to the C-N bond homolysis by the activation energy through the Arrhenius equation (equation **1**) or the Gibbs free energy of the transition state through the Eyring equation (equation **2**). The E_a for the C-N bond homolysis provides a close approximation to the bond dissociation enthalpy[147] and will be used as a means of comparison to previously published compounds.

$$k = A\mathrm{e}^{-\mathrm{E_a}/\mathrm{RT}} \qquad (\mathbf{1})$$

$$k = \frac{k_B T}{h} e^{-\Delta G^{\ddagger}/RT} \qquad (\mathbf{2})$$

When either a tetrazine (**Scheme 3.3(a)**) or alkoxyamine (**Scheme 3.3(b)**) are heated, they dissociate to produce a transient alkyl radical and the corresponding verdazyl radical or nitroxide radical with rate constant, k_a. This process is reversible and if another species is not present to trap the released transient radical then the two species will recombine with rate constant, k_b. The value of k_b has been extensively explored for alkoxyamines and found to be quite high ($k_b > 10^7$ M^{-1}s^{-1})[148-150] and while k_b

has not been determined for tetrazines it can be assumed to be similar in value to that of the alkoxyamines.

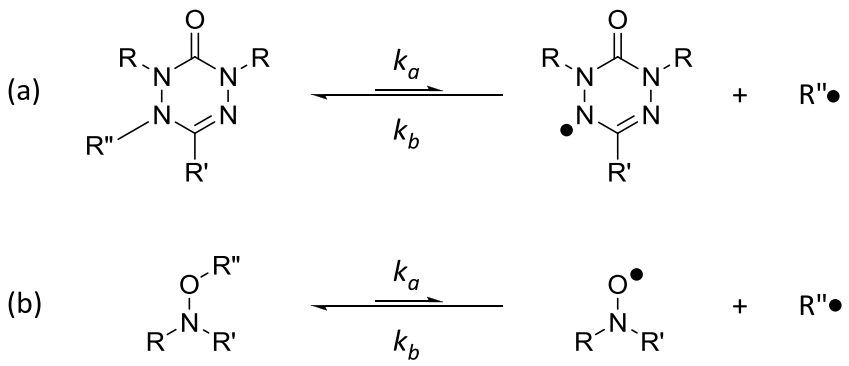

Scheme 3.3: Reversible nature of the C-N bond homolysis in (a) tetrazines and (b) alkoxyamines.

The incorporation of an excess amount of another stable radical, such as **1.9**, results in a competition between the two stable radicals, **1.9** and **3.8**, for the benzyl radicals that are generated favoring the right side of the equation according to the PRE (**Scheme 3.4**). In addition to this equilibrium, some of the benzyl radicals that are formed during the course of the reaction may couple together to form bibenzyl.

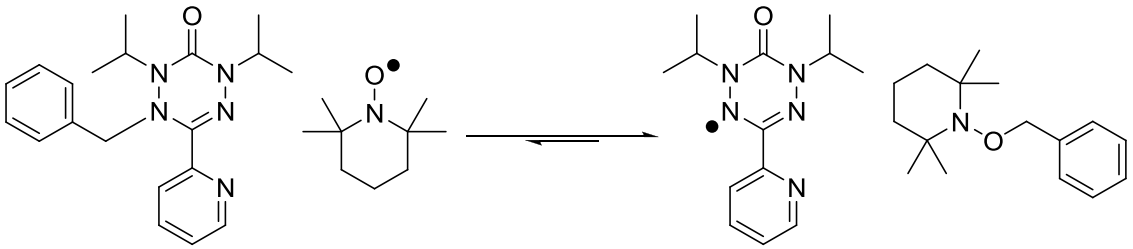

3.7 **1.9** **3.8** **3.13**

Scheme 3.4: Overall equation for the cleavage of the C-N bond in **3.7**.

Scheme 3.4 can be broken down into the individual equations that describe the simultaneous reactions that are taking place (**Scheme 3.5**). The homolysis of

compounds **3.7** or **3.7.Ru(hfac)$_2$** (represented by BnVd) into either **3.8** or **1.29** (represented by Vd·) and a benzyl radical (represented by Bn·) have a dissociation rate constant, k_{d1}, and a formation rate constant, k_{f1}. **1.9** (represented by T·) is used to trap Bn· and results in the formation of **3.13** (represented by BnT) and have a formation rate constant, k_{f2}, and a dissociation rate constant, k_{d2}. Any bibenzyl (represented by Bn_2) that is formed during the course of the reaction has a formation rate constant, k_t, and this pathway is a termination step.

$$BnVd \xrightarrow{k_{d1}} Bn\cdot + Vd\cdot$$

$$Vd\cdot + Bn\cdot \xrightarrow{k_{f1}} BnVd$$

$$T\cdot + Bn\cdot \xrightarrow{k_{f2}} BnT$$

$$BnT \xrightarrow{k_{d2}} Bn\cdot + T\cdot$$

$$Bn\cdot + Bn\cdot \xrightarrow{k_t} Bn_2$$

Scheme 3.5: Individual rate constants.

The determination of k_{d1} can be achieved by applying the rate equation to this system (equation **3**).

$$rate = \frac{d[BnVd]}{dt} = -k_{d1}[BnVd] + k_{f1}[Bn\cdot][Vd\cdot] \qquad (\mathbf{3})$$

During the course of reaction, the concentration of the benzyl radical is near zero such that the steady-state approximation can be applied. Substitution of this steady-state approximation into equation **3** gave equation **4**.

$$rate = -k_{d1}[BnVd] + k_{f1}[Vd\cdot]\left(\frac{k_{d1}[BnVd] + k_{d2}[BnT]}{k_{f1}[Vd\cdot] + k_{f2}[T\cdot] + k_t[Bn\cdot]}\right) \qquad (\mathbf{4})$$

As long as the [T·] is high enough in relation to [BnVd] then equation **4** simplifies to equation **5**. The rate is related to k_{d1} and first-order with respect to [BnVd].

$$rate = -k_{d1}[BnVd] \qquad (\mathbf{5})$$

3.4.2 Determining the Activation Energy

The rate of dissociation is a first order rate process with respect to the dissociation rate constant, k_{d1}. The value of k_{d1} can be determined using equation **6**, where $[BnVd]_0$ is the initial concentration and $[BnVd]_t$ is the concentration after heating for time t.

$$ln\frac{[BnVd]_t}{[BnVd]_0} = -k_{d1} \cdot t \qquad (\mathbf{6})$$

Once k_{d1} is obtained for various temperatures, a rearranged versions of equation **1** (equation **7**) and equation **2** (equation **8**) can be used to determine the activation energy (E_a), frequency factor (*A*), enthalpy of activation ($\Delta H^{\ddagger}$), and entropy of activation ($\Delta S^{\ddagger}$).

$$ln(k_{d1}) = \frac{-E_a}{R} \cdot \frac{1}{T} + ln(A) \qquad (\mathbf{7})$$

$$ln\left(\frac{k_{d1}}{T}\right) = \frac{-\Delta H^{\ddagger}}{R} \cdot \frac{1}{T} + ln\left(\frac{k_B}{h}\right) + \frac{\Delta S^{\ddagger}}{R} \qquad (\mathbf{8})$$

3.4.3 Selected N-Alkoxyamines

In 2000, an in-depth study of the factors that affected the C-ON bond homolysis of various *N*-alkoxyamines derived from nitroxide radicals was published by Marque *et al.*[147]. It was found that the E_a increases relative to the C-H bond energy of the corresponding R-H compound and for the same R substituent, cyclic nitroxides (**1.9**)

generally have larger values than acyclic nitroxides[151] (**1.7** and **1.8**). A summary of the E_a and k_d values for some *N*-alkoxyamines (**3.13**-**3.18**) are shown in **Table 3.4**.

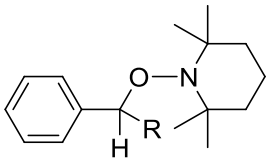

R = H **3.13**
R = Me **3.16**

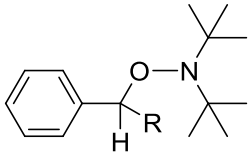

R = H **3.14**
R = Me **3.17**

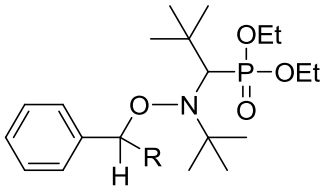

R = H **3.15**
R = Me **3.18**

Table 3.4: Summary of E_a and k_d for some *N*-alkoxyamines[147] in *tert*-butylbenzene.

Compound	E_a (kJmol^{-1})	k_d (393 K) x10^{-5} (s^{-1})
3.13	145.7	1.1
3.14	134.6	33
3.15	136.4	19
3.16	133.0	52
3.17	124.5	550
3.18	121.8	1400

This abbreviated data series shows that there is a decrease in E_a upon the addition of a methyl group at the carbon atom in the C-ON bond of the *N*-alkoxyamines. This change is accompanied by an increase in the value of k_d by at least an order of magnitude with the exception of **3.18** which increased by two orders of magnitude compared to **3.15**.

3.4.4 Selected N-Alkylated Tetrazines

In 2009, early work into the C-N bond strength of tetrazines based on verdazyl radicals was performed by Lukkarila[139]. A series of tetrazines (**3.19**-**3.22**) having a 1-

phenylethyl group at the N5 position were examined where substituents at the C6, N2, and N4 positions were varied. A summary of their E_a and k_d are given in **Table 3.5**.

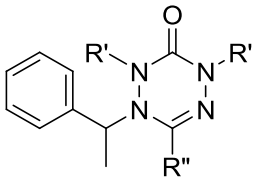

R = Me, R" = H **3.19**
R = Me, R" = Et **3.20**
R = Me, R" = Ph **3.21**
R = Ph, R" = Ph **3.22**

Table 3.5: Summary of E_a and k_d of *N*-(1-phenylethyl) tetrazines[139] in toluene.

Compound	E_a (kJmol^{-1})	k_d (393 K) x10^{-5} (s^{-1})
3.19	129	270
3.20	129	520
3.21	134	260
3.22	158	7.4

From this table, it is observed that the substituents at the C6 position had little impact on the k_d, but the substituents at the N2 and N4 positions had a much more dramatic impact. The compounds bearing methyl substituents at N2 and N4 have higher k_d and lower E_a values compared to the one with phenyl substituents. Compounds **3.19**-**3.21** were observed to have similar E_a and k_d values compared to *N*-alkoxyamines bearing a 1-phenylethyl group. The phenyl substituents at the N2 and N4 positions in **3.22** are thought to either make it more difficult for the molecule to obtain an appropriate conformation required for homolysis of the C-N bond or that the phenyl group of the (1-phenylethyl) unit at the N5 position interacts with the phenyl rings at the N4 position through a π-π stacking interaction leading to stabilization of the compound which results in an increase in E_a[139].

3.4.5 UV-Visible Spectroscopy Method

Previous methods for determining rate constants for the decomposition of alkoxyamines have used a quantitative ^{1}H NMR approach[152], detection of the released nitroxide by HPLC-UV detection[153], and a quantitative EPR method utilizing galvinoxyl radical[154] or oxygen[155] as a radical trap for the carbon-centered radical. ^{1}H NMR was not possible for this study as the overlap of peaks in the spectrum would have made it difficult to follow only one for the measurement of the disappearance of the tetrazine. HPLC-UV was not possible as there was a lack of instruments available. EPR spectroscopy was also explored, but tests involving **3.7** could not demonstrate the trapping of benzyl radicals by O_2 with the tandem release of **3.8**.

The method that was finally used to monitor species in solution was UV-Visible spectroscopy with *tert*-butylbenzene as an inert solvent. This method is applicable to the study of verdazyl radicals and their N-alkylated derivatives chiefly due to the high ε (≥ 2000 at λ_{max}) associated with these compounds compared to **1.9** (~10.5 at 469 nm); **1.9** can be applied in a high excess in relation to the tetrazine since the absorbance due to **1.9** has little effect on the absorbance readings (at the wavelengths of interest) of **3.7** and **3.8**. The UV-Vis spectrum of the alkoxyamine, **3.13**, was recorded and found to have negligible absorbance at wavelengths >300 nm. In addition, this method required that the species generated in solution do not interact with each other and the values for the ε for each species are known at their specific wavelengths. Utilizing this information, it was possible to apply linear algebra[156] to determine the concentrations of the tetrazine and verdazyl radical.

3.4.6 Experiment Preparation and Sample Acquisition for the Kinetic Studies

A 25 mL sample of known concentration was prepared and placed into a 50 mL two neck round bottom flask. It was fitted with a septum and condenser and then placed under Argon (Ar). Freeze-pump-thaw was performed four times on the sample before being placed under Ar. The sample was placed into a silicone oil bath at a desired temperature. The system was allowed ~5 min for the solution in the flask to reach the temperature of the oil bath.

Samples (1.5 mL) were removed at the desired times with a syringe and needle that were filled with Ar (taking care not to introduce oxygen into the flask). Immediately after removal of a sample it was placed into a test tube, frozen in liquid nitrogen, covered, and stored in a freezer (-20°C). After sufficient amount of time had passed to collect five data points, the run was terminated, and the UV-Vis spectra were collected at room temperature.

3.4.7 UV-Visible Data Processing

The UV-Vis spectra were recorded on a Perkin-Elmer Lambda 1050 instrument. The spectra for the kinetic studies of compound **3.7** were collected from 300-850 nm and **3.7.Ru(hfac)$_2$** were collected from 300-1300 nm. The spectra were processed using Excel. Corrections were applied to the spectra by subtracting the background, subtracting the spectrum of *tert*-butylbenzene containing no analyte at the temperature of the experiment, and having the spectrum set to zero for the range in which there is no absorbance which is 700-800 nm for **3.7** (**Figure 3.6**) and 1220-1300 nm for **3.7.Ru(hfac)$_2$**.

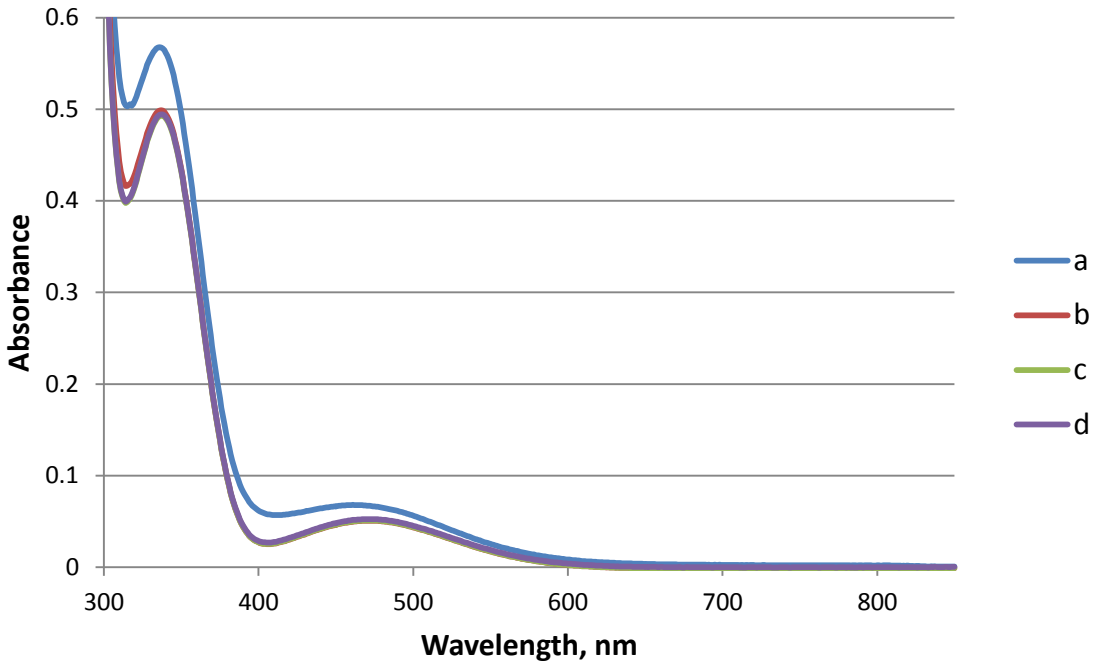

Figure 3.6: Corrections applied to a spectrum of **3.7** at 150°C (a) original spectrum, (b) blank correction, (c) *tert*-butylbenzene at 150°C correction, and (d) setting 700-800 nm to zero.

There is a noticeable decrease in the absorbance value at 338 nm in **Figure 3.6** from 0.5664 (a) to 0.4984 (b). Further corrections have a much less dramatic effect by changing the absorbance reading to 0.4929 (c) and 0.4944 (d). This method of correcting was applied to all the spectra for the homolysis of **3.7**.

3.4.8 Kinetic Data Analysis

To collect data necessary for the study of the kinetics, **3.7** was measured at three different temperatures (130, 140, and 150°C) and **3.7.Ru(hfac)$_2$** was measured at three lower temperatures (110, 120, and 130°C). A minimum of three trials at each temperature were collected for each compound.

Figure 3.7 demonstrates the change in the UV-Vis spectra for compound **3.7** over the course of one homolysis experiment performed at 150°C. There is a decrease in the amount of **3.7** (~340 nm) and an increase in **3.8** (~410 nm). There is a noticeable change in the appearance of the spectrum at ~500 nm occurring at t = 2455 s and 2912 s; this is a result of the decomposition of TEMPO (**1.9**) due to oxygen entering the system leading to a higher reading of the [**1.9**]. For this reason, the values determined at these times are unreliable and will not be used in the determination of the dissociation constant.

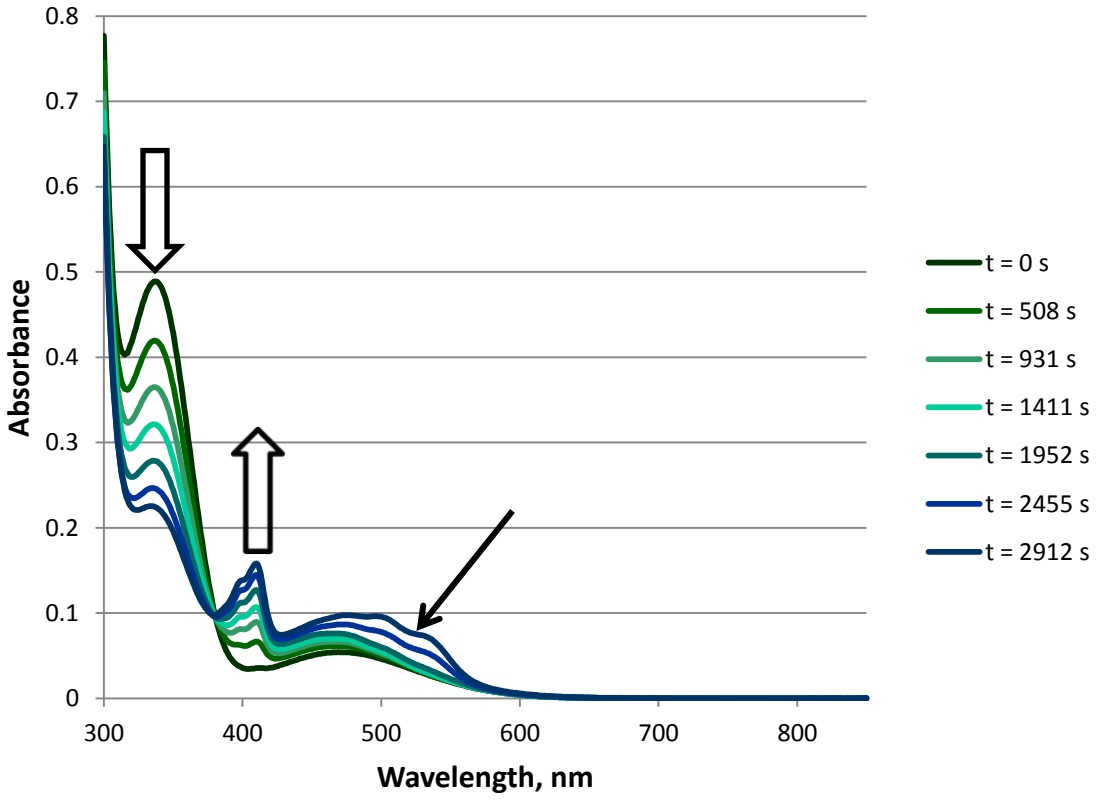

Figure 3.7: UV-Vis spectra of **3.7** with **1.9** as a scavenger at 150°C for time 0 s, 508 s, 931 s, 1411 s, 1952 s, 2455 s, and 2912 s.

The application of linear algebra allows for the determination of the [**3.7**] and [**3.8**] during the experiment and is plotted for the appropriate times in **Figure 3.8**. The values of [**3.7**]+[**3.8**] was determined through the summation of the two concentrations. The [**3.7**] is decreasing while the [**3.8**] is increasing which is as expected for the homolytic cleavage of the C-N bond in the tetrazine molecule. The sum of [**3.7**] and [**3.8**] is nearly constant illustrating that this method is reliable in the determination of each species.

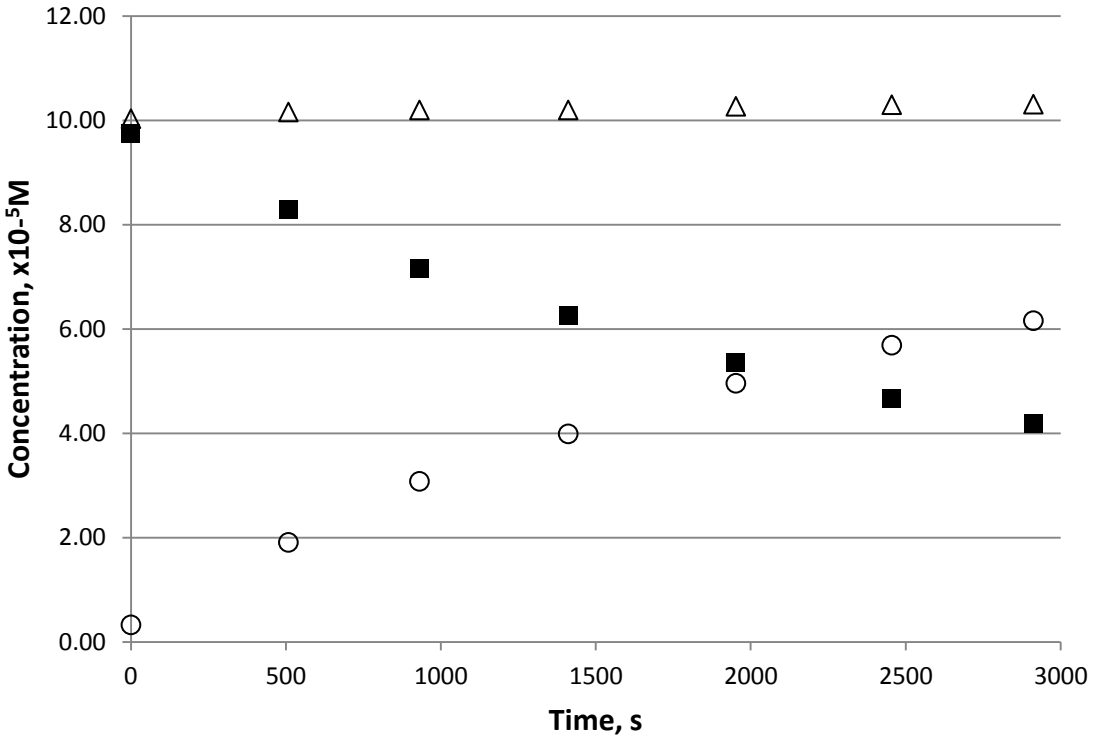

Figure 3.8: Plot of the change in the [**3.7**] ■, [**3.8**] ○, and [**3.7**]+[**3.8**] △ during the course of the experiment.

Figure 3.9 demonstrates the first-order plot of **3.7** at 150°C according to equation **6**. When a line of best fit is allowed, there is a strong correlation (R^2 = 0.998) and the value for k_d is 3.07x10^{-4} s^{-1}. When the intercept is set to zero, there is a strong correlation (R^2 = 0.998) and the value for k_d is 3.12x10^{-4} s^{-1}.

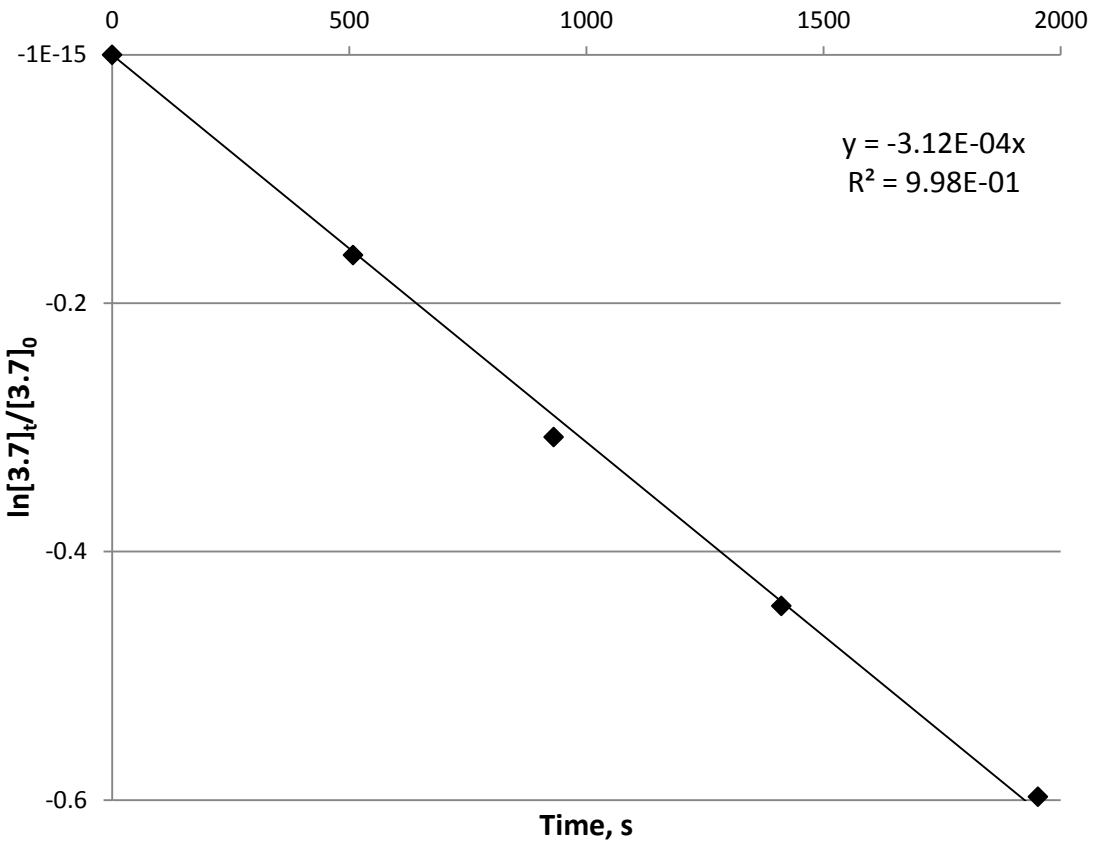

Figure 3.9: First-order plot of **3.7** at 150°C according to equation **6** (intercept set to zero).

3.4.9 Results

The k_d values obtained from the first order plots (line of best fit) of **3.7** and **3.7.Ru(hfac)$_2$** were used to generate the Arrhenius and Eyring plots of the C-N bond homolysis and are shown in **Figures 3.10** and **3.11**, respectively. A summary of the data for these compounds is given in **Table 3.6**.

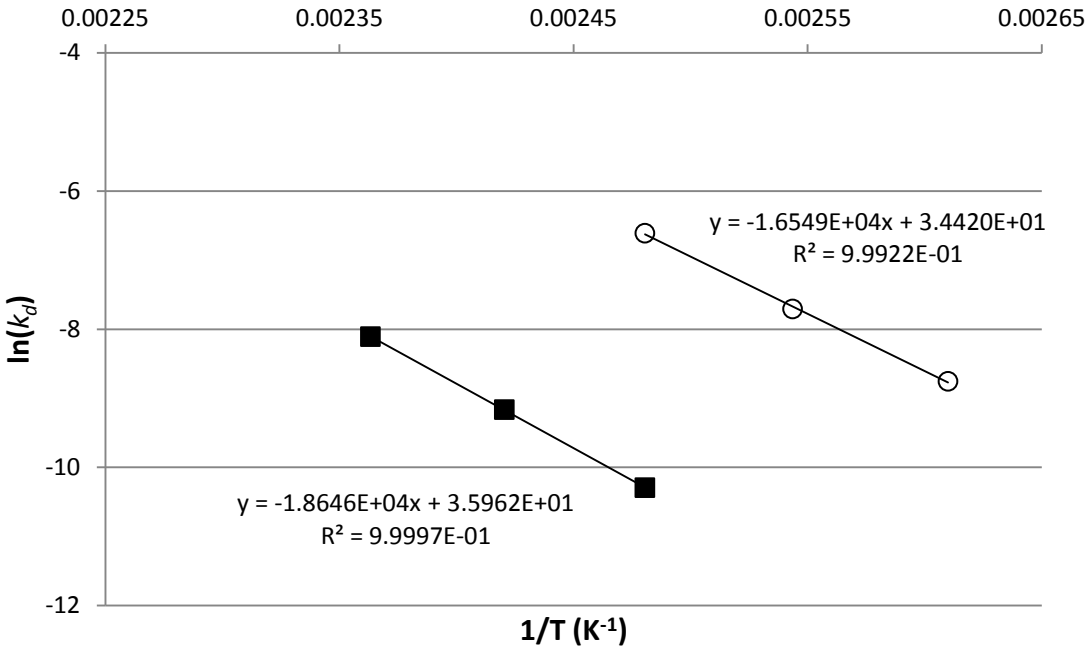

Figure 3.10: Arrhenius plot for the bond dissociation of **3.7** ■ and **3.7.Ru(hfac)$_2$** ○.

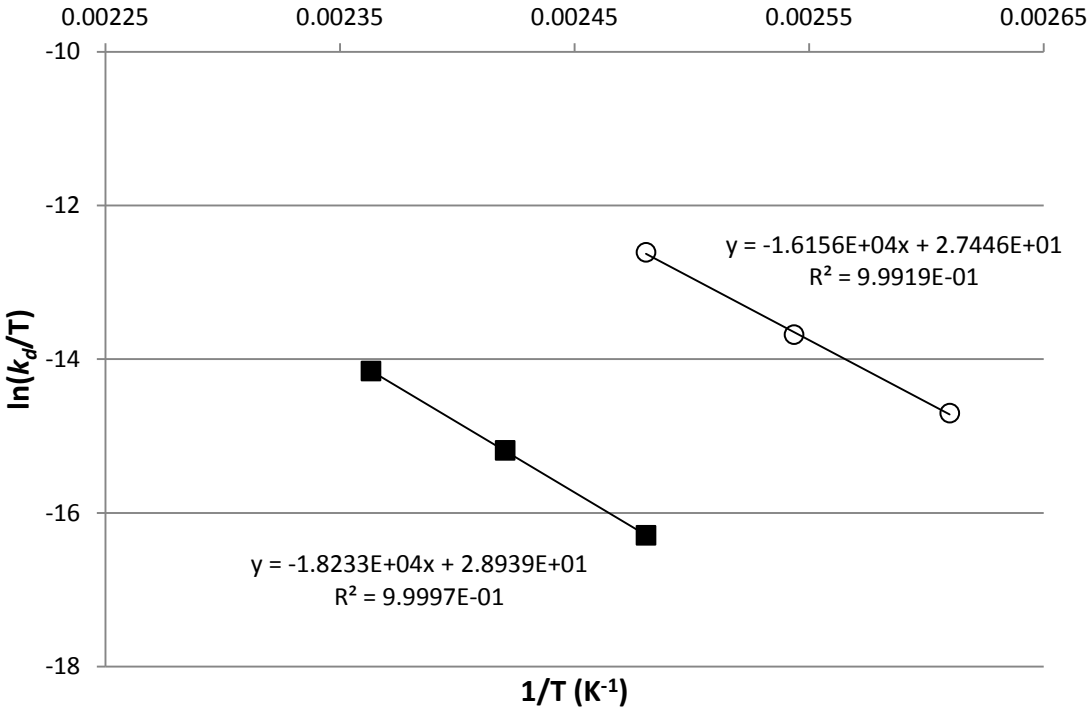

Figure 3.11: Eyring plot for the bond dissociation of **3.7** ■ and **3.7.Ru(hfac)$_2$** ○.

Table 3.6: Summary of data for the C-N bond homolysis of **3.7** and **3.7.Ru(hfac)$_2$** in *tert*-butylbenzene.

Compound	k_d (393 K) x10^{-5} (s^{-1})	E_a (kJmol^{-1})	A x10^{14} (s^{-1})	$\Delta H^{\ddagger}$ (kJmol^{-1})	$\Delta S^{\ddagger}$ (Jmol^{-1}K^{-1})
3.7	1.05 ± 0.03[a]	155 ± 2	42 ± 30	152 ± 2	43 ± 5
3.7.Ru(hfac)$_2$	45 ± 1	138 ± 2	9 ± 6	134 ± 2	31 ± 5

[a]determined for 393 K using the Arrhenius plot

3.4.10 Comments

The tetrazine, **3.7**, demonstrated both higher E_a (155 kJmol^{-1}) and A (4.2x10^{15} s^{-1}) values compared to the alkoxyamine, **3.13**, and the tetrazines, **3.19**-**3.21**. Yet, the k_d value at 393 K for **3.7** (1.1x10^{-5} s^{-1}) is the same (within error) as **3.13** (1.1x10^{-5} s^{-1}) while much lower than **3.19**-**3.21** (~3x10^{-3} s^{-1}). The higher k_d values for **3.19**-**3.22** are expected as there is greater steric bulk at the carbon atom of the C-N bond being investigated. Increasing the steric bulk at this position is known to decrease E_a and increase k_d.

3.7 demonstrated higher E_a and A values compared to **3.7.Ru(hfac)$_2$**; this resulted in **3.7** having a lower k_d (1.1x10^{-5} s^{-1} at 393 K) compared to **3.7.Ru(hfac)$_2$** (45x10^{-5} s^{-1} at 393 K). The complex, **3.7.Ru(hfac)$_2$**, had a k_d value which is nearly 40 times greater than for **3.7**. The E_a was calculated to be 17 kJmol^{-1} lower in **3.7.Ru(hfac)$_2$** compared to **3.7**.

Considering the small number of compounds in this data set, it is difficult to draw conclusions as to the reason for the differences between **3.7** and **3.7.Ru(hfac)$_2$**. A computation analysis of the energy levels of the two compounds may reveal the nature of the weakened C-N bond in the coordinated tetrazine ligand. Steric effects from the metal centre in **3.7.Ru(hfac)$_2$** causing the decrease in E_a are almost certainly not the

case as the metal is located on the opposite side of the molecule to where fragmentation of the C-N bond is occurring. The lower $\Delta H^{\ddagger}$ value of **3.7.Ru(hfac)$_2$** (134 kJmol^{-1}) illustrates that the transition state more closely resembles **1.29** compared to the resemblance of **3.7** (151 kJmol^{-1}) to **3.8**. This is a possible explanation for the decrease in E_a as the tetrazine that is coordinated to the ruthenium centre in **3.7.Ru(hfac)$_2$** is already in much the same geometry as the coordinated verdazyl in **1.29**. The role that the electronics of the metal portion plays into changing E_a and k_d can be further explored with the use of other metal centres (Fe, Ni, etc.) and the replacement of the highly electron withdrawing hfac ligands with acac or other lesser electron withdrawing ligands.

3.5 Conclusions

This work expands on the library of N-alkylated tetrazines based on verdazyl radicals by including an example of one based on the isopropyl 6-oxoverdazyl radicals (**3.7**) and the first example of a tetrazine-metal complex (**3.7.Ru(hfac)$_2$**). These compounds were fully characterized in terms of their structure, spectroscopic, and electrochemical properties. The C-N bond strength was probed to investigate the role that metal complexation has on the E_a and k_d values of **3.7.Ru(hfac)$_2$** compared to the uncoordinated ligand, **3.7**.

Examining the crystal structures of **3.7** and **3.7.Ru(hfac)$_2$**, these molecules are seen to be structurally dissimilar to **3.8** and **1.29**, respectively. Meanwhile, the lengths of most bonds in **3.7** are nearly unchanged when compared to **3.7.Ru(hfac)$_2$**. The UV-

Visible spectra of **3.7** and **3.7.Ru(hfac)$_2$** did not have the low energy transitions that were present in **3.8** and **1.29**. The N-benzylated tetrazine compounds were explored in terms of electrochemistry by CV and it was found that the reduction was at a lower potential and the oxidation at a higher potential compared to the respective radical compounds.

3.7 and **3.7.Ru(hfac)$_2$** were investigated further to determine the effect that metal complexation has on the C-N bond strength of the tetrazine. This required the development of a means for analyzing the kinetic data. A UV-Vis spectroscopy-based method and linear algebra were used to determine the concentration of tetrazine and verdazyl radical in solution. It was found that upon complexation to Ru(hfac)$_2$, there is a noticeable decrease in E_a (~17 kJmol^{-1}) and a corresponding increase in k_d (~40 times). While the true nature of this effect is still unknown, it demonstrates the potential of using metal centres in tuning the properties of the tetrazine moiety that is coordinated to the metal. This ability to tune the radical-type properties that are important for SFRP showcases the richness that verdazyl radicals will be able to offer over other systems that have previously been explored.

3.6 Experimental

3.6.1 Materials and Methods

1,5-Diisopropyl-3-pyridin-2-yl-6-oxoverdazyl[118] and [1,5-diisopropyl-3-(2-pyridyl)-6-oxoverdazyl]bis(hexafluoroacetylacetonato)ruthenium[94] were synthesized using literature methods. All solvents and reagents were purchased from Aldrich and used as received without further purification unless otherwise stated. DCM and *tert*-butylbenzene were purified according to the Purification of Laboratory Chemicals (Fifth Edition)[157].

^{1}H, ^{13}C, and ^{19}F NMR spectra were recorded on a Bruker AC300 (300 MHz), AC360 (360 MHz), and AC500 (500 MHz) instruments. The general procedures are as outlined in section 2.6.1.

5-Benzyl-2,4-diisopropyl-6-(pyridin-2-yl)-4,5-dihydro-1,2,4,5-tetrazin-3(2H)-one (3.7)

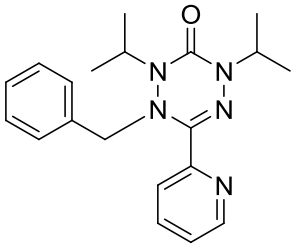

An oven dried side-arm rbf (100 mL) was flushed with Ar and to this flask was added dry, degassed DCM (30 mL). Benzyl bromide (0.15 mL, 1.2 mmol) and 1,5-diisopropyl-3-pyridin-2-yl-6-oxoverdazyl (287 mg, 1.10 mmol) were added. The solution was sparged with Ar for 30 min. A further dry, degassed DCM (10 mL) was added. $Mn_2(CO)_{10}$ (218 mg, 0.56 mmol) was added under Ar. The rbf was placed into a light box containing 6 full spectrum light bulbs and fitted with a condenser making sure to exclude air. It was stirred in the light box for 24 h after which a dark coloured solution was obtained.

The rbf was removed from the light box and DBU (0.33 mL, 2.2 mmol) was added. After 2 h, the solvent was removed *in vacuo* and the resulting black solid was stirred with Et_2O (70 mL) for 1 h. The Et_2O was collected and this process was repeated another 3 times. The Et_2O was combined with H_2O (50 mL) and extracted with 10% HCl (5X20 mL). The organic layer was discarded. The aqueous layer was washed with Et_2O (100 mL) and the organic layer was discarded. The aqueous layer was basified using a 2 M NaOH solution until pH 14 was reached and was extracted with Et_2O (4X100 mL). The organic layer was washed with H_2O until a neutral pH was reached and then it was stored on $MgSO_4$ overnight. The solvent was evaporated yielding a light tan product (220 mg, 56.8%). ^{1}H NMR (500 MHz, DCM-d_2, 250 K): δ 8.71 (d, 1H, J = 8 Hz), 7.99 (d, 1H, J = 8 Hz), 7.79 (td, 1H, J = 8,2 Hz), 7.36 (ddd, 1H, J = 7,5,1 Hz), 7.28-7.20 (m, 3H), 7.15-7.10 (m, 2H), 4.32 (sept, 1H, J = 7 Hz), 4.32 (d, 1H, J = 15 Hz), 4.00 (sept, 1H, J = 7 Hz), 3.96 (d, 1H, J = 15 Hz), 1.34 (d, 3H, J = 7 Hz), 1.03 (d, 3H, J = 7 Hz), 1.02 (d, 3H, J = 7 Hz), 0.65 (d, 3H, J = 7 Hz) ppm. ^{13}C NMR (500 MHz, DCM-d_2, 250 K): δ 156.5, 149.8, 149.7, 147.3, 136.8, 135.8, 129.5, 128.3, 128.0, 124.3, 122.8, 59.6, 52.6, 47.1, 20.8, 20.0, 19.7, 19.6 ppm. FT-IR (KBr): 3050 (w), 3032 (w), 2977 (m), 2963 (m), 2873 (w), 1675 (s), 1607 (m), 1582 (m), 1566 (m), 1474 (m), 1456 (m), 1435 (m), 1381 (s), 1361 (s), 1338 (m), 1317 (m), 1200 (m), 1180 (m), 1138 (m), 1043 (m), 966 (w), 826 (w), 790 (m), 747 (m), 706 (s), 670 (m), 608 (m) cm^{-1}. UV-Vis (MeCN): λ_{max} 258 nm (ε = $1.0x10^4$ $L{\cdot}mol^{-1}{\cdot}cm^{-1}$), 332 nm (ε = $4.8x10^3$ $L{\cdot}mol^{-1}{\cdot}cm^{-1}$). MS (ESI): *m/z* LR-MS 352 ($M+H^+$, 100%), HR-MS: theor 352.2132, expt 352.2130 ($M+H^+$, 100%). MP: 85-88°C (decomposition).

[5-Benzyl-2,4-diisopropyl-6-(pyridin-2-yl)-4,5-dihydro-1,2,4,5-tetrazin-3(2H)-one]bis(hexafluoroacetylacetonate)ruthenium(II) (3.7.Ru(hfac)$_2$)

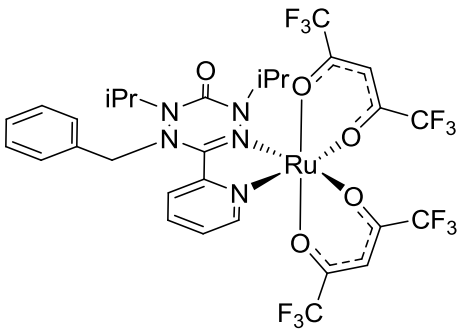

An oven dried side-arm rbf (100 mL) was flushed with Ar and to this flask was added dry, degassed DCM (40 mL). Benzyl bromide (0.22 mL, 0.176 mmol) and [1,5-diisopropyl-3-(2-pyridyl)-6-oxoverdazyl]bis(hexafluoroacetylacetonato)ruthenium (137 mg, 0.176 mmol) were added to the rbf. The solution was sparged with Ar for 30 min. A further dry, degassed DCM (10 mL) was added. $Mn_2(CO)_{10}$ (35 mg, 0.090 mmol) was added under Ar. It was placed into a light box containing 6 full spectrum light bulbs and fitted with a condenser while making sure to exclude air. It was stirred in the light box for 24 h after which a dark red solution was obtained.

It was removed from the light box and the solvent was removed *in vacuo*. Column chromatography of the dark red solid was performed (SiO_2; DCM:hexanes, 1:1) which yielded a major red fraction. The solvent was removed *in vacuo* and the product was dissolved in a minimal amount of hexanes and left to evaporate. Dark red crystals were obtained (130 mg, 84.9%) which were suitable for X-ray crystallography. ^{1}H NMR (300 MHz, DCM-d_2, 298 K): δ 8.36 (mult, 2H), 7.60-7.71 (mult, 4H), 7.13-7.27 (mult, 12H), 6.23 (s, 1H), 6.22 (s, 1H), 6.12 (s, 1H), 6.06 (s, 1H), 4.29-4.49 (mult, 7H), 3.44 (sept, 1H, J = 7 Hz), 1.46 (d, 3H, J = 8 Hz), 1.45 (d, 3H, J = 8 Hz), 1.32 (d, 3H, J = 7 Hz), 1.20 (d, 3H, J = 7 Hz), 1.06 (d, 3H, J = 7 Hz), 1.02 (d, 3H, J = 7 Hz), 1.02 (d, 3H, J = 7 Hz), 0.94 (d, 3H, J = 7

Hz) ppm. ^{13}C NMR (360 MHz, DCM-d_2, 298 K): δ 175.2 (q, $^2J_{CF}$ = 34 Hz), 174.6 (q, $^2J_{CF}$ = 34 Hz), 173.7 (q, $^2J_{CF}$ = 34 Hz), 173.5 (q, $^2J_{CF}$ = 34 Hz), 172.4 (q, $^2J_{CF}$ = 34 Hz), 171.3 (q, $^2J_{CF}$ = 34 Hz), 170.2 (q, $^2J_{CF}$ = 34 Hz), 170.2 (q, $^2J_{CF}$ = 34 Hz), 155.2, 155.1, 154.6, 154.2, 152.9, 151.6, 151.5, 151.5, 136.4, 136.2, 133.9, 133.7, 131.0, 130.8, 129.3, 129.1, 125.0, 125.0, 124.8, 124.5, 117.6 (q, $^1J_{CF}$ = 283 Hz), 117.5 (q, $^1J_{CF}$ = 283 Hz), 117.4 (q, $^1J_{CF}$ = 283 Hz), 116.9 (q, $^1J_{CF}$ = 283 Hz), 116.8 (q, $^1J_{CF}$ = 283 Hz), 116.5 (q, $^1J_{CF}$ = 283 Hz), 116.3 (q, $^1J_{CF}$ = 283 Hz), 92.8, 92.4, 92.2, 62.0, 61.8, 56.9, 56.2, 51.9, 51.6, 21.6, 21.0, 20.7, 20.3, 19.3, 19.1 ppm. ^{19}F NMR (360 MHz, DCM-d_2, 298 K): δ -74.86 (s, 3F), -74.94 (s, 3F), -75.10 (s, 3F), -75.22 (s, 3F), -75.24 (s, 3F), -75.34 (s, 6F), -75.39 (s, 3F) ppm. FT-IR (KBr): 2983 (w), 2940 (w), 1679 (s), 1570 (m), 1543 (m), 1514 (m), 1477 (m), 1402 (m), 1389 (m), 1333 (m), 1262 (s), 1205 (s), 1150 (s), 1094 (m), 1059 (m), 944 (w), 801 (w), 789 (w), 754 (m), 694 (m), 614 (w) cm^{-1}. UV-Vis (MeCN): λ_{max} 290 nm (ε = 2.5x10^4 L·mol^{-1}·cm^{-1}), 337 nm (ε = 6.4x10^3 L·mol^{-1}·cm^{-1}), 495 nm (ε = 1.2x10^4 L·mol^{-1}·cm^{-1}). MS (ESI): *m/z* LR-MS 867 (M^+, 100%), HR-MS: theor 867.08640, expt 867.08665 (M^+, 100%). Anal. Calc. for $C_{30}H_{27}N_5O_5F_{12}Ru$: C, 41.58; H, 3.14; N, 8.08. Found: C, 41.42; H, 3.20; N, 8.18. MP: 138-140°C (decomposition begins ~60°C).

CHAPTER 4

CONCLUSIONS AND FUTURE WORK

Stable organic radicals were initially realized and experimentally confirmed slightly over a hundred years ago and since that time many uses of these compounds have been explored: spin labeling, molecular magnetism, organic batteries, and many more. Verdazyl radicals, the main focus of this thesis, were discovered in 1963 and have had much of their fundamental chemistry explored. The first example of coordination chemistry involving a verdazyl radical appeared under 20 years ago, but has received much attention leading to many varieties of radical ligands and metal centres being explored. The work presented herein expands on two aspects of metal-verdazyl coordination chemistry that had not yet been investigated: the *N*,*N'*-diphenyl verdazyls as ligands, and the activation energy of the C-N bond in tetrazines and ruthenium-tetrazine compounds.

The objective of chapter 2 was to explore the coordination chemistry of new types of verdazyl radicals. The challenges associated with the synthesis of the 6-oxoverdazyl, **2.3**, resulted from the inability to synthesize the tetrazane precursor via modified literature procedures, but was accomplished after having viewed tetrazanes as aminals which are analogous to acetals. The *N*,*N'*-diphenyl verdazyls were successfully synthesized and coordination to palladium was performed.

The new metal complexes, **2.2.PdCl$_2$** and **2.3.PdCl$_2$**, are different than the more common metal-verdazyl complexes containing *N*,*N'*-dialkyl-6-oxoverdazyls. Metal complexes of the *N*,*N'*-diphenyl verdazyls have increased steric bulk at the N1 and N5 positions, the verdazyl core of the ligand in **2.2.PdCl$_2$** was able to bind tighter to palladium than the 6-oxoverdazyls and as a result it exhibited non-negligible spin density on Pd. The EPR spectra of the metal complexes demonstrated a small increase in the g-value relative to the free ligands which is characteristic of coordination of verdazyls to palladium. The electrochemistry of these new compounds was explored by the use of CV. The CVs of the free ligands and palladium-verdazyl complexes were collected and the palladium-verdazyl complexes demonstrated a positive increase in both the reduction and oxidation potentials compared to the values of the free ligands which is attributed to the presence of the electropositive palladium atom.

Future work in the area of metal-verdazyl complexes could involve the exploration of other metal centres and various other verdazyl radicals altered at the C3, C6, N1, and N5 positions. The tridentate ligands (**4.1**) having 2-pyridyl substituents at the C3 and N5 positions will allow for many new compounds to be explored. The study of the properties associated with asymmetric 6-oxoverdazyl radicals (**4.2**) bearing alkyl and aryl substituents at the N1 and N5 positions and their metal complexes is currently an understudied area of the chemistry of verdazyl radicals.

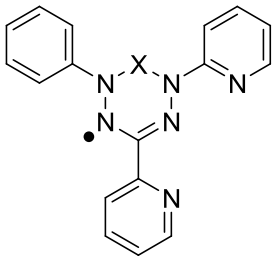

X = CH_2, CO **4.1**

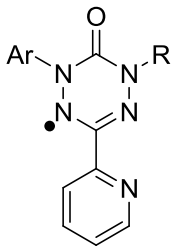

4.2

The objectives of chapter 3 were the synthesis and study of the properties of a tetrazine, **3.7**, and its ruthenium complex, **3.7.Ru(hfac)$_2$**. The synthesis of these two new compounds involved the use of dimanganese decacarbonyl and benzyl bromide to form a new C-N bond between the stable radical and a photogenerated benzyl radical. Crystal structures of these molecules were obtained and the tetrazines exhibited localized single and double bonds and a loss of planarity in the heterocycle compared to the radicals **3.8** and **1.29**. UV-Vis spectroscopy of **3.7** and **3.7.Ru(hfac)$_2$** did not have the lower energy absorptions that were present in the radical species. The CVs of **3.7** and **3.7.Ru(hfac)$_2$** showcased the reduction becoming an irreversible event and the oxidation moving to a higher potential compared to their respective radical compounds.

Investigation into the C-N bond strength of these compounds was performed by determining the E_a associated with each compound. This required the development of an analysis method by UV-Visible spectroscopy for the determination of the concentration of the tetrazine and verdazyl in solution. The k_d value at 393 K for the uncoordinated tetrazine, **3.7**, was determined by the Arrhenius equation, it was found to be comparable to the value for the alkoxyamine, **3.13**, and ~100 times less than tetrazines, **3.19**-**3.22**, which had the bulkier 1-phenylethyl substituent. In the

coordination compound, **3.7.Ru(hfac)$_2$**, the E_a of the C-N bond was decreased by ~17 kJmol^{-1} and k_d was increased by ~40 times relative to the uncoordinated **3.7**. The reason for the increase of k_d caused by the complexation of **3.7** to Ru(hfac)$_2$ is not yet fully understood, but is a significant development in the 'radical' chemistry of metal-verdazyl complexes.

The future work of this project could involve the development of a library of tetrazine and tetrazine-metal compounds (similar to what has been done for alkoxyamines based on nitroxides). This will allow for investigating the role that structure and electronics has on the strength of the C-N bond in tetrazines. Other metal centres, such as iron, need to be investigated to determine if the results for **3.7.Ru(hfac)$_2$** were specific to ruthenium. The ancillary ligands surrounding the metal can be changed to probe their role in the C-N bond strength of the metal-tetrazine complexes. Computation studies are required in regards to the electronic structure of the tetrazine-metal and verdazyl-metal complexes to help explain its role in the C-N bond strength. Overall, a greater understanding of the effect that structural changes have on the E_a and k_d will come with altering many portions of the molecule **4.3**.

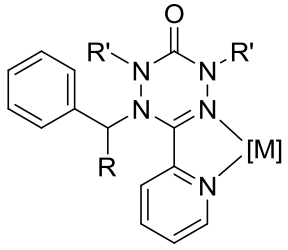

4.3

REFERENCES

1. Hicks, R. G. *Org. Biomol. Chem.* 2007, *5*(9), 1321.
2. Griller, D.; Ingold, K. U. *Acc. Chem. Res.* 1976, *9*(1), 13.
3. Gomberg, M. *J. Am. Chem. Soc.* 1900, *22*(11), 757.
4. McBride, J. M. *Tetrahedron* 1974, *30*(14), 2009.
5. McCormick, M. L.; Adriaens, P. *Environ. Sci. Technol.* 2004, *38*(4), 1045.
6. Khachatryan, L.; Vejerano, E.; Lomnicki, S.; Dellinger, B. *Environ. Sci. Technol.* 2011, *45*(19), 8559.
7. Gaudiano, G.; Koch, T. H. *Chem. Res. Toxicol.* 1991, *4*(1), 2.
8. Hyodo, F.; Matsumoto, K.-i.; Matsumoto, A.; Mitchell, J. B.; Krishna, M. C. *Cancer Res.* 2006, *66*(20), 9921.
9. Nishide, H.; Suga, T. *Electrochem. Soc. Interface* 2005, *14*(4), 32.
10. Qu, J.; Katsumata, T.; Satoh, M.; Wada, J.; Igarashi, J.; Mizoguchi, K.; Masuda, T. *Chem. Eur. J.* 2007, *13*(28), 7965.
11. Nishide, H.; Oyaizu, K. *Science* 2008, *319*(5864), 737.
12. Bowry, V. W.; Lusztyk, J.; Ingold, K. U. *J. Am. Chem. Soc.* 1989, *111*(5), 1927.
13. Bowry, V. W.; Lusztyk, J.; Ingold, K. U. *J. Am. Chem. Soc.* 1991, *113*(15), 5687.
14. Starnes, W. H. *J. Vinyl Add. Tech.* 2012, *18*(2), 71.
15. Piloty, O.; Schwerin, B. G. *Ber. Dtsch. Chem. Ges.* 1901, *34*, 1870.
16. Wieland, H.; Offenbächer, M. *Ber. Dtsch. Chem. Ges.* 1914, *47*(2), 2111.
17. Meyer, K. H.; Reppe, W. *Ber. Dtsch. Chem. Ges.* 1921, *54*(2), 327.
18. Osiecki, J. H.; Ullman, E. F. *J. Am. Chem. Soc.* 1968, *90*(4), 1078.
19. Ullman, E. F.; Call, L.; Osiecki, J. H. *J. Org. Chem.* 1970, *35*(11), 3623.
20. Hayat, H.; Silver, B. L. *J. Phys. Chem.* 1973, *77*(1), 72.

21. Ingold, K. U.; Adamic, K.; Bowman, D. F.; Gillan, T. *J. Am. Chem. Soc.* 1971, *93*(4), 902.

22. Bowman, D. F.; Brokenshire, J. L.; Gillan, T.; Ingold, K. U. *J. Am. Chem. Soc.* 1971, *93*(24), 6551.

23. Bowman, D. F.; Gillan, T.; Ingold, K. U. *J. Am. Chem. Soc.* 1971, *93*(24), 6555.

24. Grimaldi, S.; Finet, J.-P.; Zeghdaoui, A. In *ACS Polym. Prepr.* 1997; Vol. 38, p 651.

25. Grimaldi, S.; Finet, J.-P.; Le Moigne, F.; Zeghdaoui, A.; Tordo, P.; Benoit, D.; Fontanille, M.; Gnanou, Y. *Macromolecules* 2000, *33*(4), 1141.

26. Benoit, D.; Chaplinski, V.; Braslau, R.; Hawker, C. J. *J. Am. Chem. Soc.* 1999, *121*(16), 3904.

27. Hoffmann, A. K.; Henderson, A. T. *J. Am. Chem. Soc.* 1961, *83*(22), 4671.

28. Lebelev, O. L.; Kazarnovskii, S. N. *Zh. Obshch. Khim.* 1960, *30*, 1631.

29. Goldschmidt, S.; Schmidt, W. *Ber. Dtsch. Chem. Ges.* 1922, *55*(9), 3197.

30. Cook, C. D. *J. Org. Chem.* 1953, *18*(3), 261.

31. Müller, E.; Ley, K. *Z. Naturforsch., B: Chem. Sci.* 1953, *8*(b), 694.

32. Manner, V. W.; Markle, T. F.; Freudenthal, J. H.; Roth, J. P.; Mayer, J. M. *Chem. Commun.* 2008(2), 256.

33. Altwicker, E. R. *Chem. Rev.* 1967, *67*(5), 475.

34. Thomas, F. In *Stable Radicals*; John Wiley & Sons, Ltd: 2010, p 281.

35. Kuhn, R.; Trischmann, H. *Angew. Chem. Int. Ed.* 1963, *2*(3), 155.

36. Neugebauer, F. A.; Fischer, H. *Angew. Chem. Int. Ed.* 1980, *19*(9), 724.

37. Neugebauer, F. A.; Fischer, H.; Siegel, R.; Krieger, C. *Ber.* 1983, *116*(10), 3461.

38. Neugebauer, F. A.; Fischer, H.; Siegel, R. *Ber.* 1988, *121*(5), 815.

39. Milcent, R.; Barbier, G.; Capelle, S.; Catteau, J. P. *J. Heterocycl. Chem.* 1994, *31*(2), 319.

40. Hicks, R. G. In *Stable Radicals*; John Wiley & Sons, Ltd: 2010, p 245.

41. Neugebauer, F. A.; Siegel, R. *Angew. Chem. Int. Ed.* 1983, *22*(4), 320.

42. Ohnishi, S.-i.; McConnell, H. M. *J. Am. Chem. Soc.* 1965, *87*(10), 2293.

43. Janzen, E. G.; Blackburn, B. J. *J. Am. Chem. Soc.* 1968, *90*(21), 5909.

44. Janzen, E. G. *Acc. Chem. Res.* 1971, *4*(1), 31.

45. Fischer, H. *J. Am. Chem. Soc.* 1986, *108*(14), 3925.

46. Fischer, H. *Chem. Rev.* 2001, *101*(12), 3581.

47. Turek, P.; Nozawa, K.; Shiomi, D.; Awaga, K.; Inabe, T.; Maruyama, Y.; Kinoshita, M. *Chem. Phys. Lett.* 1991, *180*(4), 327.

48. Tamura, M.; Nakazawa, Y.; Shiomi, D.; Nozawa, K.; Hosokoshi, Y.; Ishikawa, M.; Takahashi, M.; Kinoshita, M. *Chem. Phys. Lett.* 1991, *186*(4–5), 401.

49. Miller, J. S.; Epstein, A. J. *Angew. Chem. Int. Ed.* 1994, *33*(4), 385.

50. Nakatsuji, S.; Anzai, H. *J. Mater. Chem.* 1997, *7*(11), 2161.

51. Otsu, T. *J. Polym. Sci., Part A: Polym. Chem.* 1956, *21*(99), 559.

52. Turner, S. R.; Blevins, R. W. *Macromolecules* 1990, *23*(6), 1856.

53. Georges, M. K.; Veregin, R. P. N.; Kazmaier, P. M.; Hamer, G. K. *Macromolecules* 1993, *26*(11), 2987.

54. Hodgson, J. L.; Namazian, M.; Bottle, S. E.; Coote, M. L. *J. Phys. Chem. A* 2007, *111*(51), 13595.

55. Manda, S.; Nakanishi, I.; Ohkubo, K.; Yakumaru, H.; Matsumoto, K.-i.; Ozawa, T.; Ikota, N.; Fukuzumi, S.; Anzai, K. *Org. Biomol. Chem.* 2007, *5*(24), 3951.

56. Bailey, W. F.; Bobbitt, J. M.; Wiberg, K. B. *J. Org. Chem.* 2007, *72*(12), 4504.

57. Lam, P. Y. S.; Vincent, G.; Clark, C. G.; Deudon, S.; Jadhav, P. K. *Tetrahedron Lett.* 2001, *42*(20), 3415.

58. Steuber, F. W.; Dimroth, K. *Ber.* 1966, *99*(1), 258.

59. Gilroy, J. B.; McKinnon, S. D. J.; Koivisto, B. D.; Hicks, R. G. *Org. Lett.* 2007, *9*(23), 4837.

60. Ochiai, E.-I. *J. Chem. Educ.* 1993, *70*(2), 128.

61. Jørgensen, C. K. *Coord. Chem. Rev.* 1966, *1*(1–2), 164.

62. Ward, M. D.; McCleverty, J. A. *J. Chem. Soc., Dalton Trans.* 2002(3), 275.

63. Ovcharenko, V. In *Stable Radicals*; John Wiley & Sons, Ltd: 2010, p 461.

64. Laugier, J.; Latour, J. M.; Caneschi, A.; Rey, P. *Inorg. Chem.* 1991, *30*(23), 4474.

65. Dickman, M. H.; Porter, L. C.; Doedens, R. J. *Inorg. Chem.* 1986, *25*(15), 2595.

66. Benelli, C.; Gatteschi, D.; Zanchini, C.; Doedens, R. J.; Dickman, M. H.; Porter, L. C. *Inorg. Chem.* 1986, *25*(19), 3453.

67. Caneschi, A.; Grand, A.; Laugier, J.; Rey, P.; Subra, R. *J. Am. Chem. Soc.* 1988, *110*(7), 2307.

68. Yoshida, T.; Kaizaki, S. *Inorg. Chem.* 1999, *38*(6), 1054.

69. Luneau, D.; Rey, P.; Laugier, J.; Belorizky, E.; Cogne, A. *Inorg. Chem.* 1992, *31*(17), 3578.

70. Oshio, H.; Watanabe, T.; Ohto, A.; Ito, T.; Ikoma, T.; Tero-Kubota, S. *Inorg. Chem.* 1997, *36*(14), 3014.

71. Fettouhi, M.; El Ali, B.; Morsy, M.; Golhen, S.; Ouahab, L.; Le Guennic, B.; Saillard, J.-Y.; Daro, N.; Sutter, J.-P.; Amouyal, E. *Inorg. Chem.* 2003, *42*(4), 1316.

72. Fegy, K.; Luneau, D.; Belorizky, E.; Novac, M.; Tholence, J.-L.; Paulsen, C.; Ohm, T.; Rey, P. *Inorg. Chem.* 1998, *37*(18), 4524.

73. Fegy, K.; Luneau, D.; Ohm, T.; Paulsen, C.; Rey, P. *Angew. Chem. Int. Ed.* 1998, *37*(9), 1270.

74. Sheldon, R. A.; Arends, I. W. C. E. *Adv. Synth. Catal.* 2004, *346*(9-10), 1051.

75. Sheldon, R. A.; Arends, I. W. C. E. *J. Mol. Catal. A: Chem.* 2006, *251*(1–2), 200.

76. Zhan, B.-Z.; Thompson, A. *Tetrahedron* 2004, *60*(13), 2917.

77. Whittaker, J. W. *Chem. Rev.* 2003, *103*(6), 2347.

78. Avigad, G.; Amaral, D.; Asensio, C.; Horecker, B. L. *J. Biol. Chem.* 1962, *237*(9), 2736.

79. Whittaker, M. M.; Whittaker, J. W. *J. Biol. Chem.* 1988, *263*(13), 6074.

80. Ito, N.; Phillips, S. E. V.; Yadav, K. D. S.; Knowles, P. F. *J. Mol. Biol.* 1994, *238*(5), 704.

81. Whittaker, M. M.; Kersten, P. J.; Cullen, D.; Whittaker, J. W. *J. Biol. Chem.* 1999, *274*(51), 36226.

82. Halfen, J. A.; Young, V. G.; Tolman, W. B. *Angew. Chem. Int. Ed.* 1996, *35*(15), 1687.

83. Halfen, J. A.; Jazdzewski, B. A.; Mahapatra, S.; Berreau, L. M.; Wilkinson, E. C.; Que, L.; Tolman, W. B. *J. Am. Chem. Soc.* 1997, *119*(35), 8217.

84. Zurita, D.; Scheer, C.; Pierre, J.-L.; Saint-Aman, E. *J. Chem. Soc., Dalton Trans.* 1996, *0*(23), 4331.

85. Zurita, D.; Gautier-Luneau, I.; Ménage, S.; Pierre, J. L.; Saint-Aman, E. *J. Biol. Inorg. Chem.* 1997, *2*(1), 46.

86. Itoh, S.; Takayama, S.; Arakawa, R.; Furuta, A.; Komatsu, M.; Ishida, A.; Takamuku, S.; Fukuzumi, S. *Inorg. Chem.* 1997, *36*(7), 1407.

87. Wang, Y.; Stack, T. D. P. *J. Am. Chem. Soc.* 1996, *118*(51), 13097.

88. Wang, Y.; DuBois, J. L.; Hedman, B.; Hodgson, K. O.; Stack, T. D. P. *Science* 1998, *279*(5350), 537.

89. Brook, D. J. R.; Lynch, V.; Conklin, B.; Fox, M. A. *J. Am. Chem. Soc.* 1997, *119*(22), 5155.

90. Hicks, R. G.; Koivisto, B. D.; Lemaire, M. T. *Org. Lett.* 2004, *6*(12), 1887.

91. Yakovenko, A. V.; Kolotilov, S. V.; Cador, O.; Golhen, S.; Ouahab, L.; Pavlishchuk, V. V. *Eur. J. Inorg. Chem.* 2009, *2009*(16), 2354.

92. Nakabayashi, K.; Ozaki, Y.; Kawano, M.; Fujita, M. *Angew. Chem. Int. Ed.* 2008, *47*(11), 2046.

93. Ozaki, Y.; Kawano, M.; Fujita, M. *Chem. Commun.* 2009(28), 4245.

94. McKinnon, S. D. J.; Patrick, B. O.; Lever, A. B. P.; Hicks, R. G. *Chem. Commun.* 2010, *46*(5), 773.

95. McKinnon, S. D. J.; Gilroy, J. B.; McDonald, R.; Patrick, B. O.; Hicks, R. G. *J. Mater. Chem.* 2011, *21*(5), 1523.

96. Barclay, T. M.; Hicks, R. G.; Lemaire, M. T.; Thompson, L. K. *Inorg. Chem.* 2001, *40*(22), 5581.

97. McKinnon, S. D. J., The University of Victoria, 2010.

98. Anderson, K. J.; Gilroy, J. B.; Patrick, B. O.; McDonald, R.; Ferguson, M. J.; Hicks, R. G. *Inorg. Chim. Acta* 2011, *374*(1), 480.

99. Barclay, T. M.; Hicks, R. G.; Lemaire, M. T.; Thompson, L. K. *Chem. Commun.* 2000, *0*(21), 2141.

100. Hicks, R. G.; Lemaire, M. T.; Thompson, L. K.; Barclay, T. M. *J. Am. Chem. Soc.* 2000, *122*(33), 8077.

101. Barclay, T. M.; Hicks, R. G.; Lemaire, M. T.; Thompson, L. K. *Inorg. Chem.* 2001, *40*(25), 6521.

102. Barclay, T. M.; Hicks, R. G.; Lemaire, M. T.; Thompson, L. K.; Xu, Z. *Chem. Commun.* 2002(16), 1688.

103. Koivisto, B. D.; Hicks, R. G. *Coord. Chem. Rev.* 2005, *249*(23), 2612.

104. Brook, D. J. R.; Richardson, C. J.; Haller, B. C.; Hundley, M.; Yee, G. T. *Chem. Commun.* 2010, *46*(35), 6590.

105. Brook, D. J. R.; Abeyta, V. *J. Chem. Soc., Dalton Trans.* 2002, *0*(22), 4219.

106. Gilroy, J. B.; Koivisto, B. D.; McDonald, R.; Ferguson, M. J.; Hicks, R. G. *J. Mater. Chem.* 2006, *16*(26), 2618.

107. Norel, L.; Pointillart, F.; Train, C.; Chamoreau, L.-M.; Boubekeur, K.; Journaux, Y.; Brieger, A.; Brook, D. J. R. *Inorg. Chem.* 2008, *47*(7), 2396.

108. Kurusu, Y.; Yoshida, H.; Okawara, M. *Tetrahedron Lett.* 1967, *8*(37), 3595.

109. Kinoshita, V. M.; Schulz, R. C. *Macromol. Chem. Phys.* 1968, *111*(1), 137.

110. Neugebauer, F. A.; Trischmann, H. *J. Polym. Sci., Part B: Polym. Lett.* 1968, *6*(3), 255.

111. Miura, Y.; Kinoshita, M.; Imoto, M. *Macromol. Chem. Phys.* 1971, *146*(1), 69.

112. Miura, Y.; Kinoshita, M.; Imoto, M. *Macromol. Chem. Phys.* 1972, *157*(1), 51.

113. Bosch, J.; Rovira, C.; Veciana, J.; Castro, C.; Palacio, F. *Synth. Met.* 1993, *55*(2–3), 1141.

114. Hmyene, M.; Naarmann, H.; Winter, H.; Pilawa, B.; Dormann, E. *J. Phys. Condens. Matter* 1994, *6*(34), L511.

115. Awadallah, A. M.; Ferwanah, A. S.; Awad, B. M.; El-Halabi, N. M. *Asian J. Chem.* 2004, *16*(2), 1176.

116. Berry, D. E.; Hicks, R. G.; Gilroy, J. B. *J. Chem. Educ.* 2009, *86*(1), 76.

117. Kuhn, R.; Trischmann, H. *Monatsh. Chem.* 1964, *95*(2), 457.

118. Pare, E. C.; Brook, D. J. R.; Brieger, A.; Badik, M.; Schinke, M. *Org. Biomol. Chem.* 2005, *3*(23), 4258.

119. Bredihhin, A.; Mäeorg, U. *Tetrahedron* 2008, *64*(28), 6788.

120. Melendez, R. E.; Lubell, W. D. *J. Am. Chem. Soc.* 2004, *126*(21), 6759.

121. Masuda, Y.; Kuratsu, M.; Suzuki, S.; Kozaki, M.; Shiomi, D.; Sato, K.; Takui, T.; Okada, K. *Polyhedron* 2009, *28*(9–10), 1950.

122. Mondal, B.; Puranik, V. G.; Lahiri, G. K. *Inorg. Chem.* 2002, *41*(22), 5831.

123. Polumbrik, O. M.; Ryabokon, I. G.; Vasilkevich, N. G. *Zh. Org. Khim.* 1985, *21*(1), 185.

124. Polumbrik, O. M.; Misyura, A. V.; Vasilkevich, N. G.; Markovskii, L. N. *Zh. Org. Khim.* 1985, *21*(4), 871.

125. Chemistruck, V.; Chambers, D.; Brook, D. J. R. *J. Org. Chem.* 2009, *74*(5), 1850.

126. Miura, Y.; Morimoto, Y.; Kinoshita, M. *Bull. Chem. Soc. Jpn.* 1975, *48*(12), 3765.

127. Miura, Y.; Morimoto, Y.; Kinoshita, M. *Bull. Chem. Soc. Jpn.* 1976, *49*(1), 253.

128. Miura, Y.; Morimoto, Y.; Kinoshita, M. *Bull. Chem. Soc. Jpn.* 1976, *49*(6), 1715.

129. Druliner, J. D. *Macromolecules* 1991, *24*(23), 6079.

130. Chung, T. C.; Janvikul, W.; Lu, H. L. *J. Am. Chem. Soc.* 1996, *118*(3), 705.

131. Lu, B.; Chung, T. C. *Macromolecules* 1998, *31*(17), 5943.

132. Steenbock, M.; Klapper, M.; Müllen, K. *Macromol. Chem. Phys.* 1998, *199*(5), 763.

133. Dasgupta, A.; Brand, T.; Klapper, M.; Müllen, K. *Polym. Bull.* 2001, *46*(2-3), 131.

134. Khelfallah, N. S.; Peretolchin, M.; Klapper, M.; Müllen, K. *Polym. Bull.* 2005, *53*(5-6), 295.

135. Yamada, B.; Tanaka, H.; Konishi, K.; Otsu, T. *J. Macromol. Sci. Part A Pure Appl. Chem.* 1994, *31*(3), 351.

136. Yamada, B.; Nobukane, Y.; Miura, Y. *Polym. Bull.* 1998, *41*(5), 539.

137. Chen, E. K. Y.; Teertstra, S. J.; Chan-Seng, D.; Otieno, P. O.; Hicks, R. G.; Georges, M. K. *Macromolecules* 2007, *40*(24), 8609.

138. Rayner, G.; Smith, T.; Barton, W.; Newton, M.; Deeth, R. J.; Prokes, I.; Clarkson, G. J.; Haddleton, D. M. *Polym. Chem.* 2012, *3*(8), 2254.

139. Lukkarila, J. L., The University of Toronto, 2009.

140. Kovisto, B. D., The University of Victoria, 2005.

141. Brown, T. M.; Cooksey, C. J. *Educ. Chem.* 1987, *24*(3), 77.

142. Gilbert, B. G.; Kalz, W.; Lindsay, C. I.; McGrail, P. T.; Parsons, A. F.; Whittaker, D. T. E. *Tetrahedron Lett.* 1999, *40*(33), 6095.

143. Gilbert, B. C.; Kalz, W.; Lindsay, C. I.; McGrail, P. T.; Parsons, A. F.; Whittaker, D. T. E. *J. Chem. Soc., Perkin Trans. 1* 2000(8), 1187.

144. Kobayashi, T.; Nishina, Y.; Shimizu, K.; Sat; ocirc; P., G. *Chem. Lett.* 1988, *17*(7), 1137.

145. Bennett, M. A.; Chung, G.; Hockless, D. C. R.; Neumann, H.; Willis, A. C. *J. Chem. Soc., Dalton Trans.* 1999, *0*(19), 3451.

146. El-Hendawy, A. M.; Alqaradawi, S. Y.; Al-Madfa, H. A. *Transition Met. Chem.* 2000, *25*(5), 572.

147. Marque, S.; Le Mercier, C.; Tordo, P.; Fischer, H. *Macromolecules* 2000, *33*(12), 4403.

148. Chateauneuf, J.; Lusztyk, J.; Ingold, K. U. *J. Org. Chem.* 1988, *53*(8), 1629.

149. Beckwith, A. L. J.; Bowry, V. W.; Ingold, K. U. *J. Am. Chem. Soc.* 1992, *114*(13), 4983.

150. Bowry, V. W.; Ingold, K. U. *J. Am. Chem. Soc.* 1992, *114*(13), 4992.

151. Moad, G.; Rizzardo, E. *Macromolecules* 1995, *28*(26), 8722.

152. Li, L.; Hamer, G. K.; Georges, M. K. *Macromolecules* 2006, *39*(26), 9201.

153. Skene, W. G.; Belt, S. T.; Connolly, T. J.; Hahn, P.; Scaiano, J. C. *Macromolecules* 1998, *31*(25), 9103.

154. Kothe, T.; Marque, S.; Martschke, R.; Popov, M.; Fischer, H. *J. Chem. Soc., Perkin Trans. 2* 1998, *0*(7), 1553.

155. Bon, S. A. F.; Chambard, G.; German, A. L. *Macromolecules* 1999, *32*(25), 8269.

156. Lay, D. C. *Linear Algebra and its Applications*; 3rd ed.; Addison Wesley: U.S.A., 2002.

157. Armarego, W. L. F.; Chai, C. L. L. In *Purification of Laboratory Chemicals (Fifth Edition)*; Butterworth-Heinemann: Burlington, 2003.

APPENDIX A: ^{1}H, ^{13}C, AND ^{19}F NMR

A.1 ^{1}H NMR of 1,5-Diphenyl-3-(pyridin-2-yl)formazan (2.7)

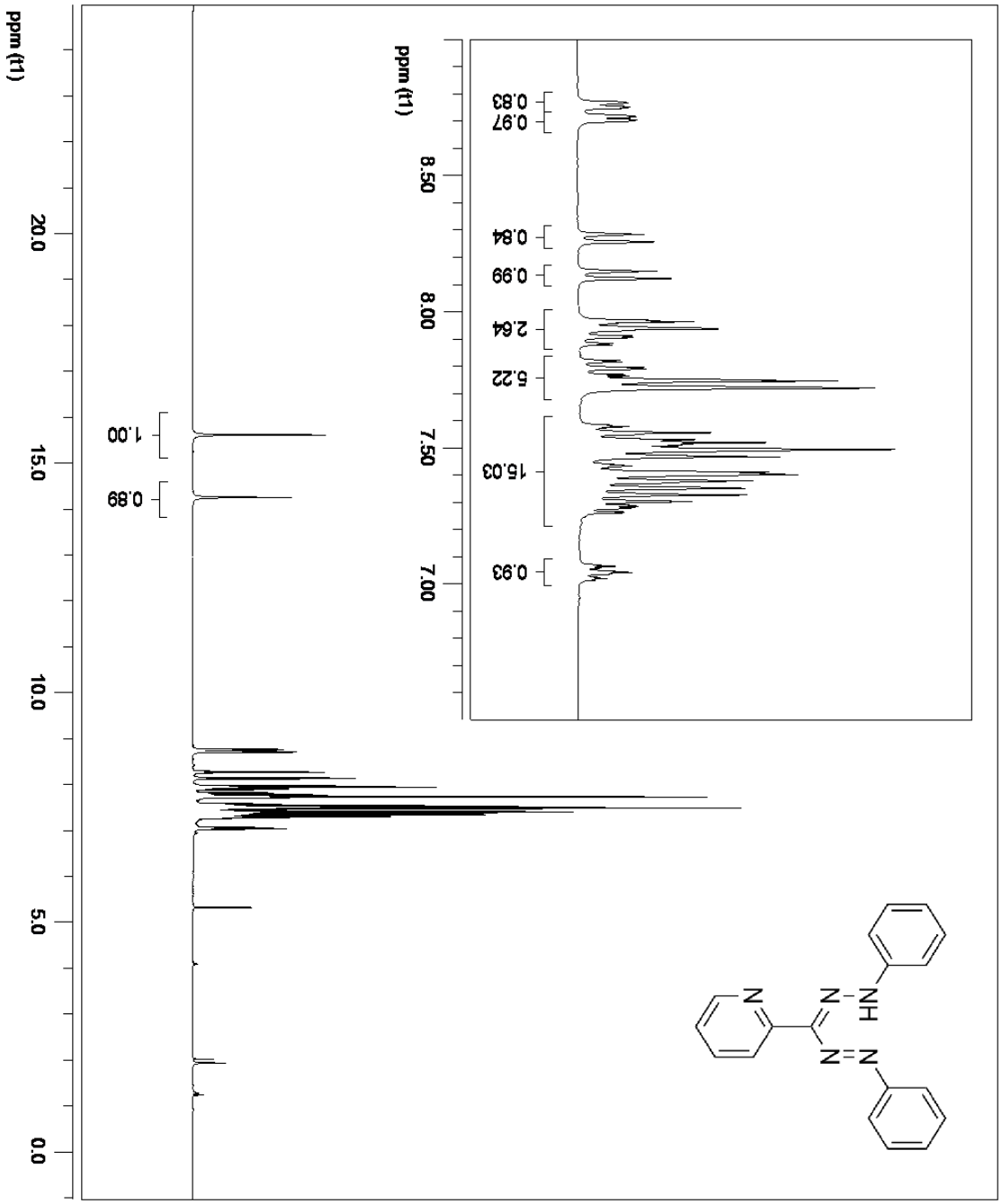

A.2 ^{13}C NMR of 1,5-Diphenyl-3-(pyridin-2-yl)formazan (2.7)

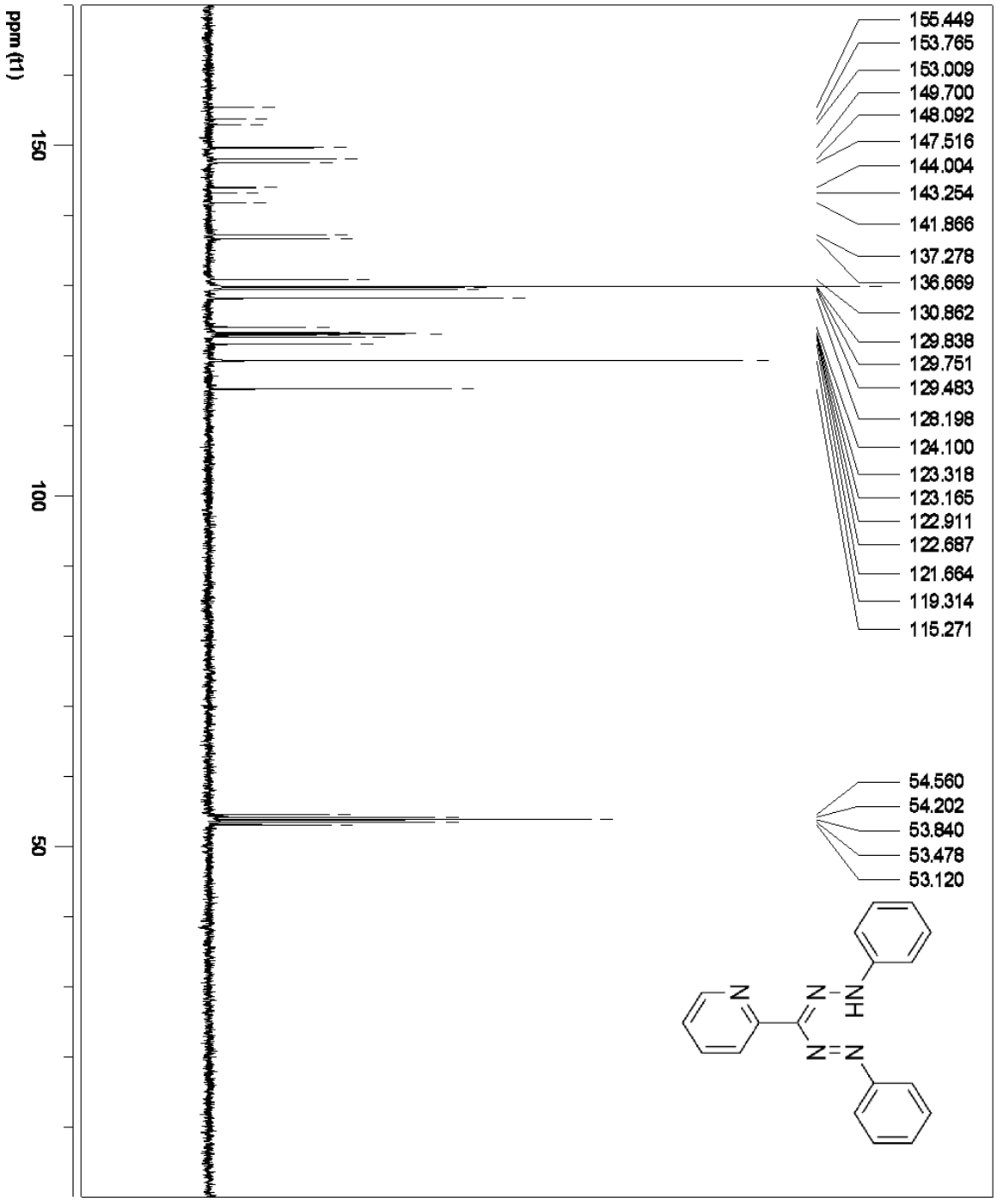

A.3 ^{1}H NMR of 2,4-Diphenylcarbonohydrazide (2.18)

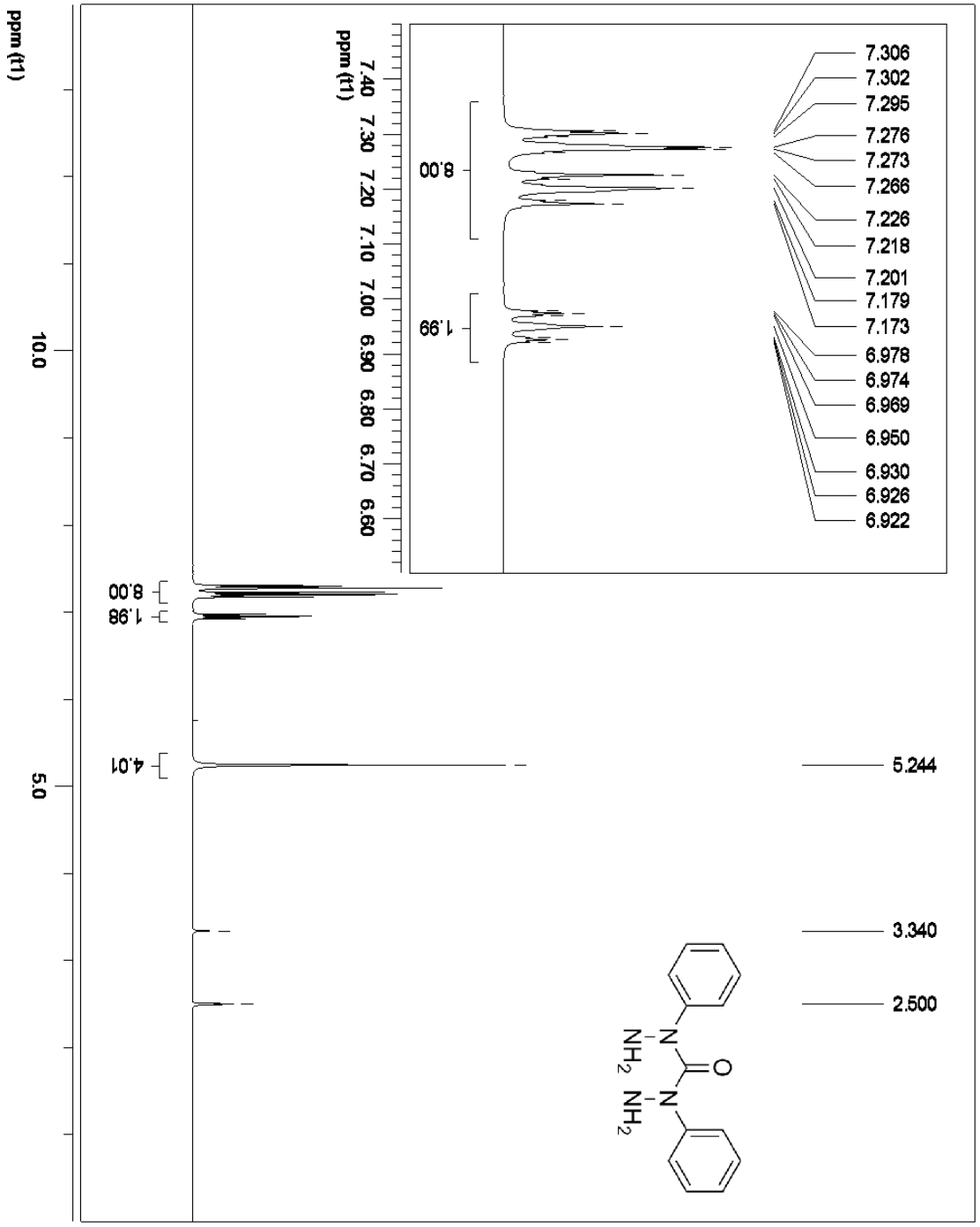

A.4 ^{13}C NMR of 2,4-Diphenylcarbonohydrazide (2.18)

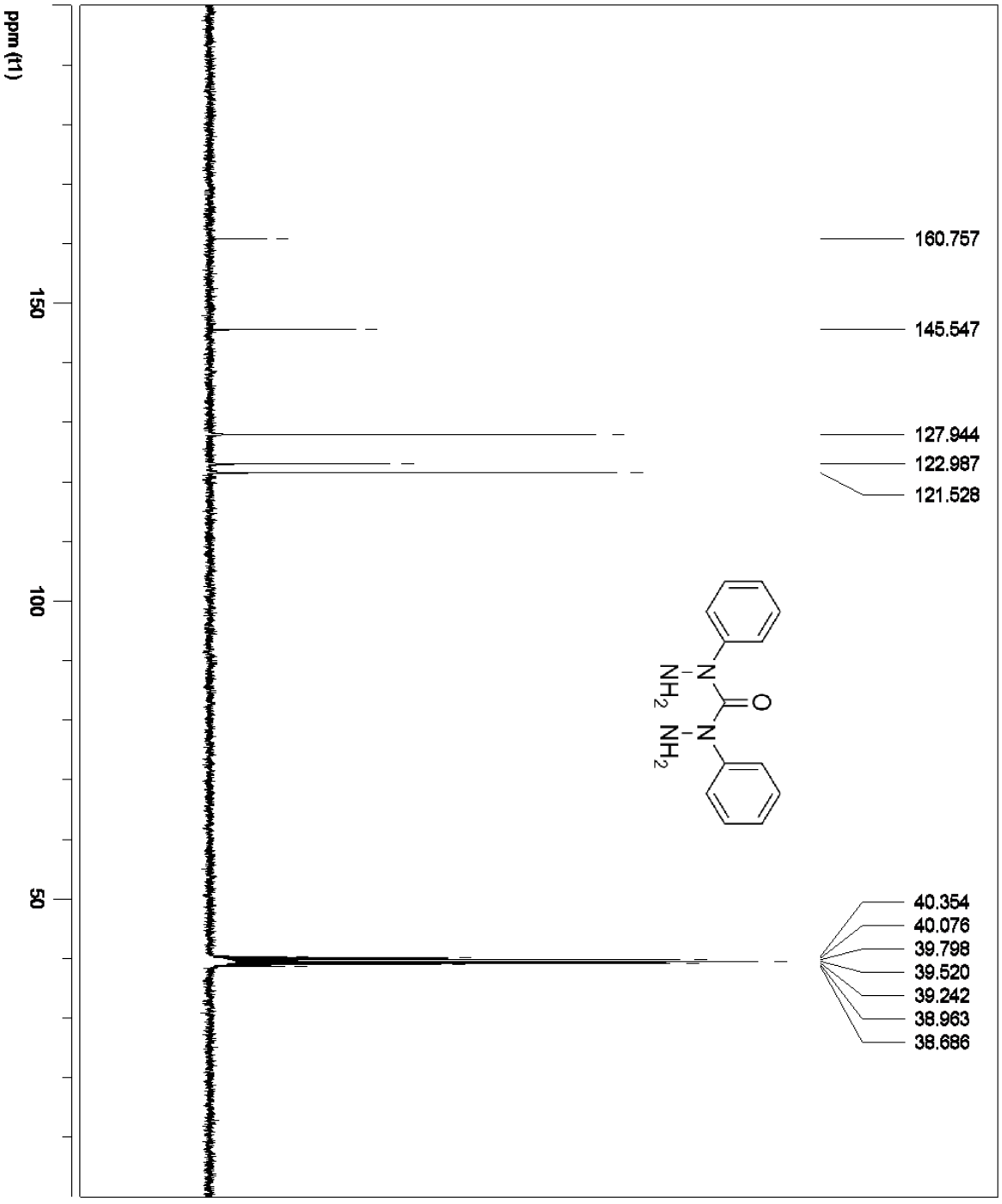

A.5 ^{1}H NMR of 2,4-Diphenyl-6-(pyridin-2-yl)-1,2,4,5-tetrazinan-3-one (2.19)

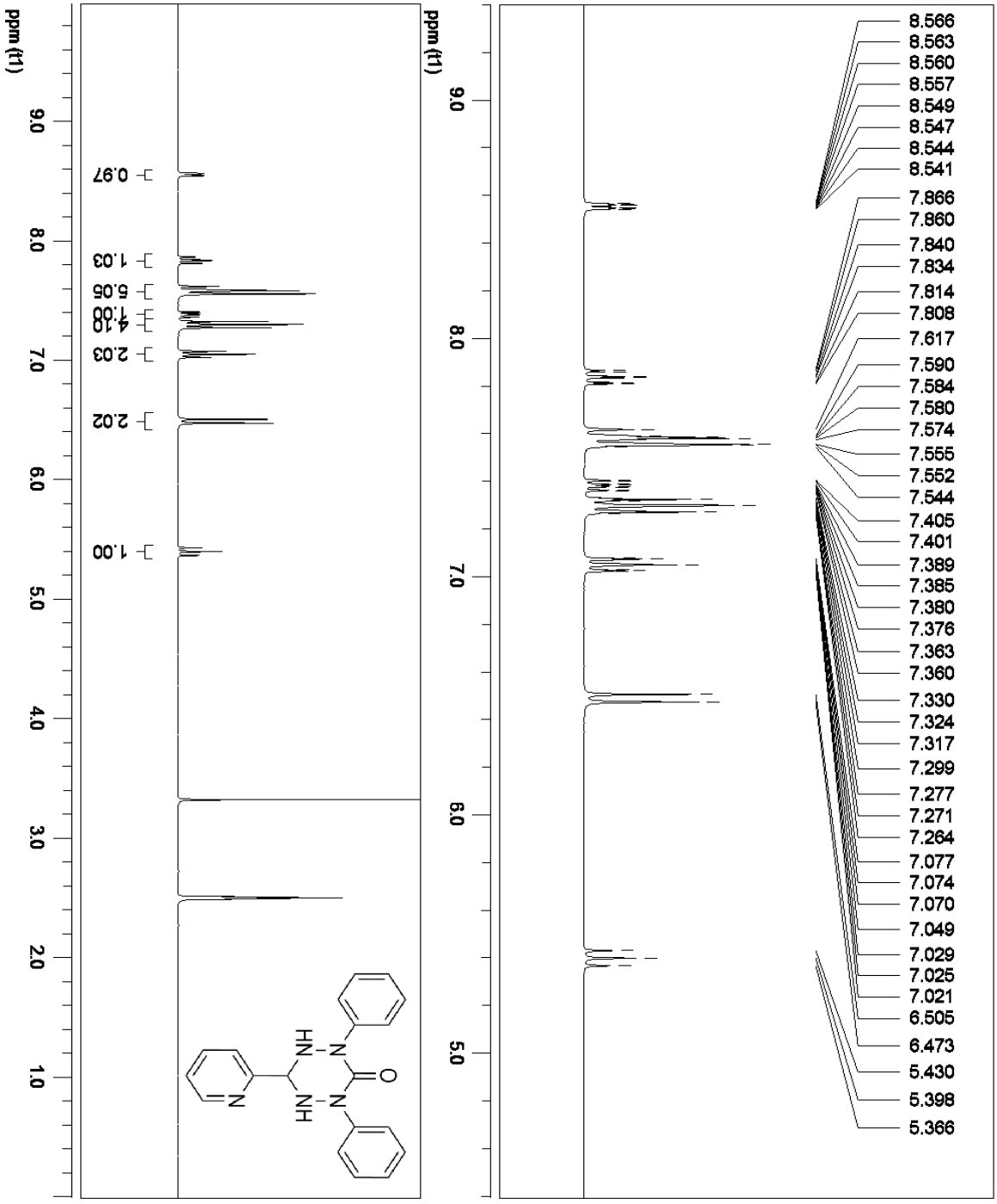

A.6 ^{13}C NMR of 2,4-Diphenyl-6-(pyridin-2-yl)-1,2,4,5-tetrazinan-3-one (2.19)

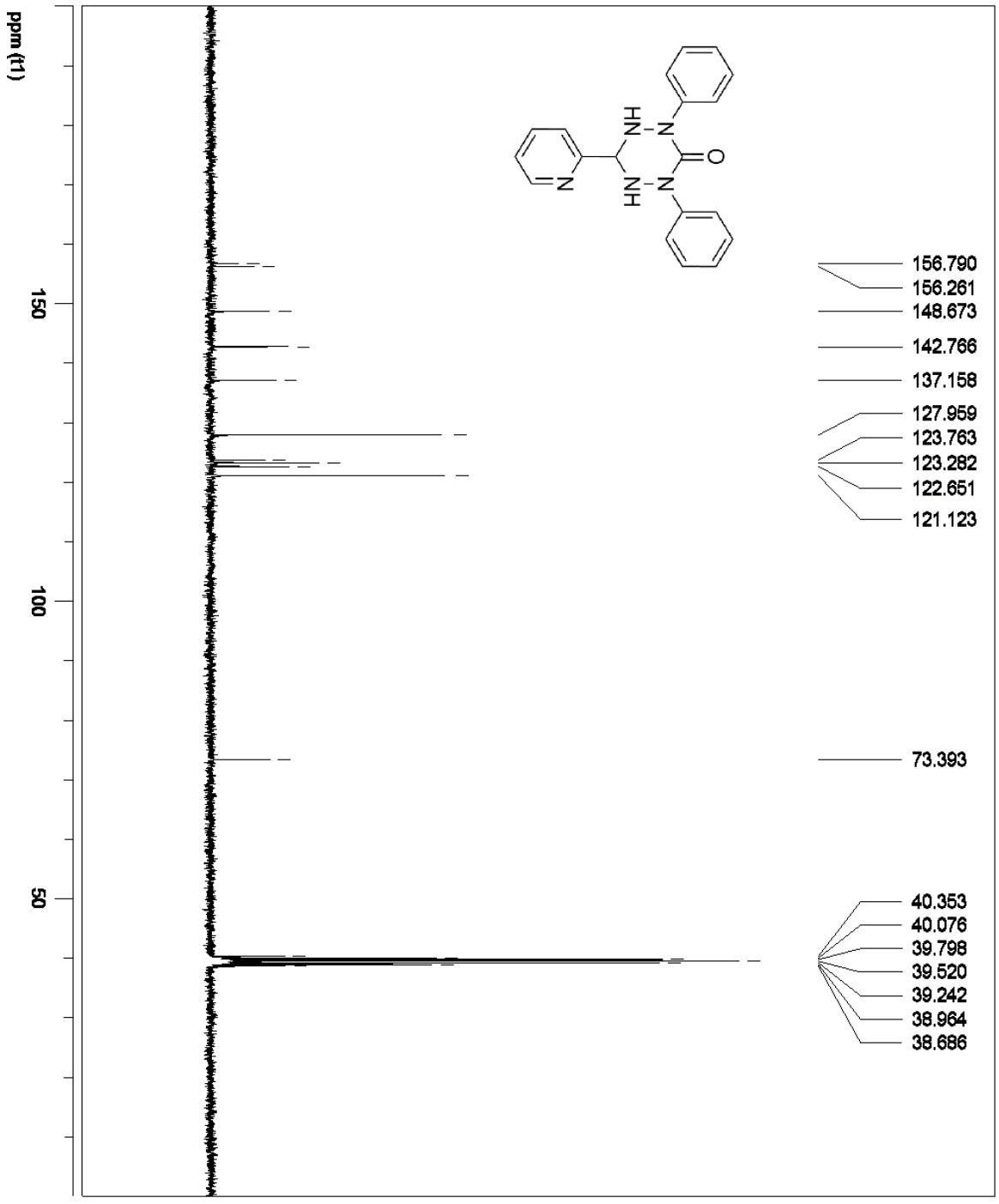

A.7 ^{1}H NMR of 5-Benzyl-2,4-diisopropyl-6-(pyridin-2-yl)-4,5-dihydro-1,2,4,5-tetrazin-3(2H)-one (3.7)

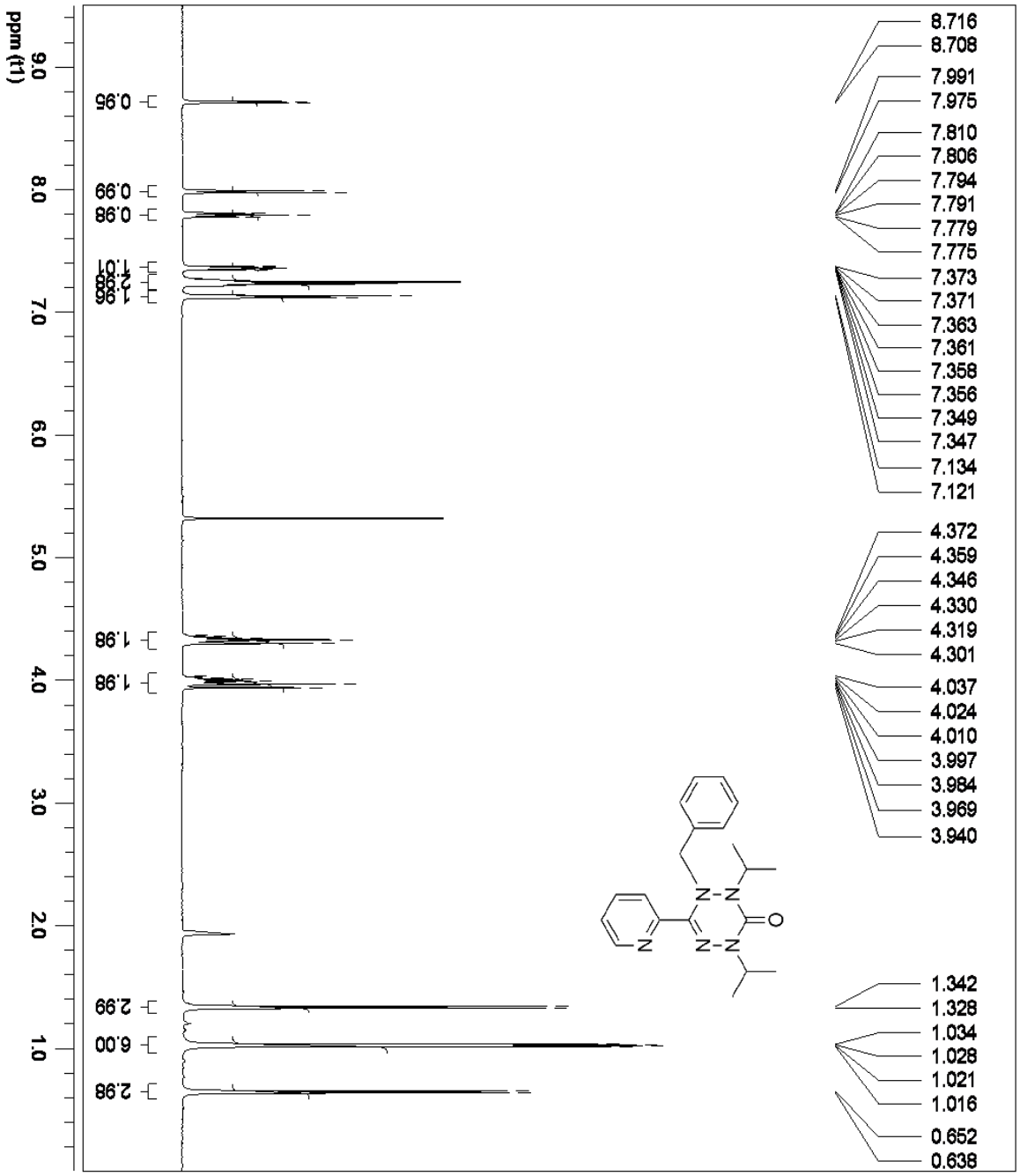

A.8 ^{13}C NMR of 5-Benzyl-2,4-diisopropyl-6-(pyridin-2-yl)-4,5-dihydro-1,2,4,5-tetrazin-3(2H)-one (3.7)

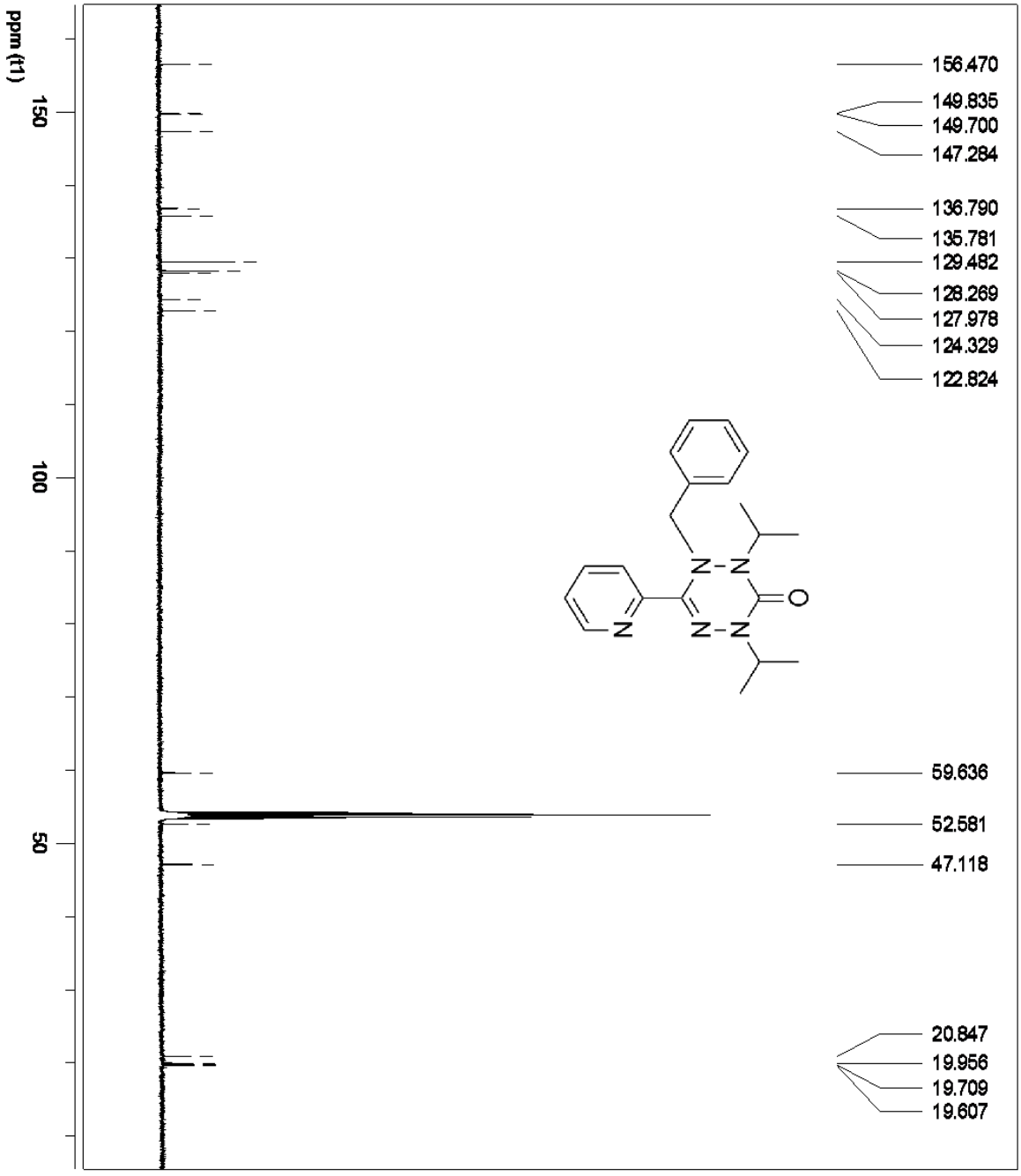

A.9 ^{1}H NMR of [5-Benzyl-2,4-diisopropyl-6-(pyridin-2-yl)-4,5-dihydro-1,2,4,5-tetrazin-3(2H)-one]bis(hexafluoroacetylacetonate)ruthenium(II) (3.7.Ru(hfac)$_2$) (Full)

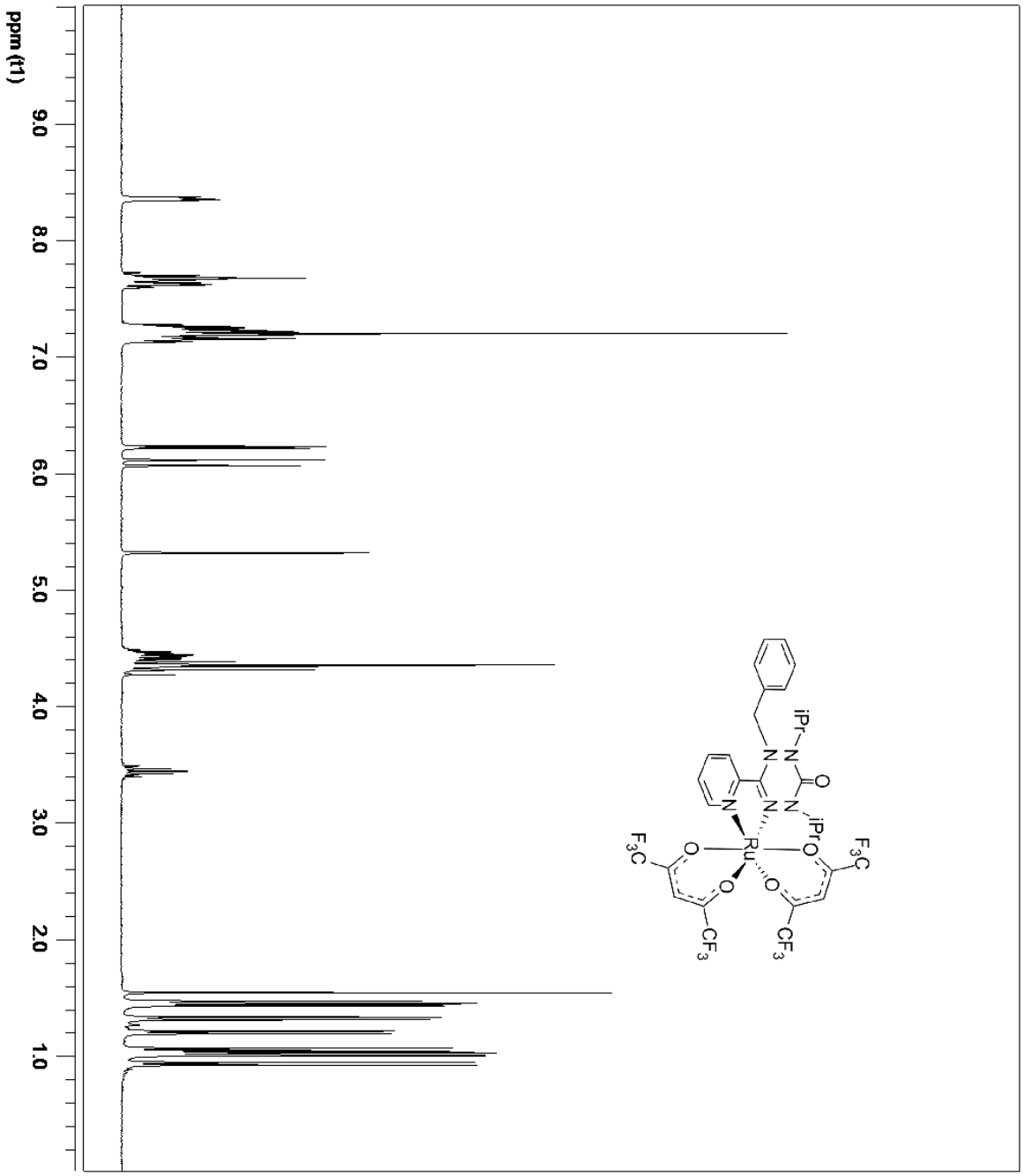

A.10 ^{1}H NMR of [5-Benzyl-2,4-diisopropyl-6-(pyridin-2-yl)-4,5-dihydro-1,2,4,5-tetrazin-3(2H)-one]bis(hexafluoroacetylacetonate]ruthenium(II) (3.7.Ru(hfac)$_2$) (Downfield)

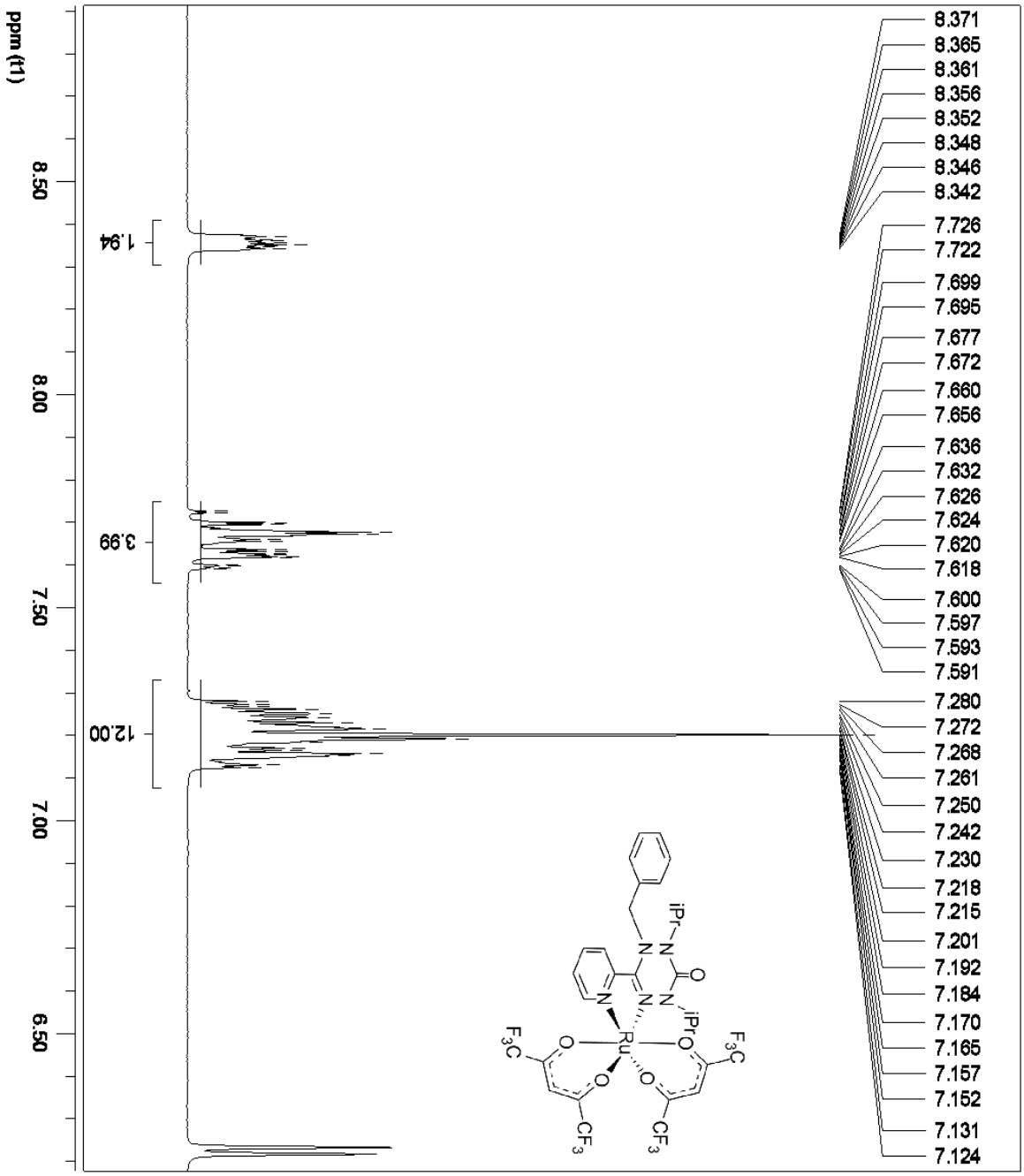

A.11 ^{1}H NMR of [5-Benzyl-2,4-diisopropyl-6-(pyridin-2-yl)-4,5-dihydro-1,2,4,5-tetrazin-3(2H)-one]bis(hexafluoroacetylacetonate)ruthenium(II) (3.7.Ru(hfac)$_2$) (Midfield)

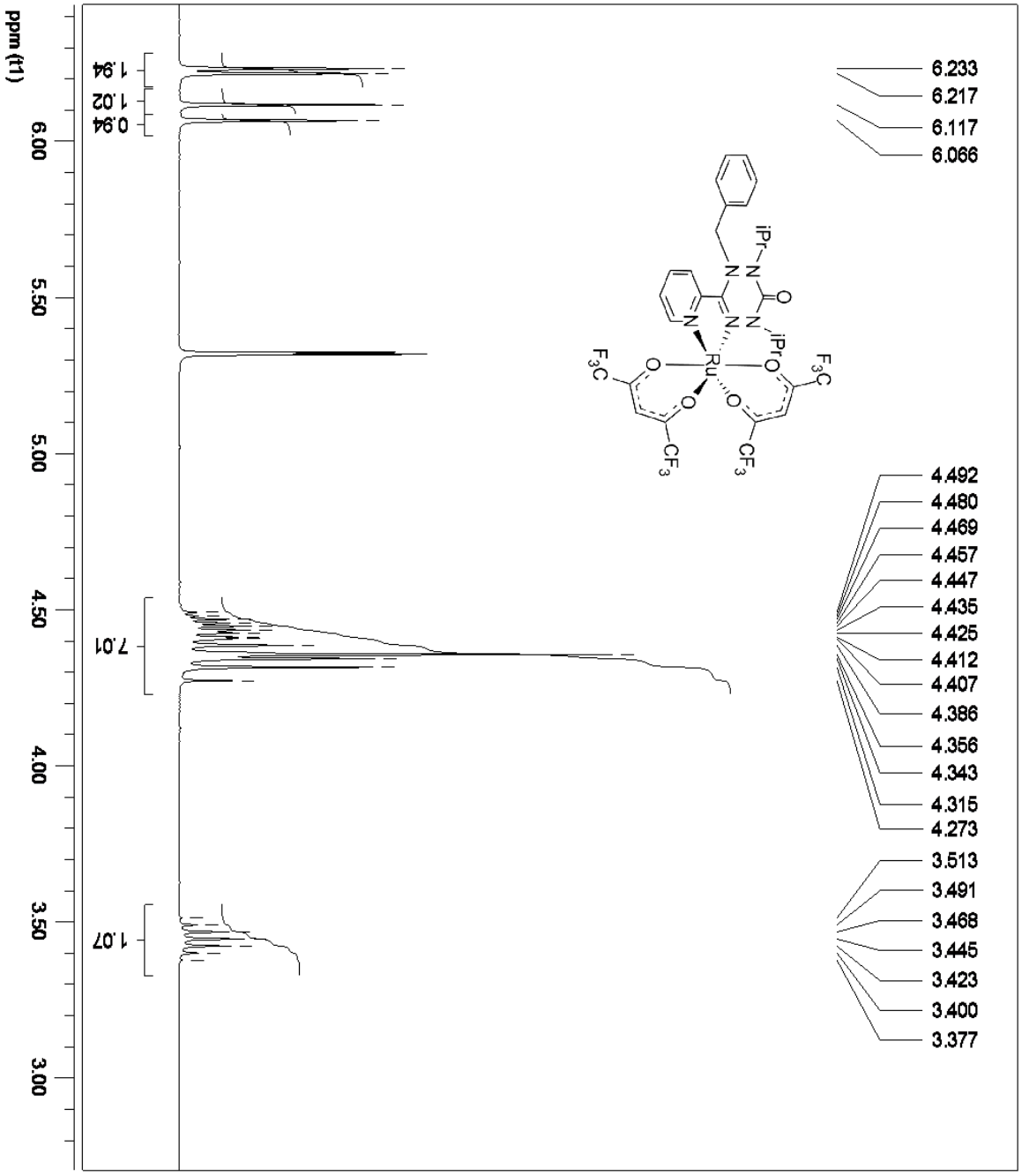

A.12 ^{1}H NMR of [5-Benzyl-2,4-diisopropyl-6-(pyridin-2-yl)-4,5-dihydro-1,2,4,5-tetrazin-3(2H)-one]bis(hexafluoroacetylacetonate)ruthenium(II) (3.7.Ru(hfac)$_2$) (Upfield)

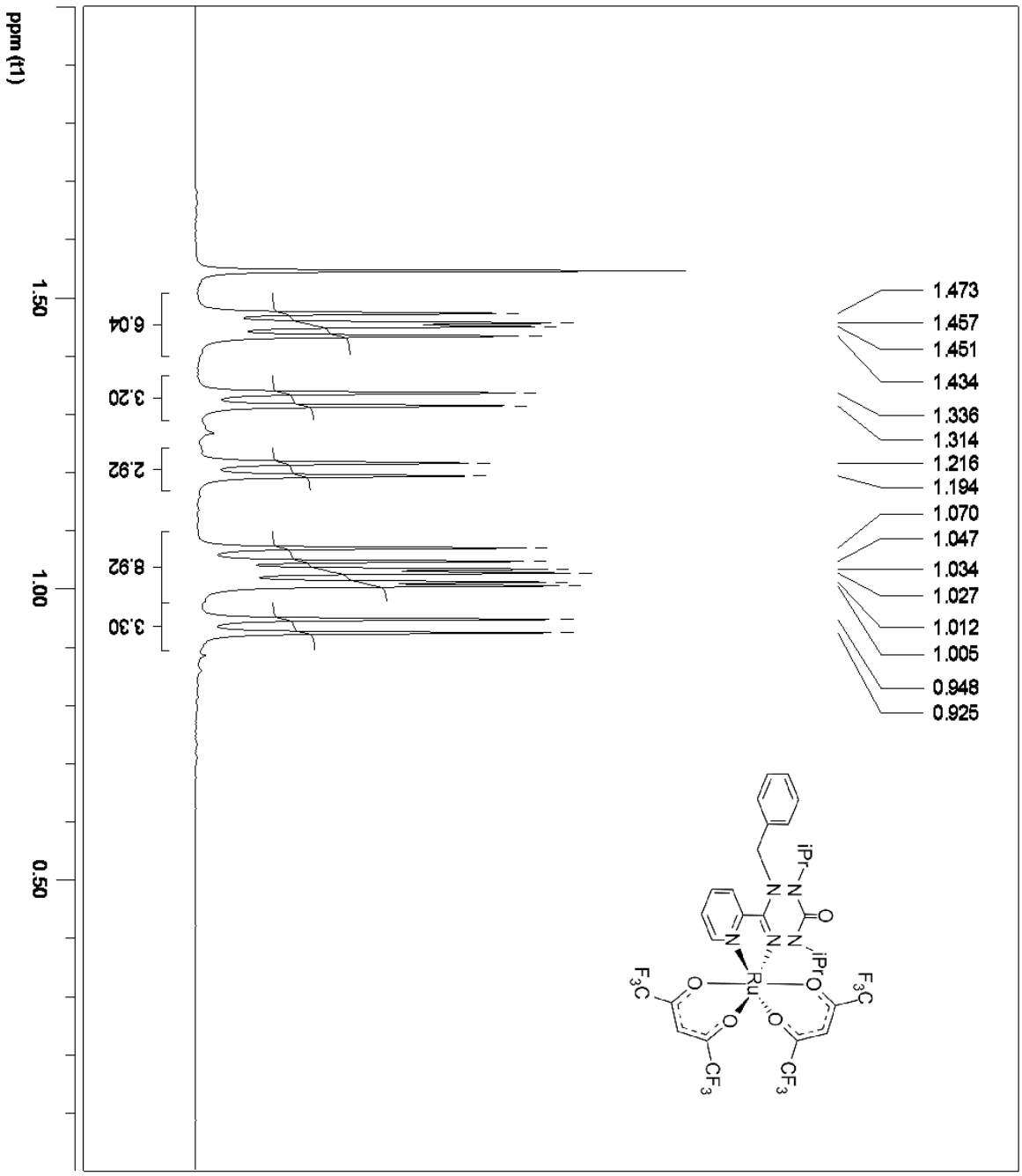

A.13 ^{13}C NMR of [5-Benzyl-2,4-diisopropyl-6-(pyridin-2-yl)-4,5-dihydro-1,2,4,5-tetrazin-3(2H)-one]bis(hexafluoroacetylacetonate)ruthenium(II) (3.7.Ru(hfac)$_2$) (Full)

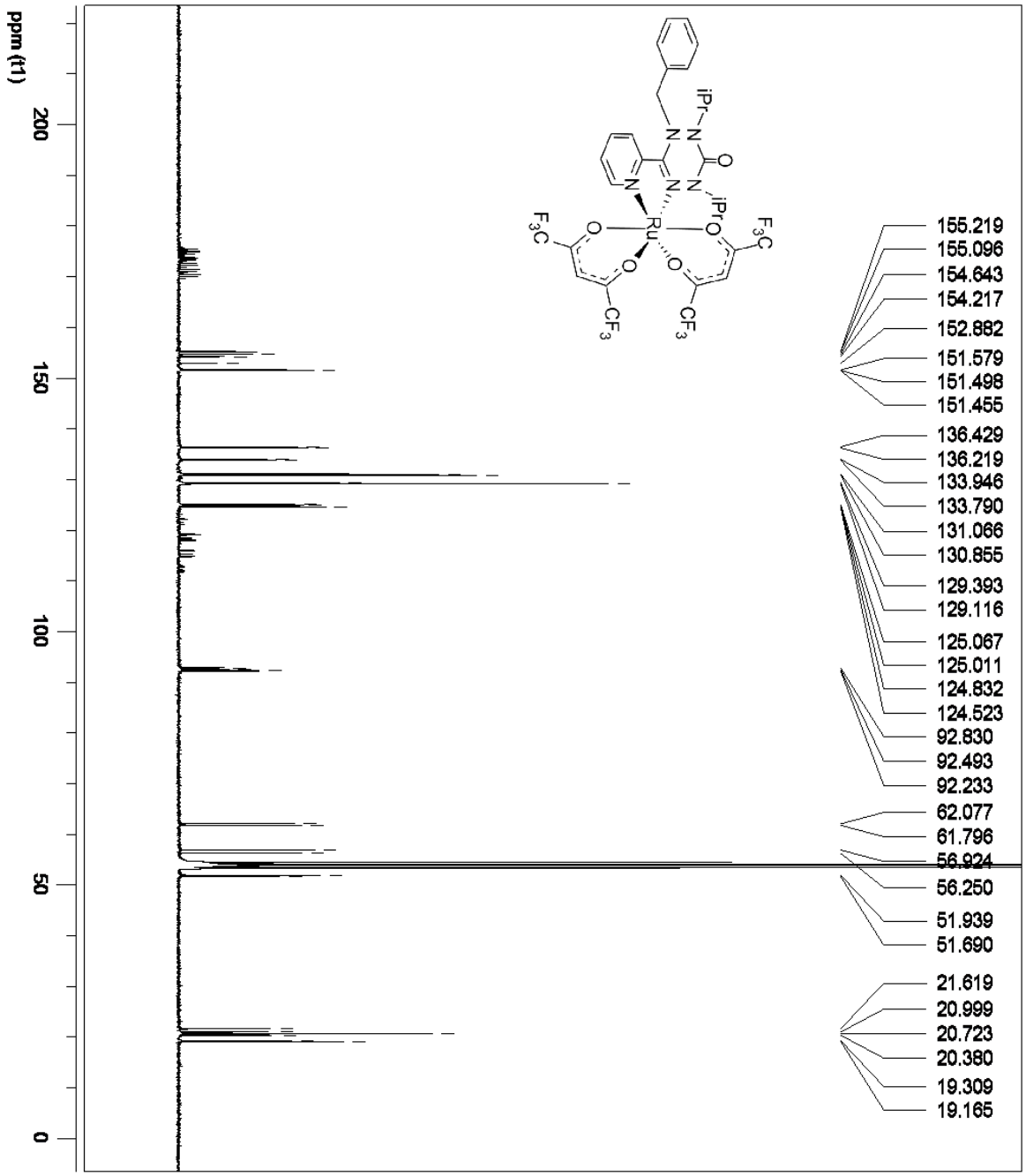

A.14 ^{13}C NMR of [5-Benzyl-2,4-diisopropyl-6-(pyridin-2-yl)-4,5-dihydro-1,2,4,5-tetrazin-3(2H)-one]bis(hexafluoroacetylacetonate)ruthenium(II) (3.7.Ru(hfac)$_2$) (CF_3)

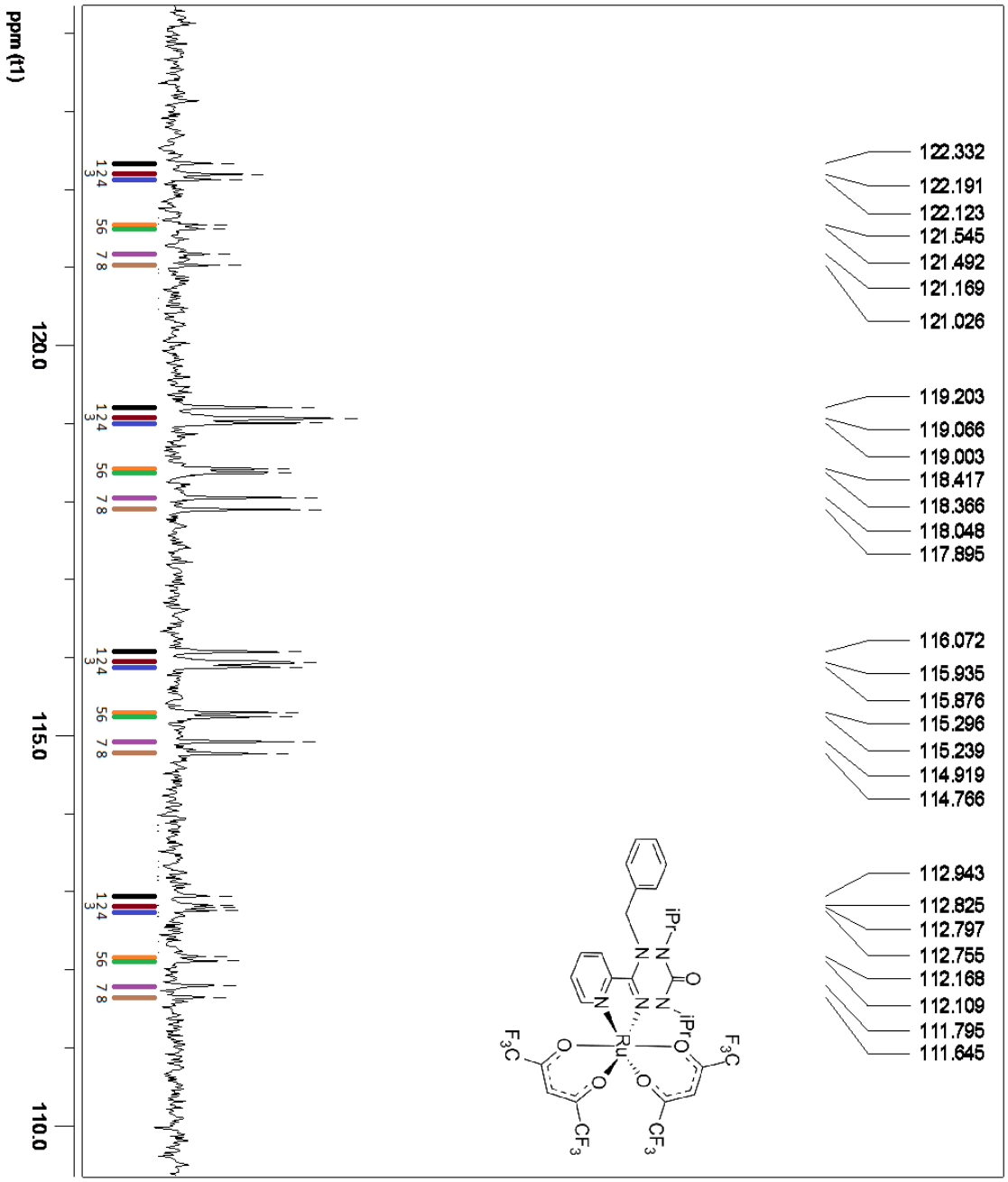

A.15 ^{13}C NMR of [5-Benzyl-2,4-diisopropyl-6-(pyridin-2-yl)-4,5-dihydro-1,2,4,5-tetrazin-3(2H)-one]bis(hexafluoroacetylacetonate)ruthenium(II) (3.7.Ru(hfac)$_2$) ($COCF_3$)

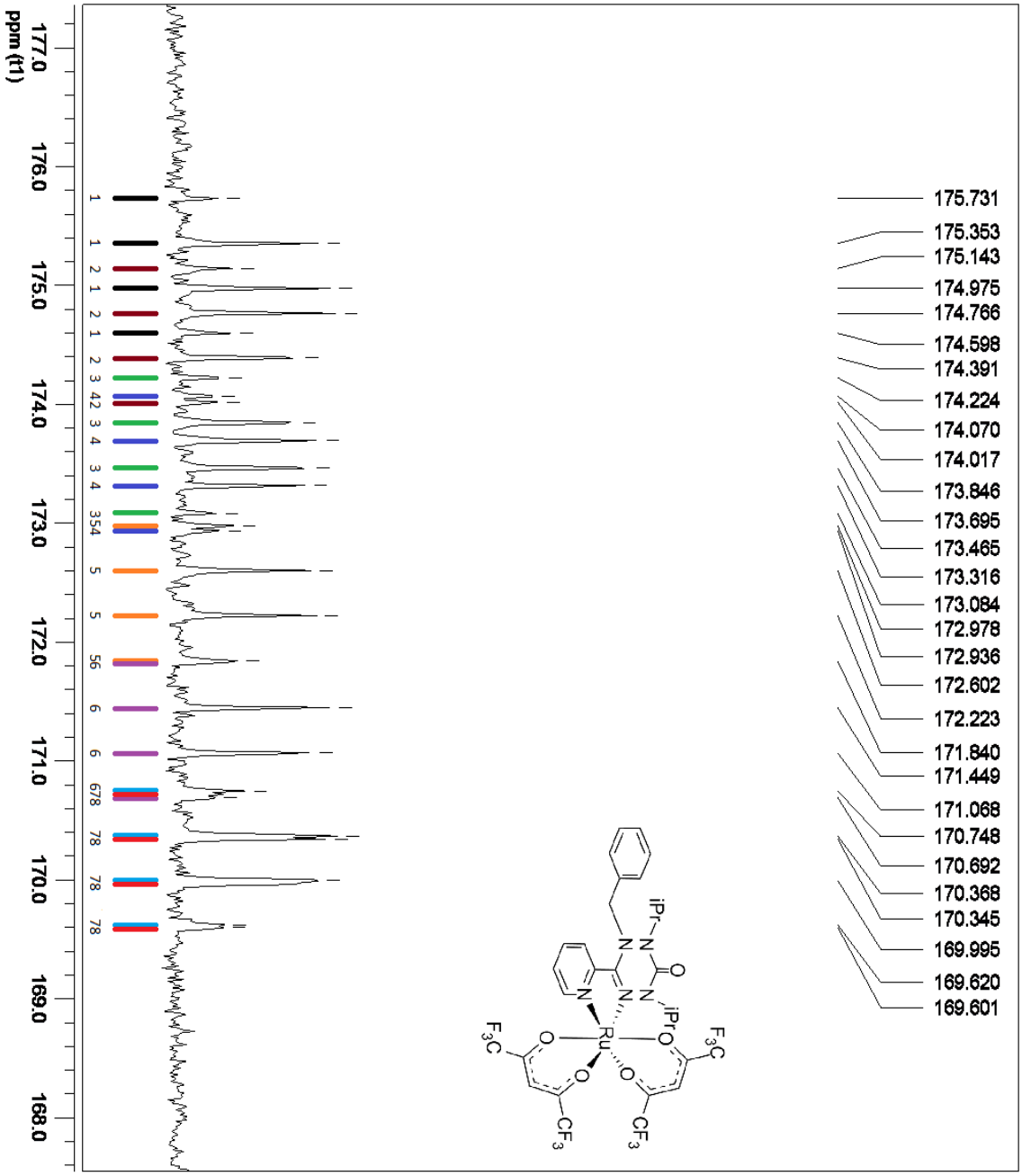

A.16 ^{19}F NMR of [5-Benzyl-2,4-diisopropyl-6-(pyridin-2-yl)-4,5-dihydro-1,2,4,5-tetrazin-3(2H)-one]bis(hexafluoroacetylacetonate)ruthenium(II) (3.7.Ru(hfac)$_2$)

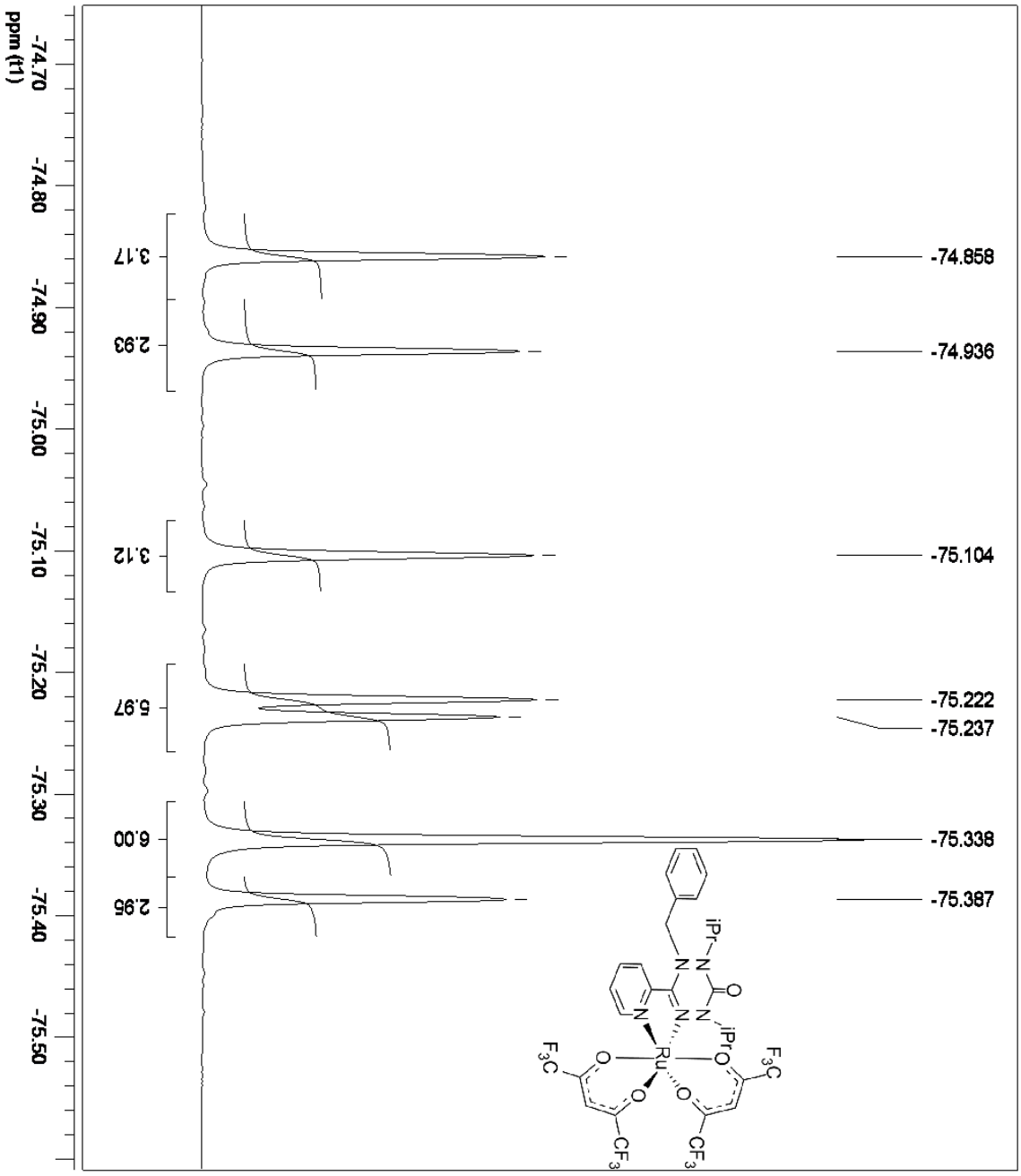

APPENDIX B: BOND HOMOLYSIS EXPERIMENTS

C-N Bond Homolysis of 3.7

Before the bond homolysis experiments could be performed on **3.7** it was necessary to obtain the experimental molar extinction coefficients for as many species as possible that are involved in the reaction. This was done by determining the molar extinction coefficients from calibration standards containing solely a pure compound of a known concentration. The samples were subjected to the same preparatory conditions that were used for the bond homolysis experiments (section 3.4.6) and aliquots of each sample were collected when the temperature of the sample had reached 110°C. This was done for the compounds **3.7**, **3.8**, **1.9**, **3.13**, and bibenzyl (**Bn_2**).

The UV-Vis spectra of each compound for the homolysis of **3.7** were collected in the range of 300-850 nm. The molar extinction coefficients of each compound were determined after application of the corrections to the spectrum was performed as described in section 3.4.7. **Figure B.1** shows an overlay of the molar extinction coefficients and **Table B.1** relates each species to the wavelengths of interest (λ_{max} of each compound, **3.13** does not have a λ_{max} at λ>300 nm).

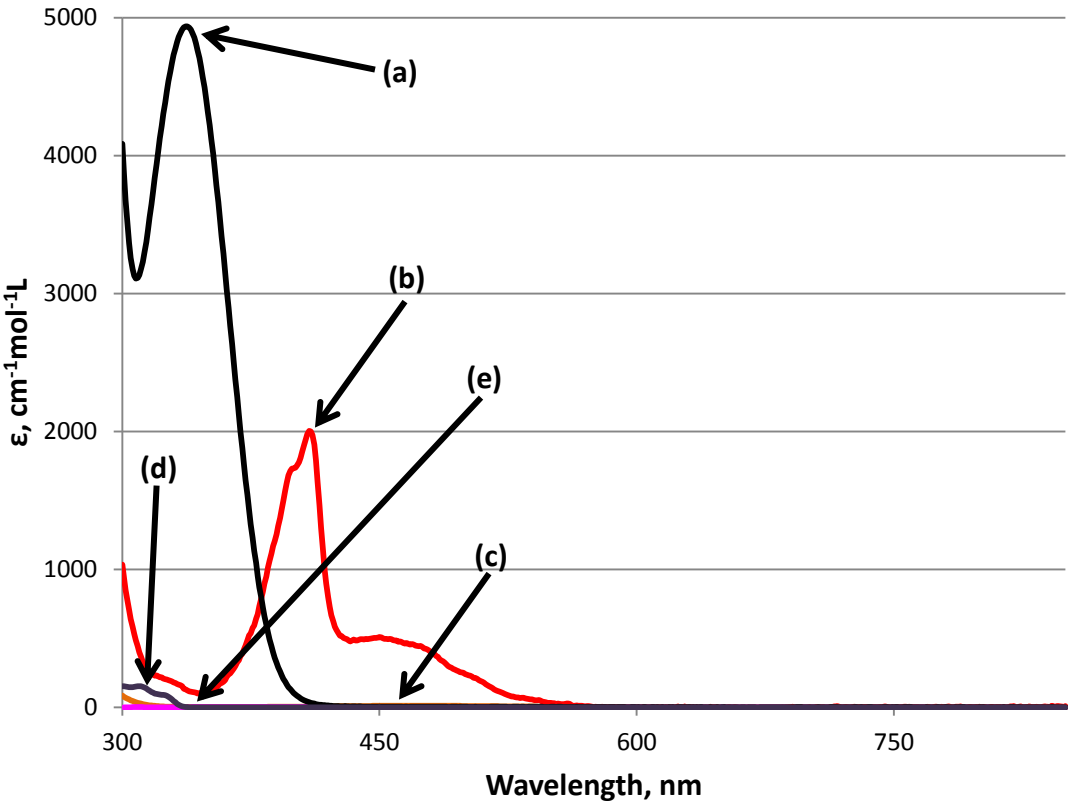

Figure B.1: Molar extinction coefficients of the compounds involved in the C-N bond homolysis of **3.7** in *tert*-butylbenzene (a, black) **3.7**, (b, red) **3.8**, (c, orange) **1.9**, (d, purple) **Bn_2**, and (e, pink) **3.13**.

Table B.1: Molar extinction coefficients for the compounds involved in the C-N bond homolysis of **3.7** in *tert*-butylbenzene at the wavelengths of interest.

Compound	Wavelength (nm)			
	310	**338**	**409**	**469**
3.13	0.292	0.110	0.483	0.325
Bn_2	152	0.616	-0.542	-0.307
3.7	3.13×10^3	4.94×10^3	36.9	3.69
3.8	399	123	2.00×10^3	4.58×10^2
1.9	29.0	1.47	5.15	10.8

In order to determine the concentrations of **3.7** and **3.8**, a series of calculations were performed. The corrected absorbance reading for each wavelength is assumed to be the sum of the absorbance due to each species in solution and thus can be represented by its own equation of the general form shown below where ε_i is the molar extinction coefficient for species i and $[S_i]$ is the concentration for species i.

$$Abs(total) = \sum Abs(individual\ species) = \sum_{i=1}^{n} \varepsilon_i * [S_i]$$

The molar extinction coefficient for **3.13** was negligible (<1 $cm^{-1}mol^{-1}L$) at the wavelengths of interest (>300 nm) and thus any absorbance due to **3.13** can be ignored. The absorbance readings for 310, 338, 409, and 469 nm are inserted into the equation along with the molar extinction coefficients for the compounds at the wavelength in question (**3.13** excluded).

Linear algebra[156] is then utilized to solve for the concentrations of **3.7** and **3.8**. A sample calculation using t = 508 s for the trial at 150°C (section 3.4.8) is shown below. This process was performed for each spectrum that was obtained to determine the concentrations of tetrazine and verdazyl radical.

nm		**1.9**	**3.8**	**3.7**	**Bn_2**	Factor	Factor **3.7**
469	6.15E-02	1.08E+01	4.58E+02	3.69E+00	-0.307	1338.75	
409	6.63E-02	5.15E+00	2.00E+03	3.69E+01	-0.542	133.88	
338	4.19E-01	1.47E+00	1.23E+02	4.94E+03	6.16E-01	1.00	
310	3.95E-01	2.90E+01	3.99E+02	3.13E+03	1.52E+02	1.58	

	1.9	3.8	3.7	Bn_2		SUB **3.7**
8.23E+01	1.45E+04	6.13E+05	4.94E+03	-4.11E+02		EQN1-EQN3
8.87E+00	6.89E+02	2.68E+05	4.94E+03	-7.26E+01		EQN2-EQN3
4.19E-01	1.47E+00	1.23E+02	4.94E+03	6.16E-01		
6.24E-01	4.58E+01	6.30E+02	4.94E+03	2.40E+02		EQN4-EQN3

	1.9	3.8	3.7	Bn_2	FACTOR	Factor**3.8**
8.19E+01	1.45E+04	6.13E+05	0	-4.12E+02	0.44	
8.46E+00	6.88E+02	2.68E+05	0	-7.32E+01	1.00	
4.19E-01	1.47E+00	1.23E+02	4.94E+03	6.16E-01	2175.83	
2.05E-01	4.43E+01	5.07E+02	0	2.39E+02	528.14	

	1.9	3.8	3.7	Bn_2		SUB **3.8**
3.57E+01	6.31E+03	2.68E+05	0	-1.80E+02		EQN1-EQN2
8.46E+00	6.88E+02	2.68E+05	0	-7.32E+01		
9.12E+02	3.20E+03	2.68E+05	1.07E+07	1.34E+03		EQN3-EQN2
1.08E+02	2.34E+04	2.68E+05	0	1.26E+05		EQN4-EQN2

	1.9	3.8	3.7	Bn_2	FACTOR	Factor **1.9**
2.73E+01	5.62E+03	0	0	-1.07E+02	1.00	
8.46E+00	6.88E+02	2.68E+05	0	-7.32E+01	8.17	
9.03E+02	2.51E+03	0	1.07E+07	1.41E+03	2.24	
9.99E+01	2.27E+04	0	0	1.26E+05	0.25	

	1.9	**3.8**	**3.7**	**Bn_2**		SUB **1.9**
2.73E+01	5.62E+03	0	0	-1.07E+02		
6.91E+01	5.62E+03	2.19E+06	0	-5.98E+02		EQN2-EQN1
2.02E+03	5.62E+03	0	2.41E+07	3.17E+03		EQN3-EQN1
2.47E+01	5.62E+03	0	0	3.13E+04		EQN4-EQN1

	1.9	**3.8**	**3.7**	**Bn_2**	FACTOR	Factor **Bn_2**
-2.00E+03	5.62E+03	0	0	-1.07E+02	-294.96	
4.18E+01	0	2.19E+06	0	-4.92E+02	-63.91	
2.00E+03	0	0	2.41E+07	3.27E+03	9.60	
-2.54E+00	0	0	0	3.14E+04	1.00	

	1.9	**3.8**	**3.7**	**Bn_2**	SUB **Bn_2**
5.89E+05	-1.66E+06	0	0	3.14E+04	EQN1-EQN4
-2.67E+03	0	-1.40E+08	0	3.14E+04	EQN2-EQN4
1.92E+04	0	0	2.31E+08	3.14E+04	EQN3-EQN4
-2.54E+00	0	0	0	3.14E+04	

	1.9	**3.8**	**3.7**	**Bn_2**			
5.89E+05	-1.66E+06	0	0	0			
-2.67E+03	0	-1.40E+08	0	0	[**3.8**]=	1.91E-05	M
1.92E+04	0	0	2.31E+08	0	[**3.7**]=	8.29E-05	M
-2.54E+00	0	0	0	3.14E+04			

C-N Bond Homolysis of 3.7.Ru(hfac)$_2$

Before the bond homolysis experiments could be performed on **3.7.Ru(hfac)$_2$** it was necessary to obtain the experimental molar extinction coefficients for as many species as possible that are involved in the reaction. This was done by determining the molar extinction coefficients from calibration standards containing solely a pure compound of a known concentration. The samples were subjected to the same preparatory conditions that were used for the bond homolysis experiments (section 3.4.6) and aliquots of each sample were collected when the temperature of the sample reached 110°C. This was done for the compounds **3.7.Ru(hfac)$_2$**, **1.29**, **1.9**, **3.13**, and bibenzyl (**Bn$_2$**).

The UV-Vis spectra of each compound for the homolysis of **3.7.Ru(hfac)$_2$** were collected in the range of 300-1300 nm. The molar extinction coefficients of each compound were determined after application of the corrections to the spectrum was performed using the process described in section 3.4.7. **Figure B.2** shows an overlay of the molar extinction coefficients and **Table B.2** relates each species to the wavelengths of interest (λ_{max} of each compound, **3.13** does not have a λ_{max} at λ>300 nm).

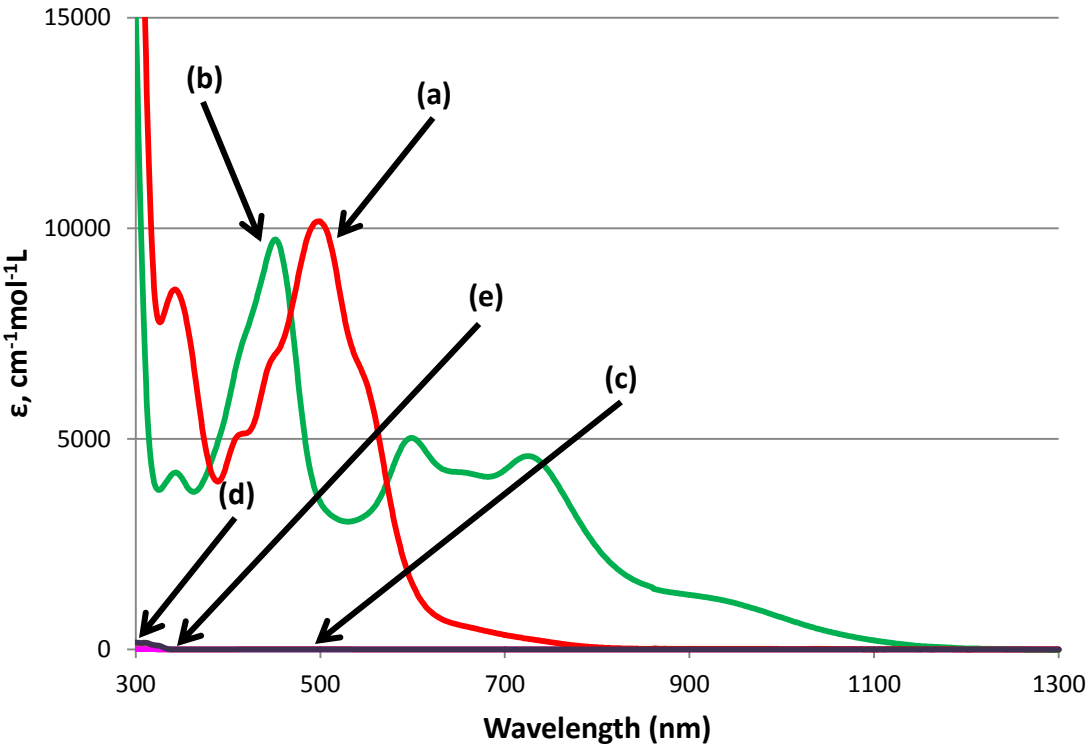

Figure B.2: Molar extinction coefficients of the compounds involved in the C-N bond homolysis of **3.7.Ru(hfac)$_2$** in *tert*-butylbenzene (a, red) **3.7.Ru(hfac)$_2$**, (b, green) **1.29**, (c, orange) **1.9**, (d, purple) **Bn$_2$**, and (e, pink) **3.13**.

Table B.2: Molar extinction coefficients for the compounds involved in the C-N bond homolysis of **3.7.Ru(hfac)$_2$** in *tert*-butylbenzene at the wavelengths of interest.

Compound	Wavelength (nm)			
	310	**451**	**469**	**498**
3.13	9.20	0.789	0.706	0.678
Bn$_2$	162	-0.266	-0.318	-0.322
3.7.Ru(hfac)$_2$	14900	7000	8100	10200
1.29	6930	9740	7800	3580
1.9	31.0	10.0	10.8	9.54

To determine if **1.29** at stable at the temperatures of the homolysis experiments, **1.29** was allowed to stand at 120°C for an extended period of time in the presence of no scavenger (**Figure B.3**) and with TEMPO (**1.9**) (**Figure B.4**). **Figure B.3** demonstrated the long-term stability of **1.29** up to 39 h. **Figure B.4** demonstrated that in the presence of TEMPO there is a change to the UV-Vis spectrum over time, but that over the length of the experiment, **1.29** is stable with respect to TEMPO.

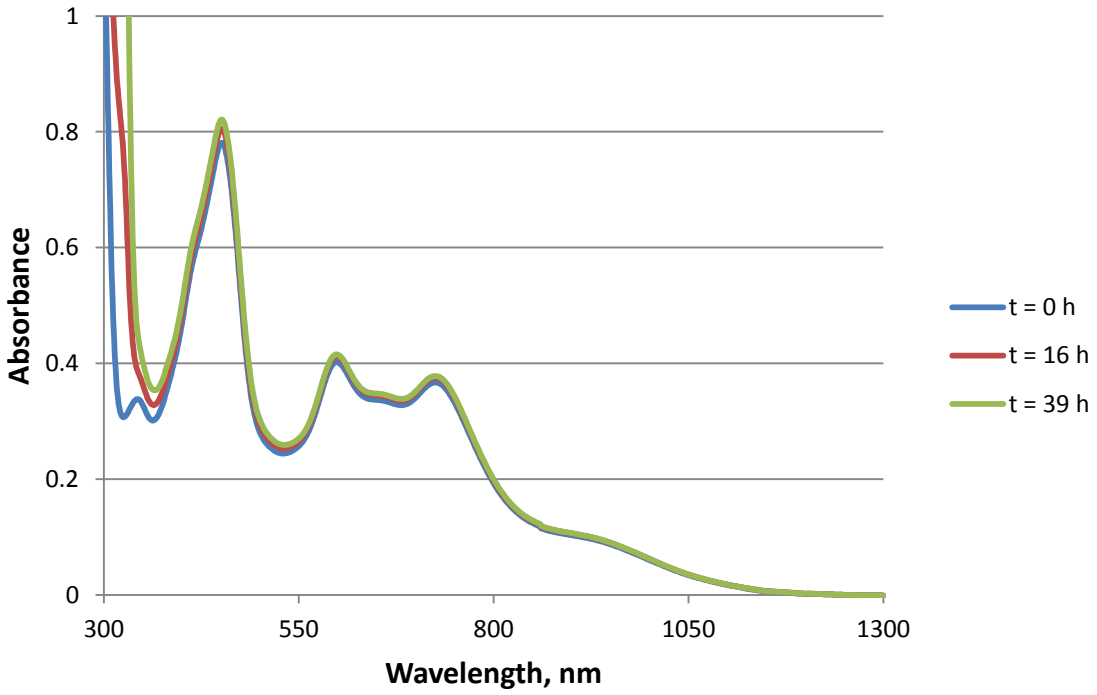

Figure B.3: Absorbance spectra for the heating of **1.29** at 120°C with no scavenger at time 0 h, 16 h, and 39 h.

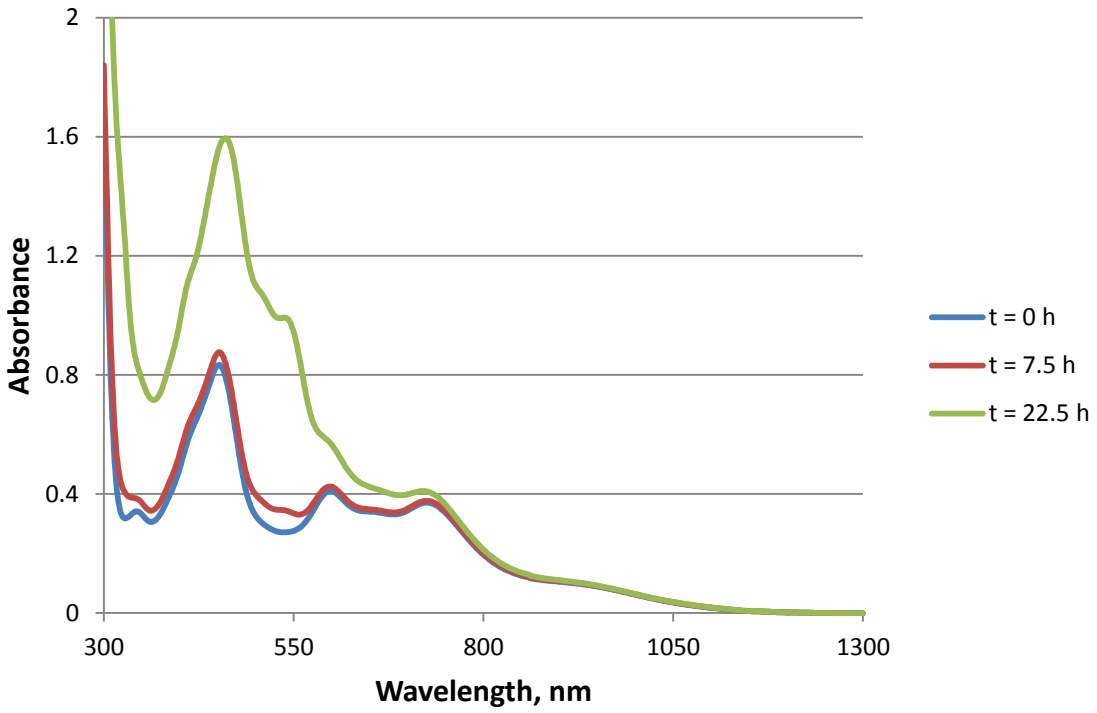

Figure B.4: Absorbance spectra for the heating of **1.29** at 120°C with TEMPO (**1.9**) as a scavenger at time 0 h, 7.5 h, and 22.5 h.

Figure B.5 demonstrates a bond homolysis experiment of **3.7.Ru(hfac)$_2$** being conducted at 120°C. There is a decrease in the amount of **3.7.Ru(hfac)$_2$** (~500 nm) and an increase in the amount of **1.29** (~450 nm). Unlike the homolysis experiments of **3.7**, it is not possible to observe if there is any decomposition of TEMPO (**1.9**).

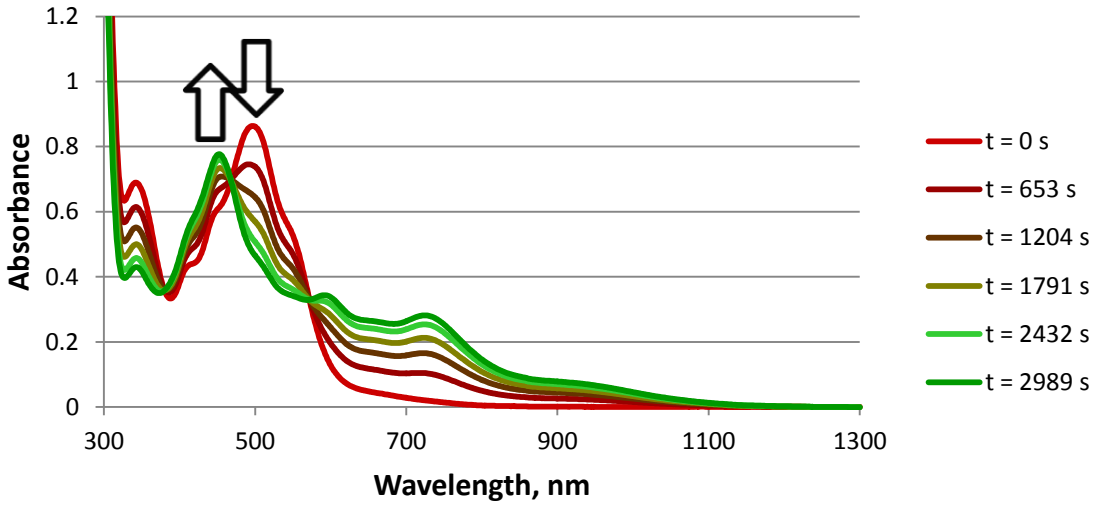

Figure B.5: UV-Vis spectra of **3.7.Ru(hfac)$_2$** with **1.9** as a scavenger at 120°C for time 0 s, 653 s, 1204 s, 1791 s, 2432 s, and 2989 s.

The molar extinction coefficient for **3.13** was negligible (<10 $cm^{-1}mol^{-1}L$) at the wavelengths of interest (>310 nm) and thus any absorbance due to **3.13** can be ignored. Linear algebra[156] was then utilized to solve for the concentrations of **3.7.Ru(hfac)$_2$** and **1.29**. A sample calculation using t = 653 s for the trial at 120°C (**Figure B.5**) is shown below. This process was performed for each spectrum that was obtained to determine the concentrations of tetrazine and verdazyl radical.

nm	ABS	**3.7.Ru $(hfac)_2$**	**1.9**	**1.29**	**Bn_2**	Factor	Factor **3.7.Ru (hfac)2**
498	0.741	1.02E+04	9.54	3.58E+03	-0.32	1.00	
469	0.701	8.10E+03	10.80	7.80E+03	-0.32	1.26	
451	0.666	7.00E+03	10.00	9.74E+03	-0.27	1.46	
310	1.155	1.49E+04	31.00	6.93E+03	162.00	0.68	

	3.7.Ru $(hfac)_2$	**1.9**	**1.29**	**Bn_2**	SUB **3.7.Ru (hfac)2**
0.741	1.02E+04	9.54	3.58E+03	-0.32	
0.883	1.02E+04	13.60	9.82E+03	-0.40	EQN2-EQN1
0.970	1.02E+04	14.57	1.42E+04	-0.39	EQN3-EQN1
0.791	1.02E+04	21.22	4.74E+03	110.90	EQN4-EQN1

	3.7.Ru $(hfac)_2$	**1.9**	**1.29**	**Bn_2**	Factor	Factor **1.29**
0.741	1.02E+04	9.54	3.58E+03	-0.32	2.96	
0.142	0	4.06	6.24E+03	-0.08	1.70	
0.229	0	5.03	1.06E+04	-0.07	1.00	
0.049	0	11.68	1.16E+03	111.22	9.12	

	3.7.Ru $(hfac)_2$	**1.9**	**1.29**	**Bn_2**	SUB **1.29**
2.198	3.02E+04	28.28	1.06E+04	-0.95	EQN1-EQN3
0.241	0	6.90	1.06E+04	-0.13	EQN2-EQN3
0.229	0	5.03	1.06E+04	-0.07	
0.449	0	106.50	1.06E+04	1014.02	EQN4-EQN3

	3.7.Ru $(hfac)_2$	**1.9**	**1.29**	**Bn_2**	Factor	Factor **1.9**
1.969	3.02E+04	23.25	0	-0.89	0.08	
0.012	0	1.87	0	-0.07	1.00	
0.229	0	5.03	1.06E+04	-0.07	0.37	
0.220	0	101.47	0	1014.08	0.02	

	3.7.Ru (hfac)$_2$	**1.9**	**1.29**	**Bn$_2$**		SUB **1.9**
0.158	2.43E+03	1.87	0	-0.07		EQN1-EQN2
0.012	0	1.87	0	-0.07		
0.085	0	1.87	3.95E+03	-0.02		EQN3-EQN2
0.004	0	1.87	0	18.70		EQN4-EQN2

	3.7.Ru (hfac)$_2$	**1.9**	**1.29**	**Bn$_2$**	Factor	Factor **Bn$_2$**
0.146	2.43E+03	0	0	0.00	-4969.41	
0.012	0	1.87	0	-0.07	-276.94	
0.073	0	0	3.95E+03	0.04	432.72	
-0.008	0	0	0	18.77	1.00	

	3.7.Ru (hfac)$_2$	**1.9**	**1.29**	**Bn$_2$**		SUB **Bn$_2$**
-727.13	-1.21E+07	0	0	18.77		EQN1-EQN4
-3.36	0	-518	0	18.77		EQN2-EQN4
31.59	0	0	1.71E+06	18.77		EQN3-EQN4
-0.008	0	0	0	18.77		

	3.7.Ru (hfac)$_2$	**1.9**	**1.29**	**Bn$_2$**
-727.12	-1.21E+07	0	0	0
-3.36	0	-518	0	0
31.60	0	0	1.71E+06	0
-0.008	0	0	0	18.77

[**3.7.Ru(hfac)$_2$**]=	6.01E-05	M
[**1.29**]=	1.85E-05	M

Figure B.6 shows a plot of the change of the [**3.7.Ru(hfac)$_2$**] and [**1.29**] during the course of the homolysis experiment. The values of [**3.7.Ru(hfac)$_2$**]+[**1.29**] was determined through the summation of the two concentrations. The [**3.7.Ru(hfac)$_2$**] is decreasing while the [**1.29**] is increasing which is as expected for the homolytic cleavage of the C-N bond in the tetrazine molecule. The sum of [**3.7.Ru(hfac)$_2$**] and [**1.29**] is nearly constant illustrating the fact that no material is being lost during this process.

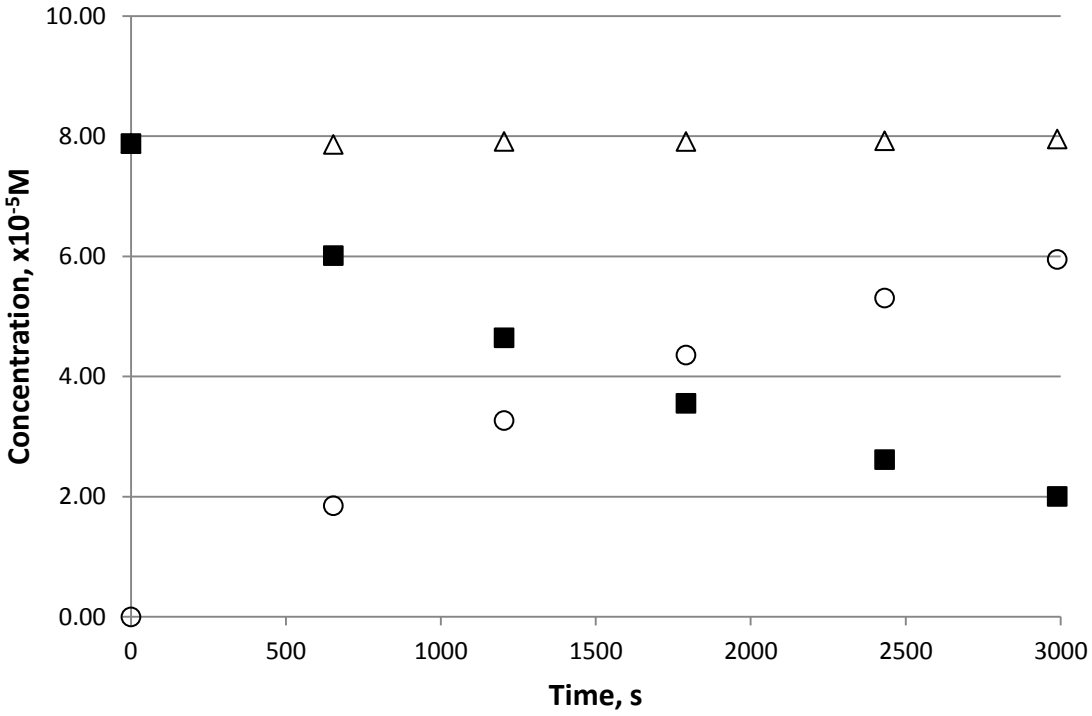

Figure B.6: Plot of the change in the [**3.7.Ru(hfac)$_2$**] ■, [**1.29**] ○, and [**3.7.Ru(hfac)$_2$**]+[**1.29**] △ during the course of the experiment.

Figure B.7 demonstrates the first-order plot of **3.7.Ru(hfac)$_2$** at 120°C according to equation **6**. When a line of best fit is allowed, there is a strong correlation (R^2 = 0.999) and the value for k_d is 4.60x10^{-4} s^{-1}. When the intercept is set to zero, there is a strong correlation (R^2 = 0.999) and the value for k_d is 4.52x10^{-4} s^{-1}.

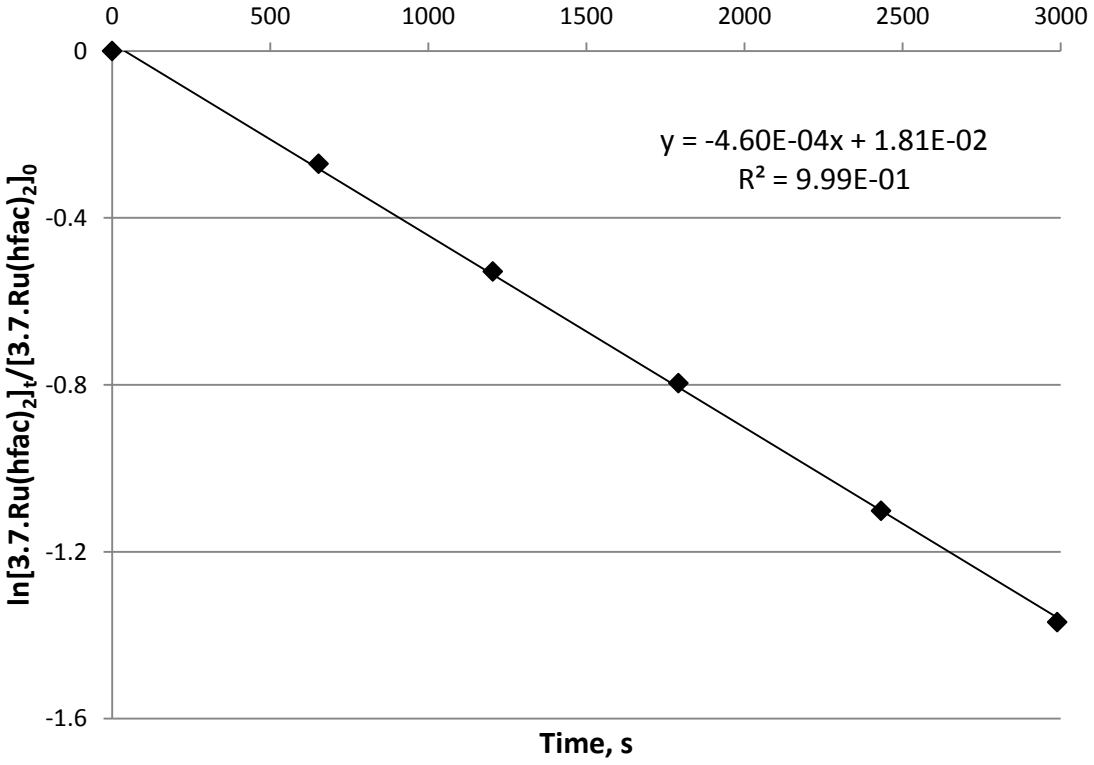

Figure B.7: First-order plot of **3.7.Ru(hfac)$_2$** at 120°C according to equation **6** (line of best fit).

APPENDIX C: CRYSTALLOGRAPHIC PARAMETERS

Table C.1: Crystallographic parameters for **2.2.PdCl$_2$**, **2.3**, and **2.3.PdCl$_2$**.

Parameter	**2.2.PdCl$_2$**	**2.3**	**2.3.PdCl$_2$**
Formula	$C_{19}H_{16}N_5PdCl_2$	$C_{19}H_{16}N_5O$	$C_{19}H_{16}N_5OPdCl_2$
FW	491.69	328.35	505.65
Dimensions (mm)	0.05X0.20X0.50	0.03X0.04X0.20	0.10X0.30X0.37
a (Å)	8.4974(8)	11.2176(4)	9.421(1)
b (Å)	14.1240(13)	19.5159(6)	10.034(1)
c (Å)	15.4290(15)	7.0585(2)	11.028(1)
α (°)	90.00	90	77.160(7)
β (°)	99.586(5)	90	77.700(6)
γ(°)	90.00	90	72.661(6)
Volume (Å^3)	1825.8(3)	1545.26(8)	958.1(2)
ρ_{calc} (g/cm^3)	1.789	1.411	1.753
System	Monoclinic	Orthorhombic	Triclinic
Space Group	P2$_1$/c (#14)	P*na*2$_1$ (#33)	*P*-1 (#2)
Z	4	4	2
μ (cm^{-1})	13.24	0.93	12.68
T (°C)	-173.0(1)	-183.0(1)	-173.0(2)
$2\theta_{max}$ (°)	60.1	50.7	45.0
Unique Reflections	5304	2837	2439
R1[a]	0.023	0.073	0.088
wR2[b]	0.050	0.199	0.156

[a] $R_1 = \Sigma||F_O| - |F_C||/\Sigma|F_O|$; [b] $wR_2 = [\Sigma w(F_O^2 - F_C^2)^2/\Sigma w(F_O^4)]^{1/2}$

Table C.2: Crystallographic parameters for **3.7** and **3.7.Ru(hfac)$_2$**.

Parameter	3.7	3.7.Ru(hfac)$_2$
Formula	$C_{20}H_{25}N_5O$	$C_{30}H_{27}F_{12}N_5O_5Ru$
FW	351.45	866.62
Dimensions (mm)	0.31x0.30x0.26	0.35x0.13x0.03
a (Å)	10.0802(8)	20.7821(4)
b (Å)	9.8139(8)	7.89150(10)
c (Å)	19.8569(15)	23.1429(4)
α (°)	90.00	90.00
β (°)	90.1493(9)	115.7100(10)
γ(°)	90.00	90.00
Volume (Å^3)	1964.36	3419.73(10)
ρ_{calc} (g/cm^3)	1.188	1.683
System	Monoclinic	Monoclinic
Space Group	$P2_1/c$ (#14)	$P2_1/c$ (#14)
Z	4	4
μ (mm^{-1})	0.077	4.746
T (°C)	-100	-100
$2\theta_{max}$ (°)	55.04	135.76
Unique Reflections	4513	5950
R1[a]	0.0410	0.0288
wR2[b]	0.1125	0.0764

[a] $R1 = \Sigma \, ||F_o| - |F_c|| / \Sigma \, |F_o|$; [b] $wR2 = [\Sigma \, w(F_o^2 - F_c^2)^2 / \Sigma \, w(F_o^4)]^{1/2}$

APPENDIX D: COMPLETE LIST OF BOND LENGTHS AND ANGLES

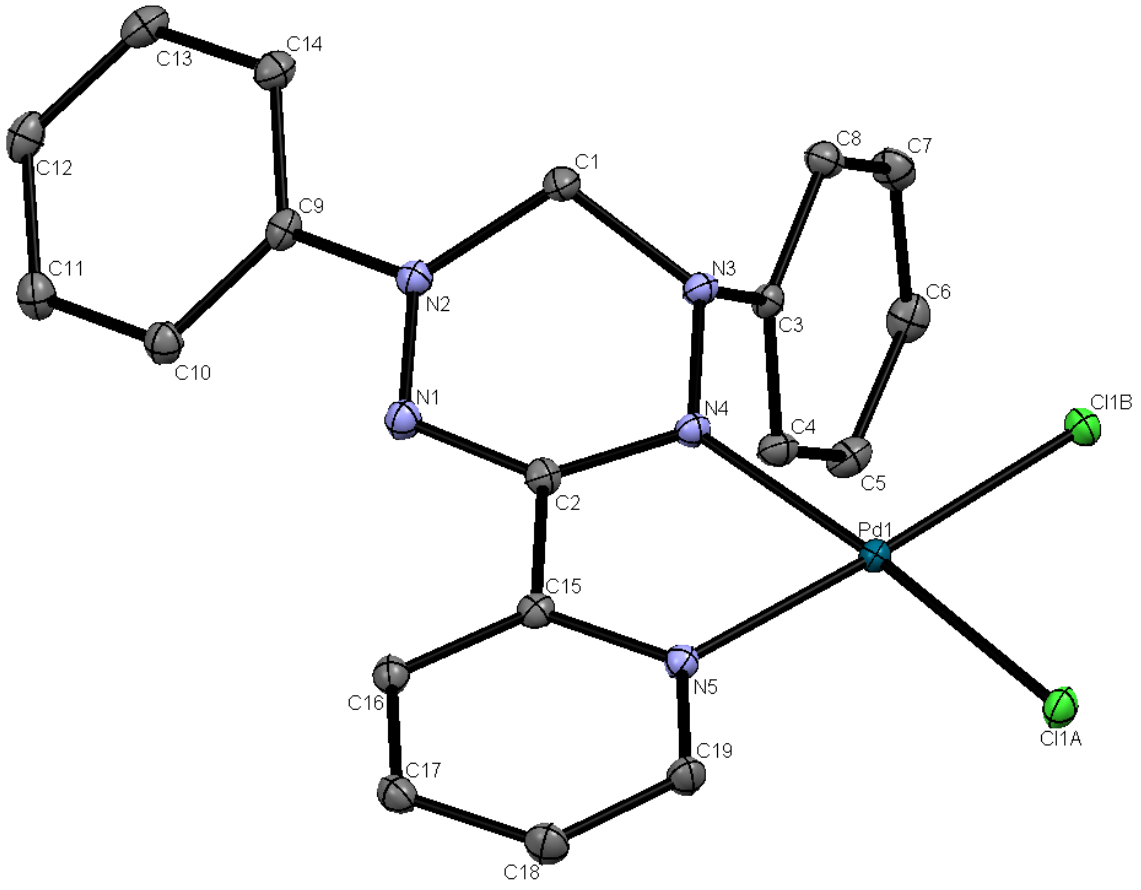

Figure D.1: ORTEP view of **2.2.PdCl$_2$**. Thermal ellipsoids at 30% probability level. Hydrogen atoms omitted for clarity.

Table D.1: Bond lengths (Å) and angles (°) for **2.2.PdCl$_2$**.

Bond	Å or °
C(1)-H(1A)	0.990(2)
C(1)-H(1B)	0.990(2)
C(1)-N(2)	1.470(2)
C(1)-N(3)	1.453(2)
C(2)-C(15)	1.469(2)
C(2)-N(1)	1.336(2)
C(2)-N(4)	1.341(2)
C(3)-C(4)	1.389(2)
C(3)-C(8)	1.394(2)

C(3)-N(3)	1.429(2)
C(4)-C(5)	1.391(2)
C(4)-H(4)	0.950(2)
C(5)-C(6)	1.387(2)
C(5)-H(5)	0.950(2)
C(6)-C(7)	1.391(2)
C(6)-H(6)	0.950(2)
C(7)-C(8)	1.385(2)
C(7)-H(7)	0.950(2)
C(8)-H(8)	0.950(1)
C(9)-C(10)	1.401(2)
C(9)-C(14)	1.397(2)
C(9)-N(2)	1.406(2)
C(10)-C(11)	1.383(2)
C(10)-H(10)	0.950(2)
C(11)-C(12)	1.396(3)
C(11)-H(11)	0.950(2)
C(12)-C(13)	1.381(2)
C(12)-H(12)	0.950(2)
C(13)-C(14)	1.393(2)
C(13)-H(13)	0.950(2)
C(14)-H(14)	0.950(2)
C(15)-C(16)	1.386(2)
C(15)-N(5)	1.351(2)
C(16)-C(17)	1.386(2)
C(16)-H(16)	0.950(2)
C(17)-C(18)	1.386(2)
C(17)-H(17)	0.951(2)
C(18)-C(19)	1.385(2)
C(18)-H(18)	0.950(2)
C(19)-H(19)	0.950(2)
C(19)-N(5)	1.337(2)
Cl(1A)-Pd(1)	2.2945(4)
Cl(1B)-Pd(1)	2.2870(4)
N(1)-N(2)	1.335(2)
N(3)-N(4)	1.381(2)
N(4)-Pd(1)	2.025(1)
N(5)-Pd(1)	2.031(1)
H(1A)-C(1)-H(1B)	108.5(1)
H(1A)-C(1)-N(2)	110.2(1)
H(1A)-C(1)-N(3)	110.2(1)
H(1B)-C(1)-N(2)	110.2(1)
H(1B)-C(1)-N(3)	110.2(1)

N(2)-C(1)-N(3)	107.6(1)
C(15)-C(2)-N(1)	117.8(1)
C(15)-C(2)-N(4)	115.4(1)
N(1)-C(2)-N(4)	126.7(1)
C(4)-C(3)-C(8)	120.8(1)
C(4)-C(3)-N(3)	120.8(1)
C(8)-C(3)-N(3)	118.4(1)
C(3)-C(4)-C(5)	119.2(1)
C(3)-C(4)-H(4)	120.4(1)
C(5)-C(4)-H(4)	120.4(2)
C(4)-C(5)-C(6)	120.5(1)
C(4)-C(5)-H(5)	119.8(2)
C(6)-C(5)-H(5)	119.7(2)
C(5)-C(6)-C(7)	119.7(2)
C(5)-C(6)-H(6)	120.2(2)
C(7)-C(6)-H(6)	120.1(2)
C(6)-C(7)-C(8)	120.5(2)
C(6)-C(7)-H(7)	119.7(2)
C(8)-C(7)-H(7)	119.8(2)
C(3)-C(8)-C(7)	119.2(1)
C(3)-C(8)-H(8)	120.4(1)
C(7)-C(8)-H(8)	120.4(2)
C(10)-C(9)-C(14)	120.6(1)
C(10)-C(9)-H(2)	119.0(1)
C(14)-C(9)-N(2)	120.4(1)
C(9)-C(10)-C(11)	119.0(1)
C(9)-C(10)-H(10)	120.5(2)
C(11)-C(10)-H(10)	120.5(2)
C(10)-C(11)-C(12)	121.0(2)
C(10)-C(11)-H(11)	119.5(2)
C(12)-C(11)-H(11)	119.5(2)
C(11)-C(12)-C(13)	119.4(2)
C(11)-C(12)-H(12)	120.3(2)
C(13)-C(12)-H(12)	120.3(2)
C(12)-C(13)-C(14)	121.0(2)
C(12)-C(13)-H(13)	119.5(2)
C(14)-C(13)-H(13)	119.5(2)
C(9)-C(14)-C(13)	119.0(1)
C(9)-C(14)-H(14)	120.5(2)
C(13)-C(14)-H(14)	120.5(2)
C(2)-C(15)-C(16)	122.9(1)
C(2)-C(15)-N(5)	114.7(1)
C(16)-C(15)-N(5)	122.4(1)
C(15)-C(16)-C(17)	118.4(1)

C(15)-C(16)-H(16)	120.8(1)
C(17)-C(16)-H(16)	120.8(2)
C(16)-C(17)-C(18)	119.2(1)
C(16)-C(17)-H(17)	120.5(2)
C(18)-C(17)-H(17)	120.4(2)
C(17)-C(18)-C(19)	119.2(2)
C(17)-C(18)-H(18)	120.4(2)
C(19)-C(18)-H(18)	120.4(2)
C(18)-C(19)-H(19)	119.0(2)
C(18)-C(19)-N(5)	122.0(1)
H(19)-C(19)-N(5)	119.0(2)
C(2)-N(1)-N(2)	114.9(1)
C(1)-N(2)-C(9)	125.7(1)
C(1)-N(2)-N(1)	115.8(1)
C(9)-N(2)-N(1)	118.4(1)
C(1)-N(3)-C(3)	119.8(1)
C(1)-N(3)-N(4)	112.4(1)
C(3)-N(3)-N(4)	116.9(1)
C(2)-N(4)-N(3)	115.2(1)
C(2)-N(4)-Pd(1)	114.9(1)
N(3)-N(4)-Pd(1)	129.0(1)
C(15)-N(5)-C(19)	118.8(1)
C(15)-N(5)-Pd(1)	114.7(1)
C(19)-N(5)-Pd(1)	126.5(1)
Cl(1A)-Pd(1)-Cl(1B)	89.61(1)
Cl(1A)-Pd(1)-N(4)	173.55(4)
Cl(1A)-Pd(1)-N(5)	93.68(4)
Cl(1B)-Pd(1)-N(4)	96.64(4)
Cl(1B)-Pd(1)-N(5)	176.72(4)
N(4)-Pd(1)-N(5)	80.08(5)

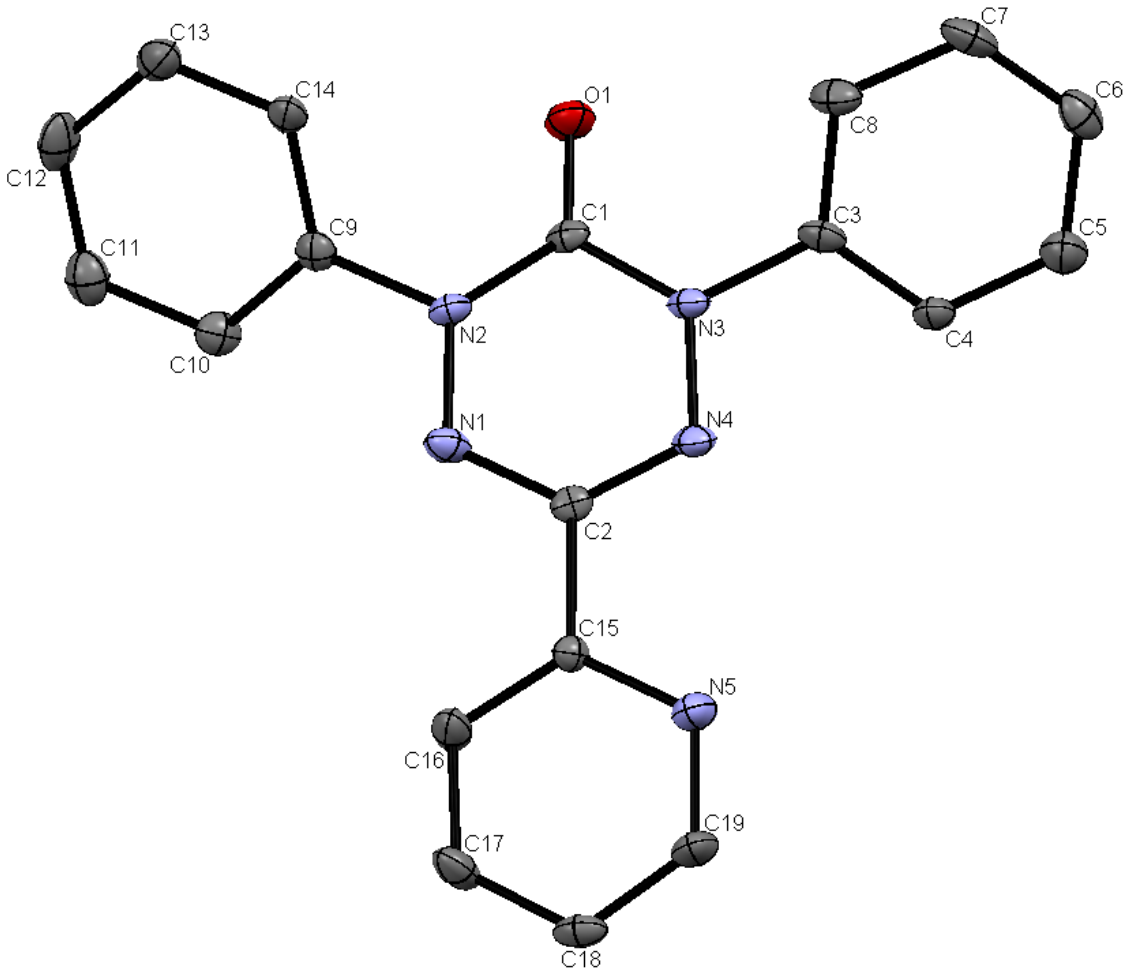

Figure D.2: ORTEP view of **2.3**. Thermal ellipsoids at 30% probability level. Hydrogen atoms omitted for clarity.

Table D.2: Bond lengths (Å) and angles (°) for **2.3**.

Bond	Å or °
C(1)-N(2)	1.363(5)
C(1)-N(3)	1.389(5)
C(1)-O(1)	1.225(5)
C(2)-C(15)	1.477(5)
C(2)-N(1)	1.337(5)
C(2)-N(4)	1.333(5)
C(3)-C(4)	1.379(6)
C(3)-C(8)	1.385(6)
C(3)-N(3)	1.441(6)
C(4)-C(5)	1.387(6)
C(4)-H(4)	0.9500

C(5)-C(6)	1.372(7)
C(5)-H(5)	0.9500
C(6)-C(7)	1.365(7)
C(6)-H(6)	0.9500
C(7)-C(8)	1.416(7)
C(7)-H(7)	0.9500
C(8)-H(8)	0.9500
C(9)-C(10)	1.375(6)
C(9)-C(14)	1.400(7)
C(9)-N(2)	1.446(5)
C(10)-C(11)	1.394(7)
C(10)-H(10)	0.9500
C(11)-C(12)	1.389(8)
C(11)-H(11)	0.9500
C(12)-C(13)	1.394(8)
C(12)-H(12)	0.9500
C(13)-C(14)	1.375(7)
C(13)-H(13)	0.9500
C(14)-H(14)	0.9500
C(19)-N(5)	1.342(6)
C(15)-C(16)	1.367(6)
C(15)-N(5)	1.367(6)
C(16)-C(17)	1.365(6)
C(16)-H(16)	0.9500
C(17)-C(18)	1.380(7)
C(17)-H(17)	0.9500
C(18)-C(19)	1.363(6)
C(18)-H(18)	0.9500
C(19)-H(19)	0.9500
N(1)-N(2)	1.369(5)
N(3)-N(4)	1.376(5)
N(2)-C(1)-N(3)	114.1(3)
N(2)-C(1)-O(1)	124.3(4)
N(3)-C(1)-O(1)	121.6(4)
C(15)-C(2)-N(1)	115.8(3)
C(15)-C(2)-N(4)	117.6(3)
N(1)-C(2)-N(4)	126.6(4)
C(4)-C(3)-C(8)	120.9(4)
C(4)-C(3)-N(3)	118.5(4)
C(8)-C(3)-N(3)	120.6(4)
C(3)-C(4)-C(5)	120.2(4)
C(3)-C(4)-H(4)	119.9
C(5)-C(4)-H(4)	119.9

C(4)-C(5)-C(6)	120.1(5)
C(4)-C(5)-H(5)	119.9
C(6)-C(5)-H(5)	119.9
C(5)-C(6)-C(7)	119.8(5)
C(5)-C(6)-H(6)	120.1
C(7)-C(6)-H(6)	120.1
C(6)-C(7)-C(8)	121.5(5)
C(6)-C(7)-H(7)	119.3
C(8)-C(7)-H(7)	119.3
C(3)-C(8)-C(7)	117.5(5)
C(3)-C(8)-H(8)	121.2
C(7)-C(8)-H(8)	121.2
C(10)-C(9)-C(14)	121.9(4)
C(10)-C(9)-N(2)	119.0(4)
C(14)-C(9)-N(2)	119.1(4)
C(9)-C(10)-C(11)	119.0(5)
C(9)-C(10)-H(10)	120.5
C(11)-C(10)-H(10)	120.5
C(12)-C(11)-C(10)	119.5(5)
C(12)-C(11)-H(11)	120.2
C(10)-C(11)-H(11)	120.2
C(11)-C(12)-C(13)	120.8(4)
C(11)-C(12)-H(12)	119.6
C(13)-C(12)-H(12)	119.6
C(12)-C(13)-C(14)	119.9(5)
C(12)-C(13)-H(13)	120.0
C(14)-C(13)-H(13)	120.0
C(9)-C(14)-C(13)	118.8(5)
C(9)-C(14)-H(14)	120.6
C(13)-C(14)-H(14)	120.6
C(2)-C(15)-C(16)	120.8(4)
C(2)-C(15)-N(5)	116.9(4)
C(16)-C(15)-N(5)	122.3(4)
C(18)-C(19)-N(5)	124.2(4)
C(18)-C(19)-H(19)	117.9
H(19)-C(19)-N(5)	117.9
C(17)-C(18)-C(19)	117.5(4)
C(17)-C(18)-H(18)	121.3
C(19)-C(18)-H(18)	121.3
C(15)-C(16)-C(17)	118.8(4)
C(15)-C(16)-H(16)	120.6
C(17)-C(16)-H(16)	120.6
C(16)-C(17)-C(18)	120.5(4)
C(16)-C(17)-H(17)	119.8

C(18)-C(17)-H(17)	119.8
C(2)-N(1)-N(2)	115.1(3)
C(1)-N(2)-N(1)	124.6(3)
C(1)-N(2)-C(9)	120.2(3)
C(9)-N(2)-N(1)	114.9(3)
C(1)-N(3)-C(3)	121.4(3)
C(1)-N(3)-N(4)	123.7(3)
C(3)-N(3)-N(4)	114.6(3)
C(2)-N(4)-N(3)	114.9(3)
C(15)-N(5)-C(19)	116.7(4)

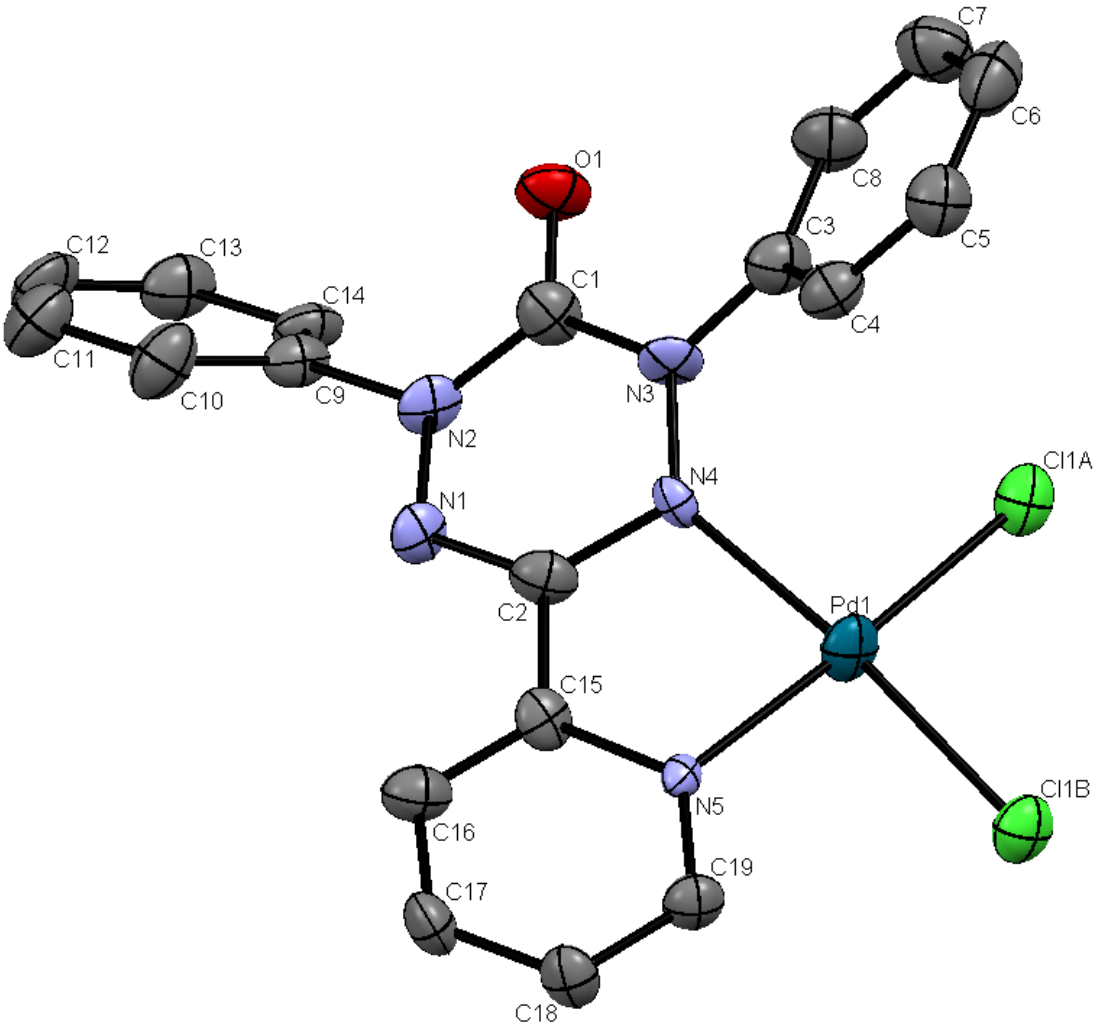

Figure D.3: ORTEP view of **2.3.PdCl$_2$**. Thermal ellipsoids at 30% probability level. Hydrogen atoms omitted for clarity.

Table D.3: Bond lengths (Å) and angles (°) for **2.3.PdCl$_2$**.

Bond	Å or °
C(1)-N(2)	1.359(13)
C(1)-N(3)	1.417(13)
C(1)-O(1)	1.220(12)
C(2)-C(15)	1.467(14)
C(2)-N(1)	1.322(13)
C(2)-N(4)	1.371(12)
C(3)-C(4)	1.391(14)
C(3)-C(8)	1.399(15)
C(3)-N(3)	1.422(13)

C(4)-C(5)	1.377(15)
C(4)-H(4)	0.9500
C(5)-C(6)	1.376(16)
C(5)-H(5)	0.9500
C(6)-C(7)	1.389(16)
C(6)-H(6)	0.9500
C(7)-C(8)	1.379(16)
C(7)-H(7)	0.9500
C(8)-H(8)	0.9500
C(9)-C(10)	1.373(15)
C(9)-C(14)	1.396(14)
C(9)-N(2)	1.454(12)
C(10)-C(11)	1.374(15)
C(10)-H(10)	0.9500
C(11)-C(12)	1.394(16)
C(11)-H(11)	0.9500
C(12)-C(13)	1.355(16)
C(12)-H(12)	0.9500
C(13)-C(14)	1.396(15)
C(13)-H(13)	0.9500
C(14)-H(14)	0.9500
C(15)-C(16)	1.382(14)
C(15)-N(5)	1.384(12)
C(16)-C(17)	1.389(14)
C(16)-H(16)	0.9500
C(17)-C(18)	1.380(14)
C(17)-H(17)	0.9500
C(18)-C(19)	1.372(14)
C(18)-H(18)	0.9500
C(19)-H(19)	0.9500
C(19)-N(5)	1.320(12)
Cl(1A)-Pd(1)	2.281(3)
Cl(1B)-Pd(1)	2.282(3)
N(1)-N(2)	1.358(11)
N(3)-N(4)	1.348(10)
N(4)-Pd(1)	2.064(7)
N(5)-Pd(1)	2.076(7)
N(2)-C(1)-N(3)	115.6(8)
N(2)-C(1)-O(1)	124.6(9)
N(3)-C(1)-O(1)	119.6(9)
C(15)-C(2)-N(1)	117.8(9)
C(15)-C(2)-N(4)	116.3(9)
N(1)-C(2)-N(4)	125.8(9)

C(4)-C(3)-C(8)	118.8(10)
C(4)-C(3)-N(3)	119.0(9)
C(8)-C(3)-N(3)	122.3(9)
C(3)-C(4)-C(5)	121.0(10)
C(3)-C(4)-H(4)	119.5
C(5)-C(4)-H(4)	119.5
C(4)-C(5)-C(6)	120.5(10)
C(4)-C(5)-H(5)	119.8
C(6)-C(5)-H(5)	119.8
C(5)-C(6)-C(7)	118.8(11)
C(5)-C(6)-H(6)	120.6
C(7)-C(6)-H(6)	120.6
C(6)-C(7)-C(8)	121.5(11)
C(6)-C(7)-H(7)	119.2
C(8)-C(7)-H(7)	119.2
C(3)-C(8)-C(7)	119.4(11)
C(3)-C(8)-H(8)	120.3
C(7)-C(8)-H(8)	120.3
C(10)-C(9)-C(14)	122.6(9)
C(10)-C(9)-N(2)	119.4(9)
C(14)-C(9)-N(2)	117.8(9)
C(9)-C(10)-C(11)	118.1(11)
C(9)-C(10)-H(10)	120.9
C(11)-C(10)-H(10)	120.9
C(10)-C(11)-C(12)	121.3(11)
C(10)-C(11)-H(11)	119.4
C(12)-C(11)-H(11)	119.4
C(11)-C(12)-C(13)	119.1(10)
C(11)-C(12)-H(12)	120.5
C(13)-C(12)-H(12)	120.5
C(12)-C(13)-C(14)	122.1(11)
C(12)-C(13)-H(13)	118.9
C(14)-C(13)-H(13)	118.9
C(9)-C(14)-C(13)	116.7(11)
C(9)-C(14)-H(14)	121.7
C(13)-C(14)-H(14)	121.7
C(2)-C(15)-C(16)	124.0(9)
C(2)-C(15)-N(5)	115.8(9)
C(16)-C(15)-N(5)	120.2(9)
C(15)-C(16)-C(17)	118.5(10)
C(15)-C(16)-H(16)	120.7
C(17)-C(16)-H(16)	120.7
C(16)-C(17)-C(18)	119.4(10)
C(16)-C(17)-H(17)	120.3

C(18)-C(17)-H(17)	120.3
C(17)-C(18)-C(19)	120.3(9)
C(17)-C(18)-H(18)	119.9
C(19)-C(18)-H(18)	119.9
C(18)-C(19)-H(19)	119.6
C(18)-C(19)-N(5)	120.8(9)
H(19)-C(19)-N(5)	119.6
C(1)-N(2)-N(1)	125.1(8)
C(2)-N(1)-N(2)	114.3(8)
C(1)-N(2)-C(9)	119.7(8)
C(9)-N(2)-N(1)	115.0(8)
C(1)-N(3)-C(3)	123.7(8)
C(1)-N(3)-N(4)	119.7(8)
C(3)-N(3)-N(4)	115.9(7)
C(2)-N(4)-N(3)	116.3(8)
C(2)-N(4)-Pd(1)	110.0(6)
N(3)-N(4)-Pd(1)	132.0(6)
C(15)-N(5)-C(19)	120.7(8)
C(15)-N(5)-Pd(1)	111.1(6)
C(19)-N(5)-Pd(1)	128.1(6)
Cl(1A)-Pd(1)-Cl(1B)	90.04(10)
Cl(1A)-Pd(1)-N(4)	95.9(2)
Cl(1A)-Pd(1)-N(5)	176.8(2)
Cl(1B)-Pd(1)-N(4)	173.8(2)
Cl(1B)-Pd(1)-N(5)	92.9(2)
N(4)-Pd(1)-N(5)	81.1(3)

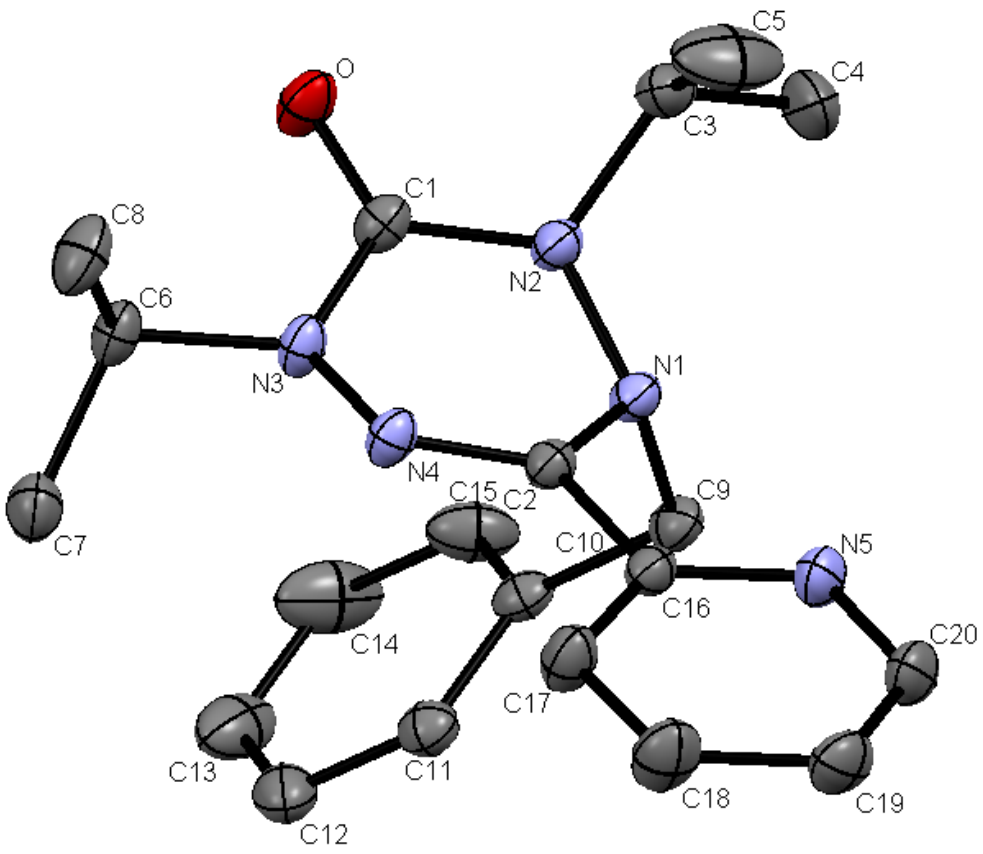

Figure D.4: ORTEP view of **3.7**. Thermal ellipsoids at 30% probability level. Hydrogen atoms omitted for clarity.

Table D.4: Bond lengths (Å) and angles (°) for **3.7**.

Bond	Å or °
C(1)-N(2)	1.379(2)
C(1)-N(3)	1.373(2)
C(1)-O(1)	1.220(1)
C(2)-C(16)	1.489(1)
C(2)-N(1)	1.407(1)
C(2)-N(4)	1.280(1)
C(3)-C(4)	1.513(2)
C(3)-C(5)	1.507(2)
C(3)-H(3)	0.999(1)
C(3)-N(2)	1.475(2)
C(4)-H(4A)	0.979(2)
C(4)-H(4B)	0.980(2)
C(4)-H(4C)	0.980(2)
C(5)-H(5A)	0.980(3)

C(5)-H(5B)	0.980(2)
C(5)-H(5C)	0.981(2)
C(6)-C(7)	1.513(2)
C(6)-C(8)	1.517(2)
C(6)-H(6)	1.000(1)
C(6)-N(3)	1.476(2)
C(7)-H(7A)	0.980(1)
C(7)-H(7B)	0.980(1)
C(7)-H(7C)	0.981(1)
C(8)-H(8A)	0.980(2)
C(8)-H(8B)	0.979(2)
C(8)-H(8C)	0.980(1)
C(9)-C(10)	1.503(2)
C(9)-H(9A)	0.989(1)
C(9)-H(9B)	0.990(1)
C(9)-N(1)	1.487(2)
C(10)-C(11)	1.390(2)
C(10)-C(15)	1.383(2)
C(11)-C(12)	1.381(2)
C(11)-H(11)	0.951(1)
C(12)-C(13)	1.374(2)
C(12)-H(12)	0.951(1)
C(13)-C(14)	1.373(3)
C(13)-H(13)	0.950(2)
C(14)-C(15)	1.387(2)
C(14)-H(14)	0.951(2)
C(15)-H(15)	0.949(2)
C(16)-C(17)	1.385(2)
C(16)-N(5)	1.337(2)
C(17)-C(18)	1.382(2)
C(17)-H(17)	0.950(1)
C(18)-C(19)	1.378(2)
C(18)-H(18)	0.950(2)
C(19)-C(20)	1.374(2)
C(19)-H(19)	0.949(1)
C(20)-H(20)	0.950(2)
C(20)-N(5)	1.343(2)
N(1)-N(2)	1.419(1)
N(3)-N(4)	1.391(1)
N(2)-C(1)-N(3)	114.8(1)
N(2)-C(1)-O(1)	122.4(1)
N(3)-C(1)-O(1)	122.8(1)
C(16)-C(2)-N(1)	118.31(9)

C(16)-C(2)-N(4)	118.3(1)
N(1)-C(2)-N(4)	123.4(1)
C(4)-C(3)-C(5)	113.3(1)
C(4)-C(3)-H(3)	107.5(1)
C(4)-C(3)-N(2)	110.2(1)
C(5)-C(3)-H(3)	107.5(1)
C(5)-C(3)-N(2)	110.7(1)
H(3)-C(3)-N(2)	107.4(1)
C(3)-C(4)-H(4A)	109.5(1)
C(3)-C(4)-H(4B)	109.4(1)
C(3)-C(4)-H(4C)	109.4(1)
H(4A)-C(4)-H(4B)	109.6(2)
H(4A)-C(4)-H(4C)	109.5(2)
H(4B)-C(4)-H(4C)	109.4(2)
C(3)-C(5)-H(5A)	109.4(2)
C(3)-C(5)-H(5B)	109.5(2)
C(3)-C(5)-H(5C)	109.5(2)
H(5A)-C(5)-H(5B)	109.4(2)
H(5A)-C(5)-H(5C)	109.5(2)
H(5B)-C(5)-H(5C)	109.5(2)
C(7)-C(6)-C(8)	112.9(1)
C(7)-C(6)-H(6)	107.6(1)
C(7)-C(6)-N(3)	109.5(1)
C(8)-C(6)-H(6)	107.6(1)
C(8)-C(6)-N(3)	111.2(1)
H(6)-C(6)-N(3)	107.7(1)
C(6)-C(7)-H(7A)	109.4(1)
C(6)-C(7)-H(7B)	109.5(1)
C(6)-C(7)-H(7C)	109.5(1)
H(7A)-C(7)-H(7B)	109.5(1)
H(7A)-C(7)-H(7C)	109.5(1)
H(7B)-C(7)-H(7C)	109.5(1)
C(6)-C(8)-H(8A)	109.4(1)
C(6)-C(8)-H(8B)	109.5(1)
C(6)-C(8)-H(8C)	109.5(1)
H(8A)-C(8)-H(8B)	109.4(1)
H(8A)-C(8)-H(8C)	109.5(1)
H(8B)-C(8)-H(8C)	109.5(1)
C(10)-C(9)-H(9A)	108.6(1)
C(10)-C(9)-H(9B)	108.6(1)
C(10)-C(9)-N(1)	114.6(1)
H(9A)-C(9)-H(9B)	107.5(1)
H(9A)-C(9)-N(1)	108.6(1)
H(9B)-C(9)-N(1)	108.6(1)

C(9)-C(10)-C(11)	120.8(1)
C(9)-C(10)-C(15)	120.7(1)
C(11)-C(10)-C(15)	118.4(1)
C(10)-C(11)-C(12)	121.1(1)
C(10)-C(11)-H(11)	119.4(1)
C(12)-C(11)-H(11)	119.4(1)
C(11)-C(12)-C(13)	119.8(1)
C(11)-C(12)-H(12)	120.1(1)
C(13)-C(12)-H(12)	120.1(1)
C(12)-C(13)-C(14)	119.8(2)
C(12)-C(13)-H(13)	120.1(2)
C(14)-C(13)-H(13)	120.1(2)
C(13)-C(14)-C(15)	120.6(2)
C(13)-C(14)-H(14)	119.7(2)
C(15)-C(14)-H(14)	119.7(2)
C(10)-C(15)-C(14)	120.3(2)
C(10)-C(15)-H(15)	119.8(1)
C(14)-C(15)-H(15)	119.9(2)
C(2)-C(16)-C(17)	120.4(1)
C(2)-C(16)-N(5)	116.6(1)
C(17)-C(16)-N(5)	123.0(1)
C(16)-C(17)-C(18)	118.8(1)
C(16)-C(17)-H(17)	120.6(1)
C(18)-C(17)-H(17)	120.6(1)
C(17)-C(18)-C(19)	118.8(1)
C(17)-C(18)-H(18)	120.6(2)
C(19)-C(18)-H(18)	120.6(2)
C(18)-C(19)-C(20)	118.7(1)
C(18)-C(19)-H(19)	120.7(1)
C(20)-C(19)-H(19)	120.6(1)
C(19)-C(20)-H(20)	118.2(1)
C(19)-C(20)-N(5)	123.6(1)
H(20)-C(20)-N(5)	118.2(1)
C(2)-N(1)-C(9)	115.20(9)
C(2)-N(1)-N(2)	112.57(9)
C(9)-N(1)-N(2)	113.76(9)
C(1)-N(2)-C(3)	117.8(1)
C(1)-N(2)-N(1)	119.57(9)
C(3)-N(2)-N(1)	114.96(9)
C(1)-N(3)-C(6)	120.0(1)
C(1)-N(3)-N(4)	120.9(1)
C(6)-N(3)-N(4)	113.86(9)
C(2)-N(4)-N(3)	115.7(1)
C(16)-N(5)-C(20)	117.2(1)

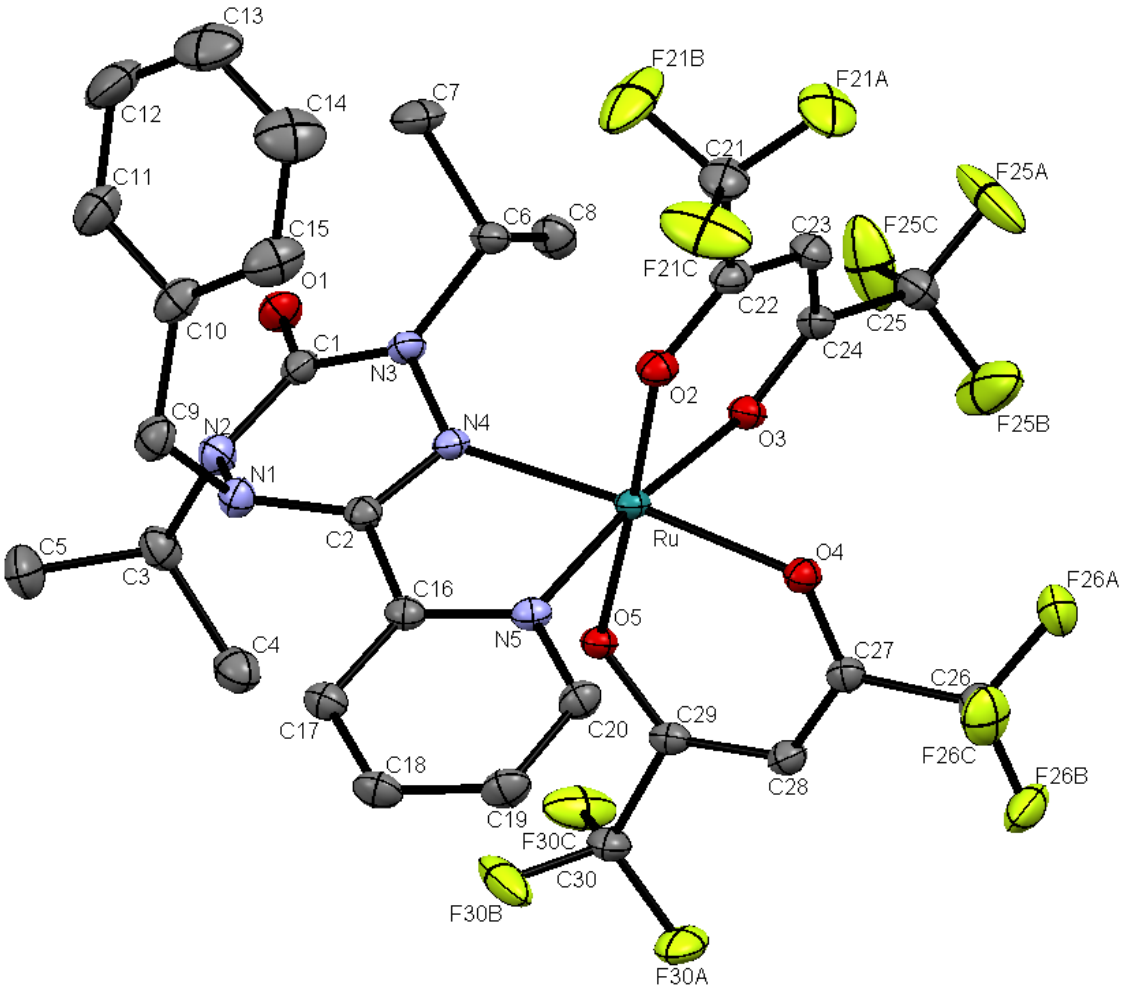

Figure D.5: ORTEP view of **3.7.Ru(hfac)$_2$**. Thermal ellipsoids at 30% probability level. Hydrogen atoms omitted for clarity.

Table D.5: Bond lengths (Å) and angles (°) for **3.7.Ru(hfac)$_2$**.

Bond	Å or °
C(1)-N(2)	1.379(3)
C(1)-N(3)	1.386(2)
C(1)-O(1)	1.217(3)
C(2)-C(16)	1.459(3)
C(2)-N(1)	1.386(3)
C(2)-N(4)	1.304(2)
C(3)-C(4)	1.524(5)
C(3)-C(5)	1.511(4)
C(3)-H(3)	1.000(2)
C(3)-N(2)	1.486(3)

C(4)-H(4A)	0.980(3)
C(4)-H(4B)	0.979(3)
C(4)-H(4C)	0.980(3)
C(5)-H(5A)	0.980(4)
C(5)-H(5B)	0.980(3)
C(5)-H(5C)	0.981(3)
C(6)-C(7)	1.524(5)
C(6)-C(8)	1.517(4)
C(6)-H(6)	1.000(2)
C(6)-N(3)	1.486(3)
C(7)-H(7A)	0.980(3)
C(7)-H(7B)	0.980(3)
C(7)-H(7C)	0.980(3)
C(8)-H(8A)	0.980(4)
C(8)-H(8B)	0.979(2)
C(8)-H(8C)	0.980(2)
C(9)-C(10)	1.507(4)
C(9)-H(9A)	0.990(2)
C(9)-H(9B)	0.991(2)
C(9)-N(1)	1.493(4)
C(10)-C(11)	1.384(5)
C(10)-C(15)	1.383(3)
C(11)-C(12)	1.387(6)
C(11)-H(11)	0.950(3)
C(12)-C(13)	1.371(5)
C(12)-H(12)	0.950(4)
C(13)-C(14)	1.379(7)
C(13)-H(13)	0.949(5)
C(14)-C(15)	1.384(6)
C(14)-H(14)	0.949(3)
C(15)-H(15)	0.951(4)
C(16)-C(17)	1.389(3)
C(16)-N(5)	1.358(3)
C(17)-C(18)	1.384(4)
C(17)-H(17)	0.951(2)
C(18)-C(19)	1.381(4)
C(18)-H(18)	0.950(2)
C(19)-C(20)	1.381(3)
C(19)-H(19)	0.951(3)
C(20)-H(20)	0.950(2)
C(20)-N(5)	1.344(3)
C(21)-C(22)	1.533(4)
C(21)-F(21A)	1.323(3)
C(21)-F(21B)	1.315(4)

C(21)-F(21C)	1.295(4)
C(22)-C(23)	1.387(3)
C(22)-O(2)	1.263(3)
C(23)-C(24)	1.392(4)
C(23)-H(23)	0.950(2)
C(24)-C(25)	1.531(3)
C(24)-O(3)	1.262(2)
C(25)-F(25A)	1.282(3)
C(25)-F(25B)	1.322(6)
C(25)-F(25C)	1.316(3)
C(26)-C(27)	1.519(3)
C(26)-F(26A)	1.331(3)
C(26)-F(26B)	1.338(4)
C(26)-F(26C)	1.329(3)
C(27)-C(28)	1.394(3)
C(27)-O(4)	1.269(3)
C(28)-C(29)	1.383(3)
C(28)-H(28)	0.950(3)
C(29)-C(30)	1.527(3)
C(29)-O(5)	1.271(3)
C(30)-F(30A)	1.327(4)
C(30)-F(30B)	1.318(3)
C(30)-F(30C)	1.315(3)
N(1)-N(2)	1.416(2)
N(3)-N(4)	1.402(3)
N(4)-Ru	2.067(2)
N(5)-Ru	2.019(2)
O(2)-Ru	2.035(2)
O(3)-Ru	2.070(1)
O(4)-Ru	2.039(2)
O(5)-Ru	2.029(2)
N(2)-C(1)-N(3)	114.4(2)
N(2)-C(1)-O(1)	123.0(2)
N(3)-C(1)-O(1)	122.6(2)
C(16)-C(2)-N(1)	120.9(2)
C(16)-C(2)-N(4)	116.5(2)
N(1)-C(2)-N(4)	122.5(2)
C(4)-C(3)-C(5)	118.2(2)
C(4)-C(3)-H(3)	107.8(2)
C(4)-C(3)-N(2)	111.1(2)
C(5)-C(3)-H(3)	107.7(2)
C(5)-C(3)-N(2)	110.6(2)
H(3)-C(3)-N(2)	107.6(2)

C(3)-C(4)-H(4A)	109.5(3)
C(3)-C(4)-H(4B)	109.5(3)
C(3)-C(4)-H(4C)	109.4(3)
H(4A)-C(4)-H(4B)	109.4(3)
H(4A)-C(4)-H(4C)	109.5(3)
H(4B)-C(4)-H(4C)	109.5(3)
C(3)-C(5)-H(5A)	109.4(3)
C(3)-C(5)-H(5B)	109.5(3)
C(3)-C(5)-H(5C)	109.5(3)
H(5A)-C(5)-H(5B)	109.4(3)
H(5A)-C(5)-H(5C)	109.5(3)
H(5B)-C(5)-H(5C)	109.5(3)
C(7)-C(6)-C(8)	111.7(2)
C(7)-C(6)-H(6)	107.3(2)
C(8)-C(6)-H(6)	107.3(2)
H(6)-C(6)-N(3)	107.4(2)
C(7)-C(6)-N(3)	109.5(2)
C(8)-C(6)-N(3)	113.3(2)
C(6)-C(7)-H(7A)	109.5(3)
C(6)-C(7)-H(7B)	109.4(3)
C(6)-C(7)-H(7C)	109.5(3)
H(7A)-C(7)-H(7B)	109.5(3)
H(7A)-C(7)-H(7C)	109.5(3)
H(7B)-C(7)-H(7C)	109.4(3)
C(6)-C(8)-H(8A)	109.5(2)
C(6)-C(8)-H(8B)	109.5(2)
C(6)-C(8)-H(8C)	109.5(2)
H(8A)-C(8)-H(8B)	109.5(3)
H(8A)-C(8)-H(8C)	109.5(3)
H(8B)-C(8)-H(8C)	109.4(3)
H(9A)-C(9)-H(9B)	107.3(2)
C(10)-C(9)-H(9A)	108.2(2)
C(10)-C(9)-H(9B)	108.2(2)
C(10)-C(9)-N(1)	116.6(2)
H(9A)-C(9)-N(1)	108.1(2)
H(9B)-C(9)-N(1)	108.1(2)
C(9)-C(10)-C(11)	120.5(3)
C(9)-C(10)-C(15)	121.0(3)
C(11)-C(10)-C(15)	118.4(3)
C(10)-C(11)-C(12)	120.3(3)
C(10)-C(11)-H(11)	119.8(3)
C(12)-C(11)-H(11)	119.9(3)
C(11)-C(12)-C(13)	120.6(4)
C(11)-C(12)-H(12)	119.8(4)

C(13)-C(12)-H(12)	119.6(4)
C(12)-C(13)-C(14)	119.7(4)
C(12)-C(13)-H(13)	120.2(4)
C(14)-C(13)-H(13)	120.1(4)
C(13)-C(14)-C(15)	119.6(4)
C(13)-C(14)-H(14)	120.1(4)
C(15)-C(14)-H(14)	120.2(4)
C(10)-C(15)-C(14)	121.3(3)
C(10)-C(15)-H(15)	119.3(3)
C(14)-C(15)-H(15)	119.4(3)
C(2)-C(16)-C(17)	124.4(2)
C(2)-C(16)-N(5)	113.4(2)
C(17)-C(16)-N(5)	122.2(2)
C(16)-C(17)-C(18)	118.4(2)
C(16)-C(17)-H(17)	120.8(2)
C(18)-C(17)-H(17)	120.8(3)
C(17)-C(18)-C(19)	119.5(3)
C(17)-C(18)-H(18)	120.3(3)
C(19)-C(18)-H(18)	120.2(3)
C(18)-C(19)-C(20)	119.4(3)
C(18)-C(19)-H(19)	120.3(3)
C(20)-C(19)-H(19)	120.3(3)
C(19)-C(20)-H(20)	119.0(3)
C(19)-C(20)-N(5)	122.1(2)
H(20)-C(20)-N(5)	118.9(2)
C(22)-C(21)-F(21A)	113.2(3)
C(22)-C(21)-F(21B)	109.7(3)
C(22)-C(21)-F(21C)	112.7(3)
F(21A)-C(21)-F(21B)	106.1(3)
F(21A)-C(21)-F(21C)	106.4(3)
F(21B)-C(21)-F(21C)	108.4(3)
C(21)-C(22)-O(2)	112.6(2)
C(21)-C(22)-C(23)	117.8(2)
C(23)-C(22)-O(2)	129.5(2)
C(22)-C(23)-C(24)	124.5(2)
C(22)-C(23)-H(23)	117.7(2)
C(24)-C(23)-H(23)	117.8(2)
C(23)-C(24)-C(25)	118.1(2)
C(23)-C(24)-O(3)	128.7(2)
C(25)-C(24)-O(3)	113.2(2)
C(24)-C(25)-F(25A)	115.1(3)
C(24)-C(25)-F(25B)	110.4(3)
C(24)-C(25)-F(25C)	112.3(2)
F(25A)-C(25)-F(25B)	107.0(3)

F(25A)-C(25)-F(25C)	108.0(3)
F(25B)-C(25)-F(25C)	103.3(3)
C(27)-C(26)-F(26A)	111.1(2)
C(27)-C(26)-F(26B)	113.3(2)
C(27)-C(26)-F(26C)	111.7(2)
F(26A)-C(26)-F(26B)	106.6(2)
F(26A)-C(26)-F(26C)	106.5(2)
F(26B)-C(26)-F(26C)	107.2(2)
C(26)-C(27)-C(28)	118.8(2)
C(26)-C(27)-O(4)	112.2(2)
C(28)-C(27)-O(4)	129.0(2)
C(27)-C(28)-C(29)	124.4(2)
C(27)-C(28)-H(28)	117.8(2)
C(29)-C(28)-H(28)	117.7(2)
C(28)-C(29)-C(30)	119.1(2)
C(28)-C(29)-O(5)	129.2(2)
C(30)-C(29)-O(5)	111.7(2)
C(29)-C(30)-F(30A)	113.7(2)
C(29)-C(30)-F(30B)	109.6(2)
C(29)-C(30)-F(30C)	112.3(2)
F(30A)-C(30)-F(30B)	106.7(2)
F(30A)-C(30)-F(30C)	106.5(2)
F(30B)-C(30)-F(30C)	107.7(2)
C(2)-N(1)-C(9)	118.0(2)
C(2)-N(1)-N(2)	112.3(2)
C(9)-N(1)-N(2)	115.3(2)
C(1)-N(2)-C(3)	118.7(2)
C(1)-N(2)-N(1)	118.4(2)
C(3)-N(2)-N(1)	115.0(2)
C(1)-N(3)-C(6)	122.3(2)
C(1)-N(3)-N(4)	119.6(2)
C(6)-N(3)-N(4)	117.0(2)
C(2)-N(4)-N(3)	114.6(2)
C(2)-N(4)-Ru	114.5(1)
N(3)-N(4)-Ru	130.6(1)
C(16)-N(5)-C(20)	118.4(2)
C(16)-N(5)-Ru	115.5(2)
C(20)-N(5)-Ru	125.2(2)
C(22)-O(2)-Ru	122.0(2)
C(24)-O(3)-Ru	121.0(1)
C(27)-O(4)-Ru	121.2(1)
C(29)-O(5)-Ru	121.1(1)
N(4)-Ru-N(5)	78.38(7)
N(4)-Ru-O(2)	91.95(7)

N(4)-Ru-O(3)	106.32(7)
N(4)-Ru-O(4)	173.32(7)
N(4)-Ru-O(5)	86.27(7)
N(5)-Ru-O(2)	93.01(7)
N(5)-Ru-O(3)	172.56(7)
N(5)-Ru-O(4)	94.97(7)
N(5)-Ru-O(5)	84.08(7)
O(2)-Ru-O(3)	92.60(6)
O(2)-Ru-O(4)	87.72(6)
O(2)-Ru-O(5)	176.84(6)
O(3)-Ru-O(4)	80.36(6)
O(3)-Ru-O(5)	90.41(6)
O(4)-Ru-O(5)	93.76(6)